NORTHWESTERN UNIVERSITY

Fundamentals of thermosensory navigation in *Drosophila*

A DISSERTATION

SUBMITTED TO THE GRADUATE SCHOOL

IN PARTIAL FULFILLMENT OF THE REQUIREMENTS

for the degree

DOCTOR OF PHILOSOPHY

Field of Engineering Sciences and Applied Mathematics

By

Joshua I. Levy

EVANSTON, ILLINOIS

September 2021

ABSTRACT

Fundamentals of thermosensory navigation in *Drosophila*

Joshua I. Levy

Processing of sensory information in the brain is a pervasive and fundamental phenomenon across animal species and is involved in both "hard-wired" innate responses as well as learned and adaptive behaviors. Here, I show that the avoidance of hot temperature, a simple innate behavior, contains unexpected plasticity and complex processing in *Drosophila*. First, I demonstrate that the hot receptor neurons of the antenna and their molecular heat sensor, Gr28B.d, are essential for flies to produce escape turns away from heat. By integrating modeling of the thermal environment with behavioral data, I show that even minute temperature differences (0.1°C-1.0°C) between the antennae are sufficient to determine turning direction. Based on these measurements, I evolve a fly/vehicle model with two symmetrical sensors and motors (a "Braitenberg vehicle") which closely approximates basic fly thermotaxis. Critical differences between real flies and the hard-wired vehicle reveal that fly heat avoidance involves decision-making, relies on rapid learning, and is robust to new conditions, features generally associated with more complex behavior. Next, I show that the innocuous heat sensors are also involved in processing of diffuse thermal signals, and identify key neural

circuitry enabling flies to chart a course away from dangerous heat. By comparing fly behavior with that of a modified vehicle model, I find that separate but interacting processing underlies navigation of steep and shallow thermal gradients.

Acknowledgments

During my time in Evanston, I've had the honor of working with so many brilliant, hard-working, and scientifically curious people. Although life as a graduate student has been a struggle at times, my colleagues here have pushed me to think about problems in new and exciting ways, and have changed me for the better, both as a scientist and a person.

In particular, I have to thank Marco Gallio, who inspired and supervised this work, and José Miguel Simões, a postdoc in the Gallio lab who I've worked with closely over the last few years. Both of these gentlemen have an undying desire and intuition for great science, and it has been a privilege to work with them.

I also owe a great deal to my ESAM advisor, Bill Kath, who encouraged me to do impactful and interdisciplinary science, and was supportive as I explored a range of research topics. I'd also like to thank Neda Bagheri, who incorporated me into her lab and enabled me to work on a broad range of problems in systems biology, and Madhav Mani, who helped me believe that by immersing myself in a lab, I'd gain access to a spectrum of new and unexplored problems, and whose fervor for rigorous, data-driven science is unparalleled.

I would like to thank the remaining members of the Gallio lab, especially Michael Alpert, Dominic Frank, Oscar Arenas, Jenna Jouandet, Alessia Para, and Fred Zhao, who welcomed me into the group and were remarkably patient with me as I got up to speed. I would also like to thank the members of the Bagheri lab, especially Jessica Yu, Joe Muldoon, Narasimhan Balakrishnan, Justin Finkle, Alex Prybutok, Jason Cain, and Kate Dray, who pushed me to

think deeply about the role of modeling in science, and helped me better communicate my work.

I would also like to acknowledge my fellow ESAM grad students that have made this journey immeasurably more enjoyable, in particular Noah Ford, Thomas Lynn, Joseph Johnson, Eric Johnson, Brita (Schneiders) Young, Rebecca Menssen, Hammad Faizi, Gerardo Pradillo, and Nicolas Daffern (honorary). They have been there for everything from daily lunches and Thanksgiving dinners, intellectual (and not so intellectual) discussions, sporting events, and weekend rendezvous.

Last, but certainly not least, this would not have been possible without my family and Camila, who have supported me throughout the ups and downs of graduate school. Having them nearby throughout this process has been an incredible luxury and has made all the difference.

Table of Contents

List of Figures

Preface

All life is intimately connected to the environment and its fluctuations of light and dark, hot and cold, wet and dry. It is in part due to such interactions that organisms have evolved to exist within particular niches and manage to thrive in accordance with the dynamic conditions of Earth. While the fundamental rules of biology unite all organisms — as Jacques Monod famously claimed, "What is true of *E. coli* must also be true of elephants" — at the level of behavior there is no single strategy for survival, as evidenced by the vast array of behavioral solutions observed in nature. However, among animals with a central brain, the fundamental components of neural processing are often conserved, even though behavior may vary wildly across species.

This thesis presents results from my time at Northwestern, during which I have attempted to answer the question: How do animals, from flies to humans, depend on and navigate their environment?

To do so, I use the thermosensory system of the fruit fly (*Drosophila melanogaster*) to investigate the fundamental rules of sensory processing and navigation. This work is a close collaboration with the Gallio lab at Northwestern, and fuses experimental and mathematical approaches to further our understanding of the links between genes, cells, and behavior.

CHAPTER 1

Fundamentals of thermosensory navigation

Temperature is among the most fundamental determinants of cellular state. At one extreme, it can rapidly lead to degradation of cellular material and at the other, it can arrest cellular reactions and inhibit motion. Yet, neural processing of temperature by the brain is also one of the least understood modes of sensory processing.

In this chapter, we discuss the basics of hot temperature sensation and processing, focusing on the fruit fly *Drosophila melanogaster*. We start our discussion at the molecular level, examining key classes of sensors, eventually making our way to known neuronal circuitry. Finally, we will discuss ways to conceptualize and categorize the behaviors flies use to navigate their thermal environment.

1.1. Transducers of hot stimuli

Animals sense temperature through the use of molecular receptors, which transform changes in the environment into changes of conformation or state. When stimulated, receptors can adjust the chemical and electrical conditions of an animal's cells, often with exquisite precision. However, only in the last few decades have we developed the experimental tools to identify and study these fundamental sensory components.

One key class of temperature receptors are ion channels called Transient Receptor Potential (TRP) channels. Originally discovered in the fruit fly as sensors of bright light, TRP

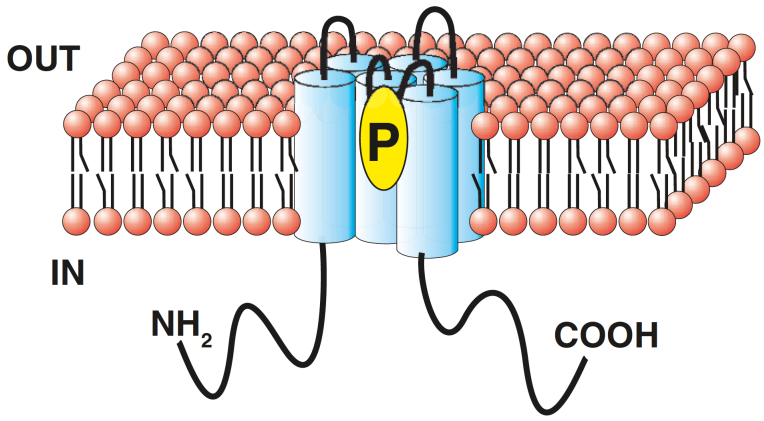

Figure 1.1. Structure of TRP membrane proteins. Six transmembrane domains (blue) and channel pore (P). Adapted from [**1**].

channels can often detect multiple sensory modalities and can be targeted by molecular agonists [**2**]. When activated, TRP channels open their central pore (which contains many negatively charged residues), allowing for positively charged ions to flow into the cell, and their large conductance is often sufficient to depolarize a neuron and drive firing of action potentials.

TRPV1, the first mammalian TRP receptor to be described, was identified using a genetic screen against capsaicin, the ingredient that gives "hot" peppers their characteristic spiciness [**3**]. In this same work, it was shown that this cation channel is activated when exposed to temperatures known to elicit pain in mammals. Accordingly, mammalian TRPV1 is termed a "noxious" temperature receptor, as it contributes to the sensing of painful thermal stimuli *in vivo* ($> 43°C$), known as nociception. Later studies identified other mammalian TRP channels tuned to distinct thermal ranges (see Figure 1.2a): TRPV2 responds to temperatures greater than $52°C$, TRPV3 to the high 30s, TRPV4 to the low 30s, TRPM8 below $26°C$ and TRPA1 to noxious cold temperatures [**4**]. Together, these responses cover

nearly the entire range of observable temperatures. Despite these differences in tuning, these channels all use a similar mechanism.

Notably, homologous versions of TRP proteins have been shown to have wildly variable tuning (Figure 1.2b). For example, while mammalian TRPA1 responds to noxious cold, the polar opposite response is found in its homolog in *Drosophila*, which responds to temperatures above $40°C$. A recent study showed that this is likely not due to a a different mechanism, but rather TRPA1 is responding to the presence of hydrogen peroxide and reactive oxygen species, which can arise in both noxious hot and cold temperature regimes [**5**]. Interestingly, while the *painless* TRP channel has been shown to be important for nociception in larvae [**6**], its role in adults remains unclear.

Although TRP channels are thought to be the dominant thermosensory receptors in mammals, recent research has found that other types of molecular receptors may play a role in fly sensing. In *Drosophila*, TRPA1 is mostly inactive since flies generally remain far from noxious heat. Below the noxious range, it turns out that a protein that shows similarities with a gustatory receptor, termed Gr28B.d, actually confers heat sensitivity [**7**]. While gustatory receptors show structural similarities with G-protein coupled receptors [**8, 9**], recent work suggests that it may function as a non-selective cation channel, similar to several TRP channels [**10**].

Although the molecular receptors that confer sensitivity to thermal stimuli are often similar across organisms, many differences arise in the organization and use of those sensors. To study the way thermal input is used, we focus on the fruit fly *Drosophila melanogaster* to identify core principles underlying the processing of temperature.

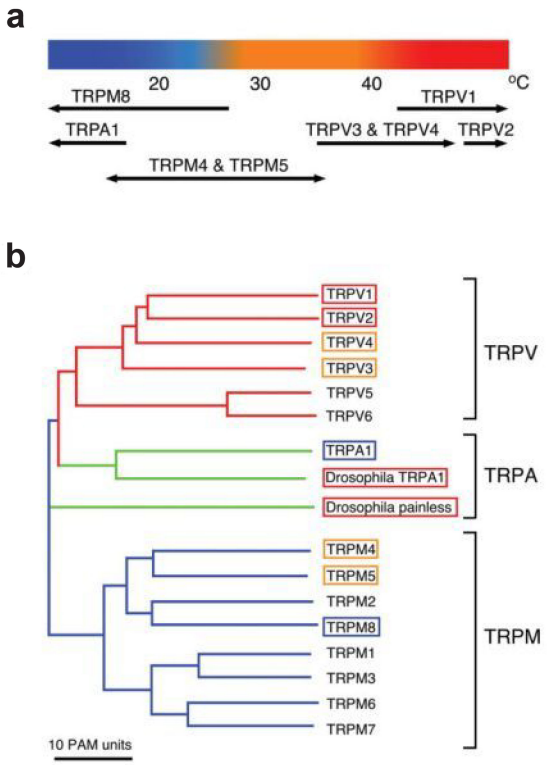

Figure 1.2. TRP receptor proteins. **a.** TRP channels are tuned to sense many different temperature ranges. **b.** Classes of mammalian and *Drosophila* TRP proteins. From [**4**].

1.2. Studying thermosensation in the fruit fly

Measuring just about 3mm in length in adulthood, yet possessing a a central brain of roughly 100,000 neurons and a host of complex behaviors, the fruit fly *Drosophila melanogaster* has long been a crucial model organism in neuroscience and biology. Research on *Drosophila* has led to some of the greatest breakthroughs in our understanding of genetics, especially the role of genes in determining behavior.

Fruit flies are an excellent model system to study how animals sense and process thermal stimuli. As poikilotherms, flies are strongly dependent on rapid and robust temperature processing at a range of spatial and temporal scales, and in the modern lab setting, flies

are both genetically and physiologically tractable. This permits incredibly precise study of individual cellular components like receptors, and even previously "invisible" phenomena like neural firing.

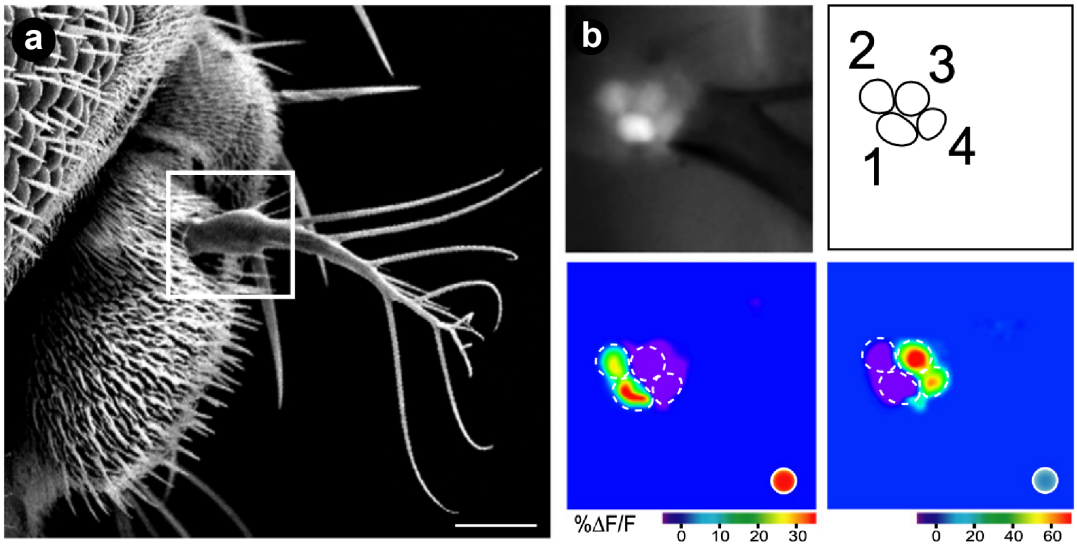

Figure 1.3. Hot and cold receptor neurons in the antennae. **a.** Thermosensory neurons are housed in the base of the arista, the final segment of the fly antenna. **b.** Hot and cold sensing cells are found in clusters of three neurons, totaling 6 cells(only two of each are shown). Calcium response of hot and cold neurons to thermal stimuli (hot on left, cold on right). From [**11**].

One of the most important tools we have for studying the fly brain is the GAL4-UAS system [**12**]. This method uses a yeast transcription factor (GAL4) and its corresponding enhancer (Upstream Activation Sequence, or UAS) to drive expression of a desired gene in a particular cell type. Using the GAL4-UAS system we can even express fluorescent markers and optical indicators like GFP (green fluorescent protein) and GCaMP (a fluorescent calcium indicator) in cells of interest, allowing us to visualize their morphology and firing behavior in the brain. While study of neural activity had historically relied on electrical measurements, the invention of genetically encoded calcium indicators (GECIs) like

GCaMP dramatically shifted the experimental paradigm, allowing researchers to simultaneously study the activity of many neurons in the brain, and with cell-type specificity offered by the GAL4-UAS system.

This tool has proven crucial in the study of temperature sensation. Although findings from the lab of Seymour Benzer, one of the godfathers of modern behavioral genetics, suggested that the antennae of the fly housed temperature receptor neurons [**13**], it was not until the development the GAL4-UAS system that these cells could be studied in detail [**11**]. As it turns out, the final segment of the antennae, a feather-like protrusion called the arista, contains a group of six cells, three of which are dedicated hot sensors (Hot Cells or HCs) and three that are cold sensors (Figure 1.3a).

The three hot cells each express the molecular receptor Gr28B.d, while the cold sensory triad expresses a TRP channel receptor. Importantly, since these neurons are inaccessible to traditional electrophysiological patching without destroying the arista, the UAS-GCaMP element allows for optical measurement of cellular state via calcium driven changes in fluorescence, as shown in Figure 1.3b. Experimentally, we observe that heating reliably activates hot cells, while inhibiting cold cells [**11**]. Similarly, cooling inhibits hot cells while activating cold cells. Importantly, the hot cells are required for sensation of innocuous heating ($< 35°$C) above the fly's preferred temperature of 25°C. However, more intense heat stimuli engage noxious thermosensory cells, which express TRPA1.

In the fly, TRPA1-expressing neurons are present throughout the brain and body. The group of TRPA1-expressing cells located within the brain, also known as Anterior Cells (ACs), have been suggested to mediate thermal preference even at innocuous temperatures [**14**]. Outside of the brain, TRPA1 is expressed throughout the body of the fly and is required for avoidance of temperatures greater than $35°C$ [**5**].

Using just these sensory modules, the fly is able to detect almost any perceivable warm or hot stimulus. However, converting this information into behavior requires additional processing in the brain.

1.2.1. Processing of heat in the fly brain

When sensory neurons are activated, they send information to the central brain, where this information aggregated and converted into a behavioral response. Recent studies of *Drosophila* have allowed us to uncover some of this circuitry involved in fly responses to heat and begin to interrogate the nature of the underlying computations [**15**]. Unlike mammalian brains, the fly brain is often thought to be largely hard-wired [**16**]. In fact, individual neurons can be unambiguously identified across animals using the GAL4-UAS method, and the connectivity among neurons within the brain is remarkably reproducible. This incredible consistency is also evident in the heat processing circuitry of the fly, from the level of sensory neurons to higher order processing.

Following innocuous heating, activity registered in the hot cells is relayed to a key distribution hub of the brain, known as the Antennal Lobe (AL, see Figure 1.4). There, neurons receiving synaptic input from the hot glomerulus are triggered to signal other areas of the brain for further processing. These second order neurons (also known as projection neurons or 2Ns) are comprised of a number of canonical types, which recently have been identified [**15, 17**].

When studied experimentally, the 2Ns are found to have a range of different properties that provide insight into their role in temperature sensing. One important characteristic of these cells is their adaptation speed. Based on the amount of time required for the cell to return to baseline activity following thermal stimulation, we can roughly categorize 2Ns as

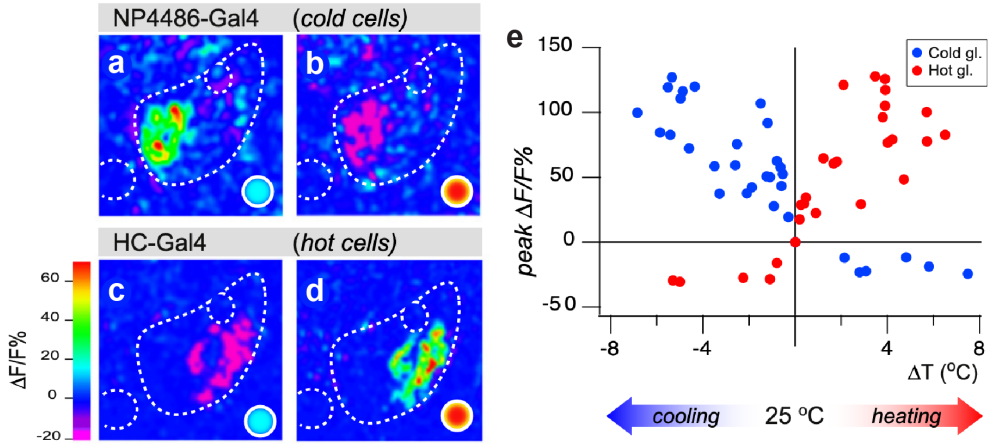

Figure 1.4. Response to thermal stimuli in posterior antennal lobe (PAL). **a,b.** Cold cell responses to cold and hot stimuli. **c,d.** Hot cell reponses. **e.** Calcium responses grow linearly above the preferred temperature of 25 $^{\circ}C$. From [**11**].

slow-adapting or fast-adapting. Cells that adapt slowly tend to integrate information over time, suggesting that they may be better suited to conveying information about stimulus magnitude, while fast-adapting cells are better suited to detection of changes in input.

As an example, the R95C02-GAL4 driver specifies a class of second order neurons that innervate the lateral horn (LH), a well known sensory processing area, as well as the lesser known posterior lateral protocerebrum (PLP) (Figure 1.5). When stimulated, a subset of these neurons responds rapidly, but this response quickly decays to baseline. Notably, the response intensity of each does not does scale with the intensity of the stimulus. Following termination of the stimulus, additional neurons in this class show a similar pulse of response. Together, this suggests that these neurons convey temporal information regarding the start and stop of the stimulus (commonly described as ON and OFF responses).

On the other hand, slow-adapting hot neurons have a rather different role and morphology. For example, one class of slow-adapting neuron identified by the VT40053-GAL4 driver

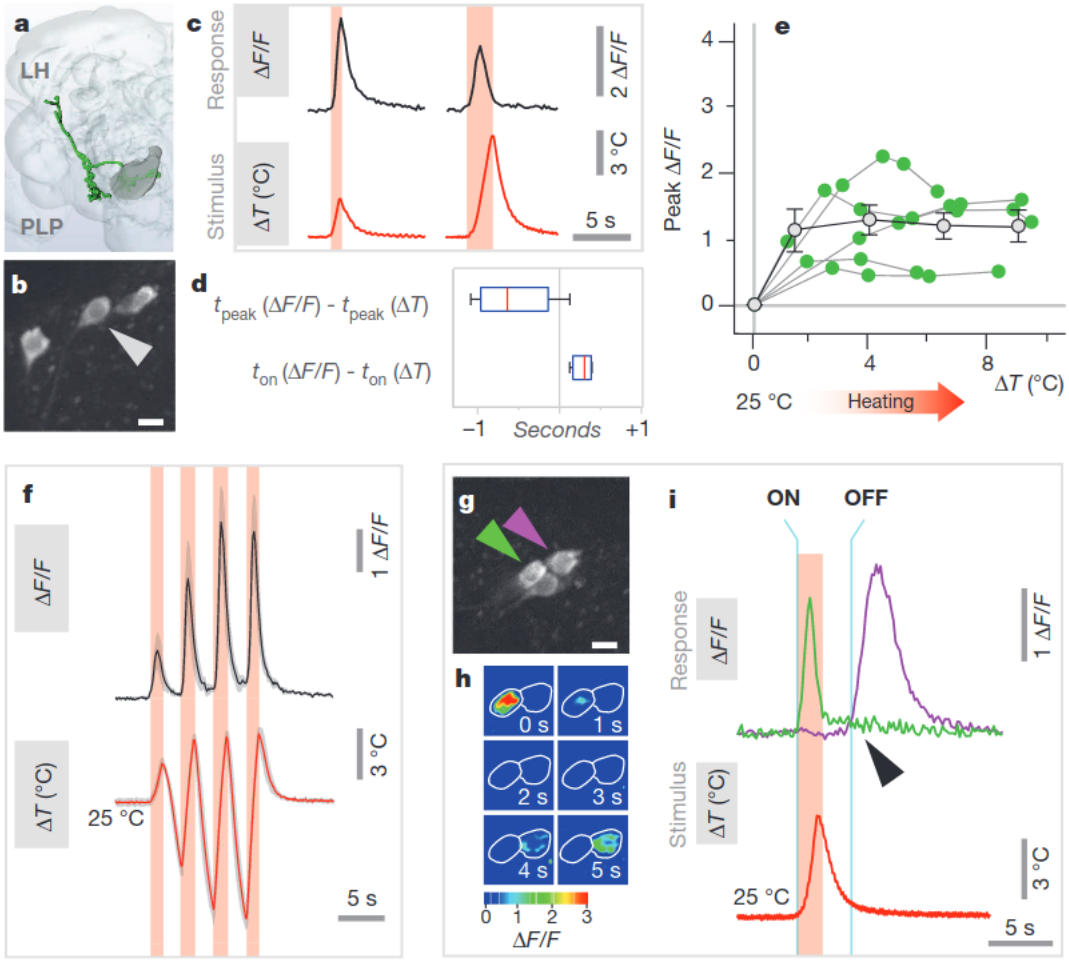

Figure 1.5. Firing behavior of fast-adapting hot projection neurons. **a,b.** Morphology of R95C02-expressing neurons and position of hot sensitive cell (arrow). **c,d.** response properties relative to stimulus. **e,f.** Response to hot stimuli, has intensity independent of that of the thermal stimulus. **g-i.** Two separate cells respond to ON and OFF events. From [**15**].

responds to both hot and cold stimuli with elevated intensity throughout the duration of the stimulus, followed by a slow descent to baseline (Figure 1.6). In addition, the intensity of the response seems to scale with the that of the stimulus, suggesting that these slow cells may convey the magnitude of the change in temperature. These "broadly tuned" neurons then

extend into the brain, relaying information to known processing areas like the mushroom body (MB) and lateral horn (LH), as well as the posterior lateral protocerebrum (PLP).

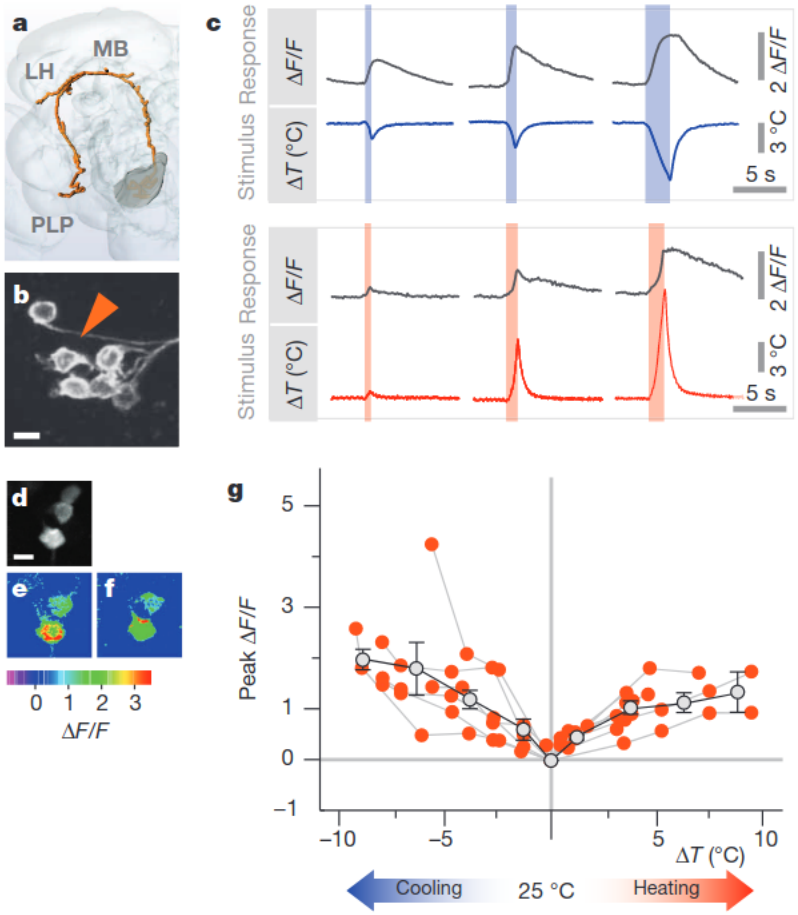

Figure 1.6. Firing behavior of slow adapting, broadly tuned neurons. **a,b.**VT40053 neuron morphology and cell bodies. **c-g.** This class of neurons respond to both hot and cold stimuli and with intensity corresponding to that of the thermal stimulus. From [**15**].

Although the aforementioned circuitry and processing at the neuronal level provides an indispensible glimpse into the logic of the fly brain, it is only through examination of behavior that we can understand if and how this information is used. Generally, this requires the use of perturbation experiments, in which genetic and physical manipulations are used to selectively

target, activate or silence parts of a circuit. One powerful approach involves the selective expression (mediated by GAL4) of transgenes that are capable of silencing neural activity. For example, expression of Kir-2.1, an inwardly rectifying potassium channel, in a desired cell type, induces persistent hyperpolarization and is commonly used to prevent neuronal firing.

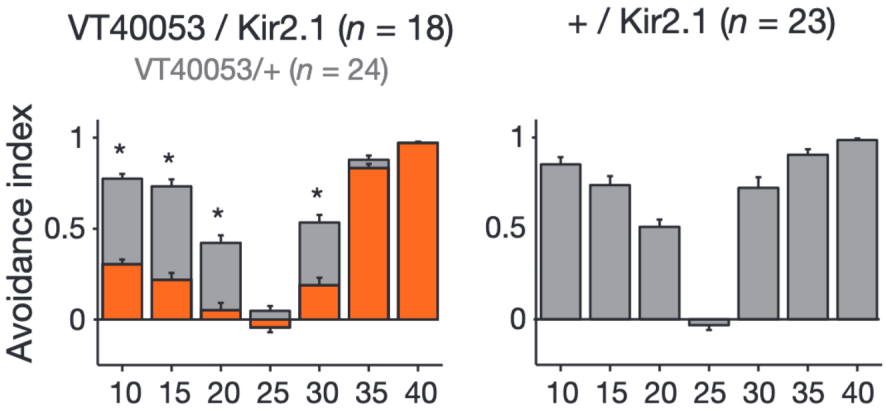

Figure 1.7. Heat avoidance behavior in VT40053/Kir mutants. Silencing VT40053-expressing cells with UAS-Kir leads to a loss of innocuous heat avoidance, in addition to a loss of cold avoidance (orange), distinct from controls (grey). From [**15**].

Indeed, when slow adapting VT40053 neurons are silenced with UAS-Kir, flies show a clear change in their heat avoidance behavior when tested in a two-choice thermal preference experiment, as shown in Figure 1.7. In this experiment, flies are forced to choose between a region at their preferred $25°C$ (Base temperature, or BT) and a test temperature (TT). Their occupancy in each region is used to calculate a simple statistic called an Avoidance Index (or AI). The AI ranges from -1 (strong preference of the test temperature) to 1 (strong preference of $25°C$). This simple measure is often written

$$\text{AI} = \frac{\text{time spent at BT} - \text{time spent at TT}}{\text{total time}}. \tag{1.1}$$

By considering changes in AI, it is evident that unlike control flies, these mutants have a decreased ability to avoid innocuous temperatures including innocuous cold ($20°C$) and hot ($30°C$), yet remain capable of avoiding noxious heat (Figure 1.7). This information suggests that VT40053 neurons process key thermal input from the antennae, and play a role in innocuous warm temperature processing.

Genetic knock-out experiments have also shown that noxious heat avoidance requires TRPA1 expression. Indeed, in two-choice behavioral experiments between their preferred $25°C$ and a harmful $40°C$, TRPA1 mutants do not robustly avoid heat (Figure 1.8). Rather, they explore the hot region as if it were only set to an innocuous warm temperature ($30°C$) [**5**]. Interestingly, the TRPA1 mutant phenotype could be rescued by a Drosophila TRPA1 variant that is not sensitive to heat (TRPA1-C, Figure 1.8b,c), or even by planarian (heat insensitive) or human TRPA1 (cold sensitive). This result suggested that a chemical intermediate (H_2O_2) may mediate noxious heat sensing by TRPA1.

The cellular substrates and processing mediating TRPA1-dependent noxious heat avoidance are not well understood, but likely involves multidendritic neurons that tile the fly epidermis [**18**].

1.3. Innate vs learned behavior

How are temperature stimuli processed into directed behavior? In neuroscience, we often categorize neural processing and its corresponding behavior as either being innate or learned.

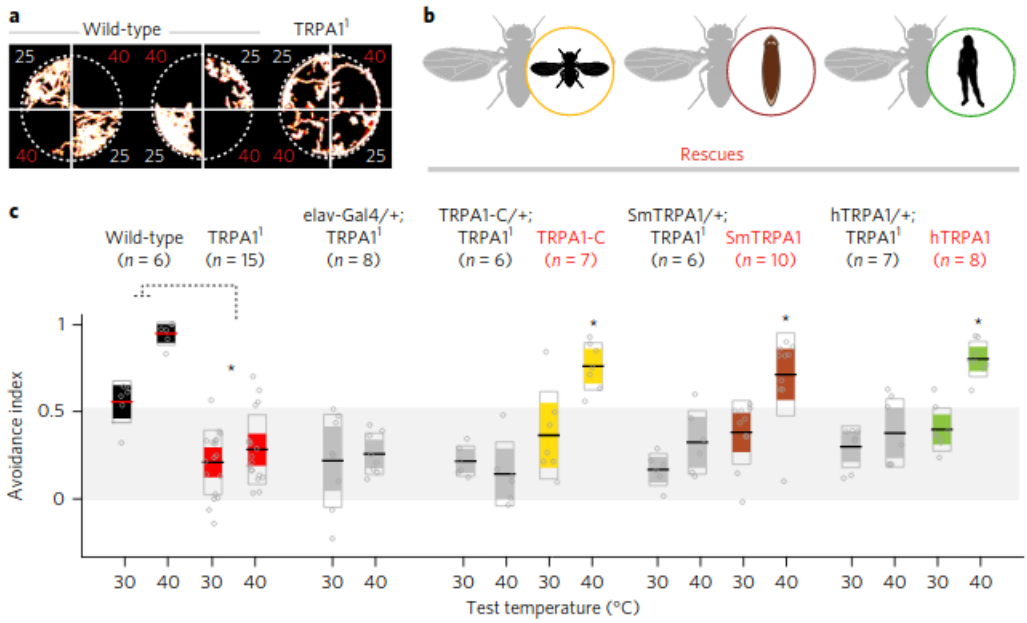

Figure 1.8. Mutation of TRPA1 leads to a loss of noxious heat avoidance. **a.** Wild type and TRPA1 mutant fly trajectories in a two-choice experiment. ,c. Schematic and results of rescue experiments. TRPA1[1] mutants show reduced heat avoidance in a two-choice experimental assay. Rescue experiments heat insensitive TRPA1 transgenes from *Drosophila*, planarian, and human restore avoidance behavior. From [**5**].

Innate behavior is believed to be genetically encoded or hard-wired into the brain, while learned behavior is the result of interaction between experience and neuronal plasticity.

From an evolutionary perspective, it is evident why innate behavior is important. Once an animal is born, it has only a short period of time, ranging from a few days to a few years, to figure out what it needs to do to survive and pass on its genetic material. For example, many insects are remarkably capable at birth and are known to engage in behaviors like walking, flying, and even hunting [**16**]. In contrast, humans are a major outlier in relation to most other animals, spending many years learning while in an immature, vulnerable state. Still, as almost all animals, a large portion of our sensory representation and behavior is innate. Without any previous experience, monarch butterflies migrate thousands of miles

to escape dangerous winter temperatures [**19**], moths are attracted to sources of light [**20**], turtle hatchlings can dig their way out from under layers of sand [**21**], and many mammals perform shaking maneuvers when wet [**22**].

To contemplate the range of behaviors producible by a hard-wired circuit, the cybernetic-ist Valentino Braitenberg proposed a series of thought experiments, in which he constructed "vehicles" using only a simple arrangement of sensors, wires, and motors [**23**]. With just a handful of these components, Braitenberg suggested that he could reproduce animal behaviors like curiousity, cowardice, love, and hate. Although these behaviors may appear appear complex, even intelligent, the underlying circuitry may be encoded using relatively simple rules.

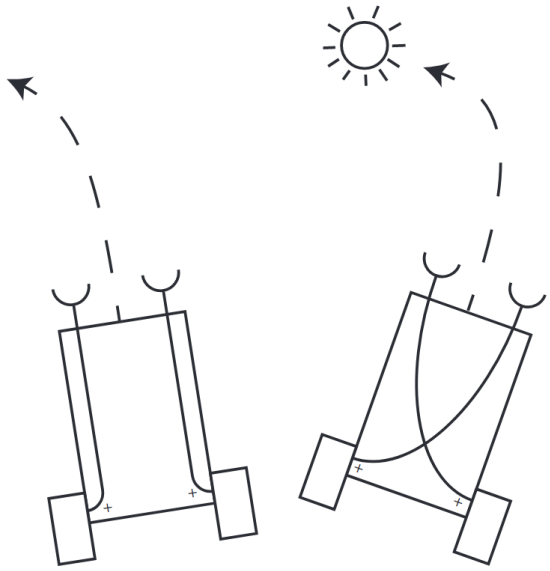

Figure 1.9. Braitenberg vehicles can perform apparently complex behavior. Even simple vehicles, as proposed by Valentino Braitenberg, are produce behaviors like "hate" (left) and "love" (right). From [**23**].

In reality, "hard-wired" brain circuits are not entirely rigid, and neither are the behaviors they produce. While fruit fly behavior is often considered to be completely genetically

encoded, its "innate" behavior appears to be state dependent. For example, after mating, female flies show strong changes in food preference, consuming more protein and carbohydrate-rich food than virgin flies [**24, 25**]. Similarly, when protein deprived flies are given a choice between yeast and an alternative food source, the flies prefer the yeast.

Innate behaviors can be modulated by even more subtle environmental changes. While flies innately display aggressive behavior when threatened or in danger of losing a competition, its frequency and intensity are intimately linked to its state and experience [**26**]. When socially isolated, male flies display an increased propensity to fight compared to group-housed controls. Further, repeated winners and losers of fights clearly acquire lasting positive and negative internal states, which impacts their willingness to take risks, engage in courtship, and overall fitness.

Although recent research has only begun to show that innate behavior can be flexible, behavior requiring learning and memory formation have been the subject of considerable study. Flies are known to rapidly form visual, olfactory, and place memories that guide their future preferences [**27**]. For example, nearly 50 years ago the Benzer lab showed that flies can form a stable negative association (lasting at least 24 hours) between a neutral odor and an electric foot shock [**28**].

1.4. Sensory navigation

Perhaps one of the most distinguishing characteristics of animals is their ability to navigate their environment. Animals navigate to find food, avoid predators, locate a mate, and to escape hazardous environmental conditions, some of the most fundamental requirements for survival. To accomplish these behaviors, animals must interpret information received at

their sensors and craft a behavioral response. However, as mentioned, the way in which they do so is still being uncovered.

The organism whose navigation that we understand best may actually be the bacterium *E. coli*, which is able to navigate towards a chemical source without the use of a brain. Remarkably, using only a relatively small group of simple molecular machines, bacteria can alternate between running and "tumbling" modes in a biased fashion that leads them up concentration gradients to a desired source [**29**]. Specifically, they decrease their turning probability when moving in a direction of increasing concentration, and when they experience no gradient or a decrease in concentration, they maintain turning frequency at a baseline value, leading to unbiased motion.

In the field of systems neuroscience, we aspire to achieve a similar level of clarity on the behaviors and underlying mechanisms used for sensory navigation in animals. Armed with recent advances in behavioral tracking, molecular genetics, and mapping of brain circuitry (connectomics), we are now equipped to analyze neural processing in unprecedented detail.

A recent blossoming of the field has led to significant progress. For example, we now know that owls are able to target their prey by comparing inter-aural sonic arrival times [**30**], that moths use wind sensing and olfaction to orient themselves towards an odor source [**31**], and that ants robustly track conspecific pheromones to reliably travel to and from their nest [**32**]. These behaviors often occur over large distances, and represent navigational strategies that are quite distinct from those of a bacterium.

However, we are generally still learning how these neural circuits achieve these behaviors, and the types of computation they perform. We have evidence suggesting that some animals can use spatial memory to form maps of a sensory landscape [**33, 34**], potentially even

fusing multiple sensory modes to guide navigation [**35**]. Yet, to date, behavioral modeling of navigation remains largely theoretical, largely divorced from the underlying neural circuitry.

Inspired by evidence of spatial memory, some algorithms have suggested a Bayesian-like computation may integrate sensory input and step towards a target [**36, 37**], while others suggest reflex-like responses to local changes in the environment may be sufficient for navigation [**38**]. Although this research is ongoing, it is clear that there is no single strategy for all forms of navigation or all types of animals. As with most designed systems, behavior (and brain wiring) is heavily context dependent, a consequence of factors like environment, competition, and efficiency.

1.4.1. Sensori-motor integration in the *Drosophila* nervous system

In order to navigate through complex environments, animals depend on rapid integration of sensory information to perform motor commands. Achieving robust and flexible navigation requires adjustable neural circuits that integrate external and internal sensors to control movement.

For some stereotyped behavior, animals depend on direct (or nearly direct) sensory neuron to motor neuron communication known as reflexes. For example, both vertebrates and invertebrates employ "stretch" reflexes to maintain posture [**39**]. These reflexes depend on just three basic components working in a loop: a sensory neuron, a motor neuron and a muscle. When the muscle is stretched, the sensory neuron is activated, thereby exciting the motor neuron, leading to muscle contraction and decreased muscle stretch. Accordingly, these circuits are essential to stabilize an animal during changes in mechanical load.

However, dynamic behaviors rely on different types of circuitry in order to generate complex motion. One class of control mechanisms, known as central pattern generators (CPGs)

can be driven following processing in the central brain and are responsible for driving rhythmic patterns like walking or breathing [**40**]. By integrating feedback from proprioceptive mechanosensors as well as descending signals from the brain, these local circuits enable many behaviors essential to survival [**41**].

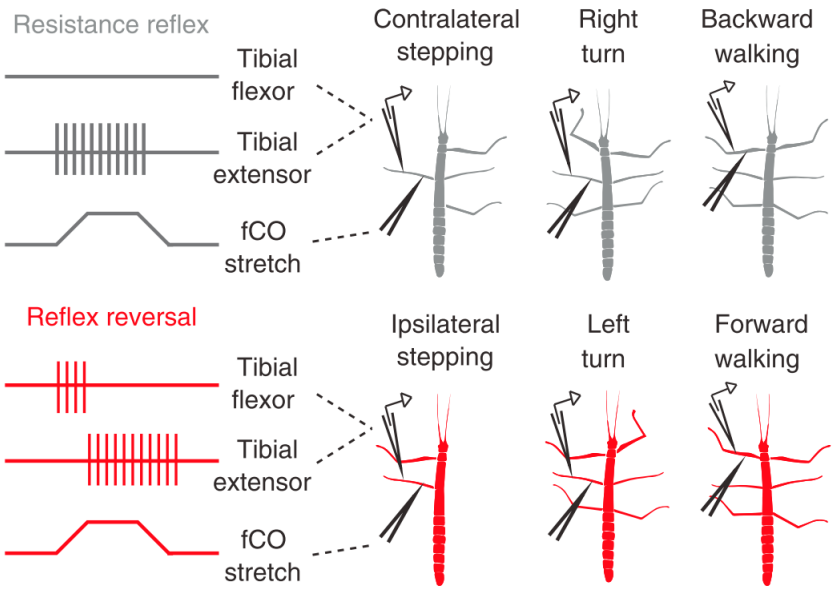

Figure 1.10. Motor control in invertebrates. Stick insects use a combination of reflex and CPG circuits to maintain stability and maneuver. From [**39**].

In *Drosophila* there is a small, but growing body of literature on how the sensorimotor system works, previously impeded by their diminutive size but now accelerated by a wealth of genetic and computational tools. One well studied model of sensorimotor integration is the stick insect, *Phasmatodea*, which relies on a delicate balance of both reflex and CPG driven behavior. For example, stretch reflexes in the legs of the stick insect naturally maintain stability through a reflex that inhibits tibial motor neurons, which would ordinarily prevent voluntary leg motion (e.g., walking). To handle this, CPG signaling can "reverse" the reflex, allowing for the tibial flexion required for maneuvering. Further processing in the brain

can then turn off CPG activity, returning the motor control to a posture maintaining state. Importantly, this showcases the fundamental tradeoff between stability and maneuverability during animal behavior.

While long considered to be no more than simple automatons, insects have emerged as one of the most tractable examples of flexible sensorimotor control. Even amidst changing conditions, insects are able to perform diverse behaviors including running, flying, grooming, courting, or even building. They also provide key lessons for development in robotics, though the most promising insect-inspired robots still can only mimic a small fraction of fly behaviors [**42**], and are much more prone to mishaps, particularly in uneven terrain. This flexibility is one of the great uncovered secrets of insect sensorimotor processing, and further discovery of how the brain accomplishes it may lay the groundwork for a new generation of robust robotics.

1.5. Neural coding of sensory space

As an animal moves about its environment, its sensors continuously gather information and send it to the brain for processing. This processing results in a representation of the sensory environment, also known as a spatial map, that can be used to guide behavior.

First described in the lab of Edward Tolman during a study of rats navigating a maze [**43**], these spatial maps are thought to take two forms:

(1) Egocentric, or body-centric representations, reflect a focus on relative position with respect to the animal. Common examples are directional descriptors (e.g., left, right, forward, back).

(2) Allocentric, or world-centric representations, integrate simple sensory input to form a global map of sensory space using the relative positions of features in the environment. Examples include spatial grids and heading direction, which describe characteristics independent of current position and orientation (e.g., north, east, south, west).

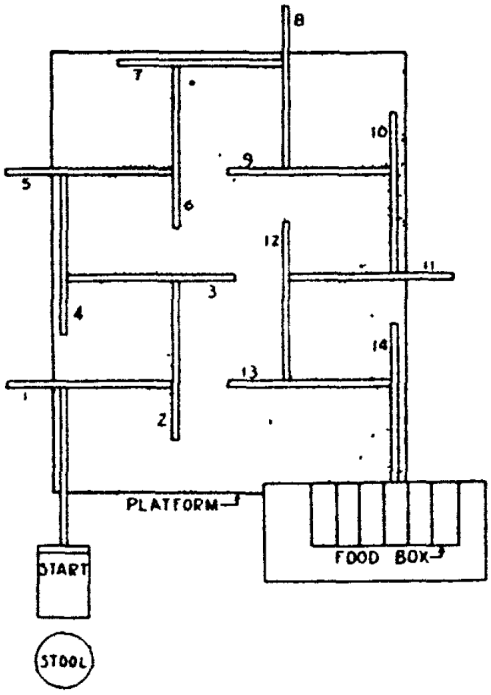

Figure 1.11. Tolman's maze experiment. Rats were trained to navigate a complex T-maze, igniting discussions on the types of sensory processing required for completing this task. From [**43**].

In Tolman's experiment, rats learned how to navigate the maze rapidly over multiple trials, but the nature of their underlying strategy remained unclear. Were rats learning a sequence of walking and turning maneuvers? Or were they somehow building a "field map" from key landmarks to be used for navigating the maze?

This remains an active area of research, but it is clear that elements of both spatial encodings guide navigation. Recent research on rats suggests that egocentric stimulus-response processing may occur in the dorsal striatum [**44**], while "grid" and "boundary" cells in the hippocampus are known to encode specific regions of space, regardless of animal orientation [**45**].

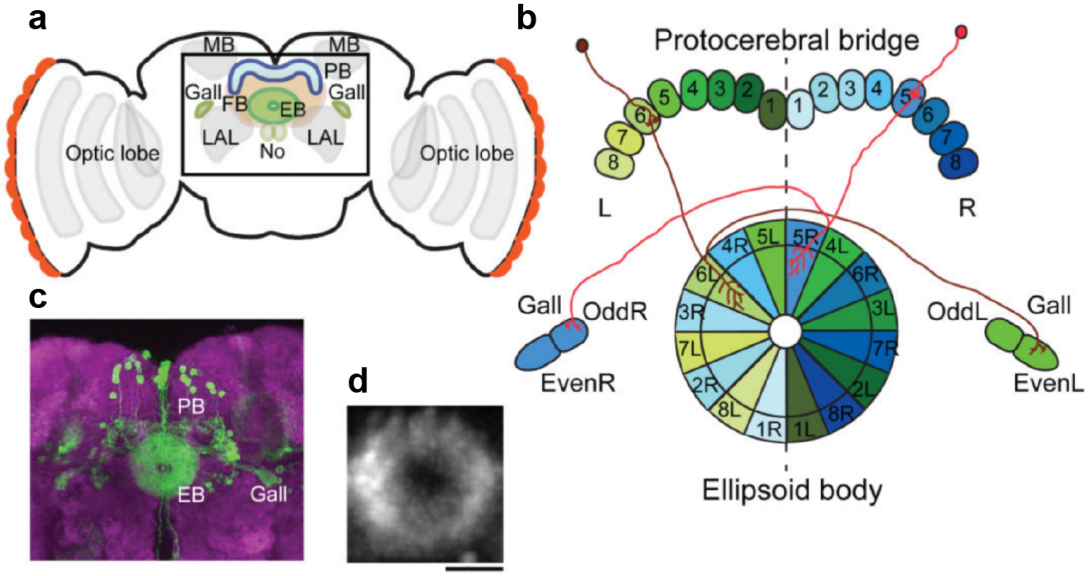

Figure 1.12. Allocentric heading cells in the fly brain. **a.** Schematic of the fly brain and central complex (box), showing the fan-shaped body (FB), protocerebral bridge (PB), ellipsoid body (EB), mushroom body (MB), lateral accessory lobe (LAL), noduli (NO), and gall. **b.** EPG neurons, which form 16 wedges tiling the EB, innervate the central 16 columns of the PB (which has 18 total columns) as well as the gall. **c.** Fluorescence of EPG neurons expressing GFP. **d.** Example of activity bump in EPG neurons expressing GCaMP. Scale bar: 20 μm. From [**46**].

Insects also display both egocentric and allocentric processing, likely coordinated in the central complex (CX), a conserved region of the brain involved in many aspects of navigation [**47, 48, 49**]. For example, in the CX, allocentric head direction cells tile an annular region known as the Ellipsoid Body (EB), while also forming arbors in both the protocerebral bridge

(PB) and gall (G) [**46, 50**]. These EPG, or "compass", neurons as they are often called, maintain a bump of activity that corresponds to the fly's heading angle, relative to cues in the environment. Recent findings have shown that they are required to maintain a constant heading with respect to salient features of the environment, also known as menotaxis, and are involved in sensory pathways including visual and wind processing [**51, 52, 53**]. Another group of EB neurons, known as PEN neurons, are required to rotate the position of the activity bump as the fly turns [**50, 54**].

However, the EB is not required for all types of goal-directed navigation. Compass-silenced flies remain capable of positive taxis, in which they walk in the direction of a spatial landmark, a form of egocentric processing [**51, 52**], and both flies and bees are known to use optical flow input to make corrective adjustments to their trajectory as they proceed towards a target [**55, 56**]. In the fly brain, optical flow information is thought to be encoded in part by LNO and SpsP neurons, which innervate the Noduli (NO) and PB brain regions of CX [**57**]. Importantly, while these cells are strongly effected by optic flow stimuli, they likely integrate a host of other egocentric cues (e.g., proprioception of translational velocity), and are activated even in total darkness [**56**].

Another form of egocentric representation is observed in a group of neurons targeting the fan-shaped body (FB) region of the CX, known as PFN cells, which are thought to encode airflow and walking velocity [**57, 58**]. Silencing of a subset of these neurons, the ventral PFNs, was found to prevent flies from selecting appropriate corrective turns following changes in airflow direction, suggesting they may be required for proper orientation to a stimulus [**58**]. Although little is known about the role of the FB in navigation, and whether or not it operates distinctly from the EB, there are some indications that it may exert a strong influence on locomotor activity. For example, FB stimulation evokes stereotypical walking

behavior in flies [**59**], and FB output neurons have been suggested to drive steering [**49**]. However, most of the neural substrates that support these behaviors remain unknown.

1.6. Fundamentals of thermosensory processing in *Drosophila*

In this dissertation, I present two investigations of fly navigation in response to hot thermal stimuli. This work aims to develop quantitative frameworks to describe animal behavior by integrating approaches from fields including computer vision, mathematical modeling, and optimization, with experimental measurements in the lab. The core objective of these efforts is to identify fundamental principles that explain the sensorimotor processing underlying complex behavior.

The work presented in Chapter 2 illustrates how the antennae (and the hot receptor molecule they express, Gr28B.d) are essential for flies to produce escape turns away from heat. Combining high-resolution tracking with 3D simulation of the thermal environment, I show that, in steep thermal gradients, direction of escape turns is determined by minute temperature differences between the antennae (0.1-1.0°C). Following additional experiments in the Gallio lab that confirm this sensitivity, I evolve a fly-sized *in silico* vehicle model with symmetrical sensors and motors (a "Braitenberg vehicle") which approximates basic fly thermotaxis. By critically examining differences between real flies and the hard-wired vehicle, I show that fly heat avoidance involves decision-making, relies on rapid learning, and is robust to new conditions, features generally associated with more complex behavior.

In Chapter 3, I extend our study of thermosensory navigation to a novel context, a linear temperature gradient, in which the physical parameters of the system are chosen such that temperature differences between the antennae are negligible. Using tracking and modeling of the thermal environment, I show that the antennal thermosensors are also necessary for

rapid descent of the thermal gradient. Although the "naive" vehicle of described in Chapter 2 does not efficently descend the gradient, I show that successful navigation is restored by incorporating a "compass"-like modulator of turning behavior, prompting further study of the role of the compass cells in this context. Experimental silencing of fly "compass" cells suggests that allocentric heading, established by spatio-temporal processing of thermal cues, is essential for rapid navigation of the shallow gradient, but does not effect the predictability of escape turn direction in a steep gradient. In parallel, silencing of PFNv cells does not effect performance in the linear gradient, but leads to a loss of turning bias at the steep thermal boundary, suggesting that these cells may play a role in egocentric processing of heat stimuli. Using network analysis of the fly brain connectome, I identify neurons that may relay heat input to both the compass and PFNv cells.

Overall, these results suggest that flies use elements of both vehicle-like steering, as well as compass modulated navigation. Direct comparison of a vehicle model with actual flies reveals unexpected complexity in fly navigation, and enables identification and study of key processing circuitry.

CHAPTER 2

Robustness and plasticity in *Drosophila* heat avoidance

2.1. Forward

Developed in close collaboration with the Gallio Lab, this chapter uses a fusion of computational, statistical, and experimental methods to establish a detailed understanding of *Drosophila* heat avoidance. A shorter version of this work was published in Nature Communications in 2021 [**60**]. This work is the product of a close collaboration with José Miguel Simões of the Gallio lab, who engineered mutant flies and performed recordings of behavior as well as neural activity, while I developed the quantitative methods to analyze the raw data, and built and analyzed the models used in our approach. Smaller contributions from other members of the lab are mentioned in the text. Additional detail on experimental and statistical procedures is provided in the Appendix.

2.2. Introduction

Innate behaviors can be performed in response to a cue without prior experience. As such they are considered hard-wired in the nervous system, particularly in the more "simple" nervous system of invertebrates. At the extreme, the cyberneticist Valentino Braitenberg famously proposed that a broad range of seemingly complex animal behavior (e.g., "aggression", "love", and "hate" [**23**]) could be reproduced by hypothetical vehicles purely as a result of the wiring pattern of a set of symmetric sensors and motors.

Here, we report the first high-resolution characterization of heat avoidance and thermotaxis in adult Drosophila melanogaster. Our first goal is to define the basic functional organization of the sensory system that guides these innate behaviors in adult fruit flies. Our next objective is to compare fly heat avoidance with the behavior of a Braitenberg-inspired in silico vehicle model, explicitly probing the notion that the fly's innate avoidance of hot temperature can be understood as a combination of hard-wired responses.

The avoidance of unfavorable temperatures is a fundamental behavior in the repertoire of all motile animals, from flatworms to whale sharks [**61**]. Due to its ancestral nature, heat avoidance is an ideal system to test the idea that simple innate behavior may be largely hardwired. The fruit fly Drosophila melanogaster is an excellent model to address this question. A genetically and physiologically tractable animal capable of elaborate short and long-range navigation [**62, 63**], flies have been extensively used to study and model the sensory processing that informs navigational decisions [**64, 65**].

When given a choice, adult Drosophila melanogaster prefer 25°C over colder or warmer temperatures [**11, 13**]. Flies are, in particular, very sensitive to heat: in laboratory conditions, adults of both sexes are incapacitated if confined to ∼35-37°C [**66**], and exposure to 40°C proves quickly lethal. As a consequence, adult flies display increasingly robust avoidance of temperatures higher than their preferred 25°C, spanning the innocuous (i.e., not harmful, 25-35°C) and noxious (i.e., potentially harmful or even lethal, >35°C) range.

In the fly nervous system, rapid temperature changes are detected by dedicated populations of hot- and cold-activated temperature receptor neurons (TRNs) residing in the last antennal segment, the arista [**11**]. The projections of these neurons form two distinct, adjacent glomeruli in the Posterior Antennal Lobe (PAL) region of the brain, where afferent activity defines a simple map for temperature representation [**11, 15**]. In addition to

the hot-activated receptors of the antenna ("Hot Cells" or HC), adult flies possess internal heat sensors within the head capsule ("Anterior Cells" or AC [**14**]), and multi-modal thermal/mechanical nociceptors innervate the body of both the larva and adult [**18, 6**] (Figure 2.1a shows a schematic of the cell types and gene functions involved in heat sensing in the adult).

Despite this basic knowledge, we still do not understand how the activity of distinct cellular sensors may be coordinated to produce heat avoidance, nor how aversive heat responses become integrated in the navigational programs that steer animals away from thermal danger (thermotaxis).

2.3. Characterization of thermal sensors and role in heat avoidance

To develop a more detailed picture of how thermosensory input is processed into navigational responses, we used a two-choice behavioral assay [**11**] to study the thermal preferences of control and mutant flies. All analysis was performed on groups of flies, with 5-10 flies per trial. Our results directly demonstrate that both noxious and innocuous signals play a role during rapid heat avoidance:

(1) Transgenic silencing or ablation of heat-activated TRNs of the arista abolished avoidance of 30°C heat, while avoidance of 35°C was only partially reduced, and avoidance of 40°C was not affected (Figure 2.1a-e; note that silencing of AC neurons had no effect on this behavior, Figure 2.1f, see Figure 2.1g and Figure 2.2 for controls).

Identical results to the silencing of hot cells were obtained from a null mutant (produced for this study) of the candidate heat receptor ion channel Gr28B [**7**]. Importantly, the Gr28B mutant phenotype was completely rescued by expression

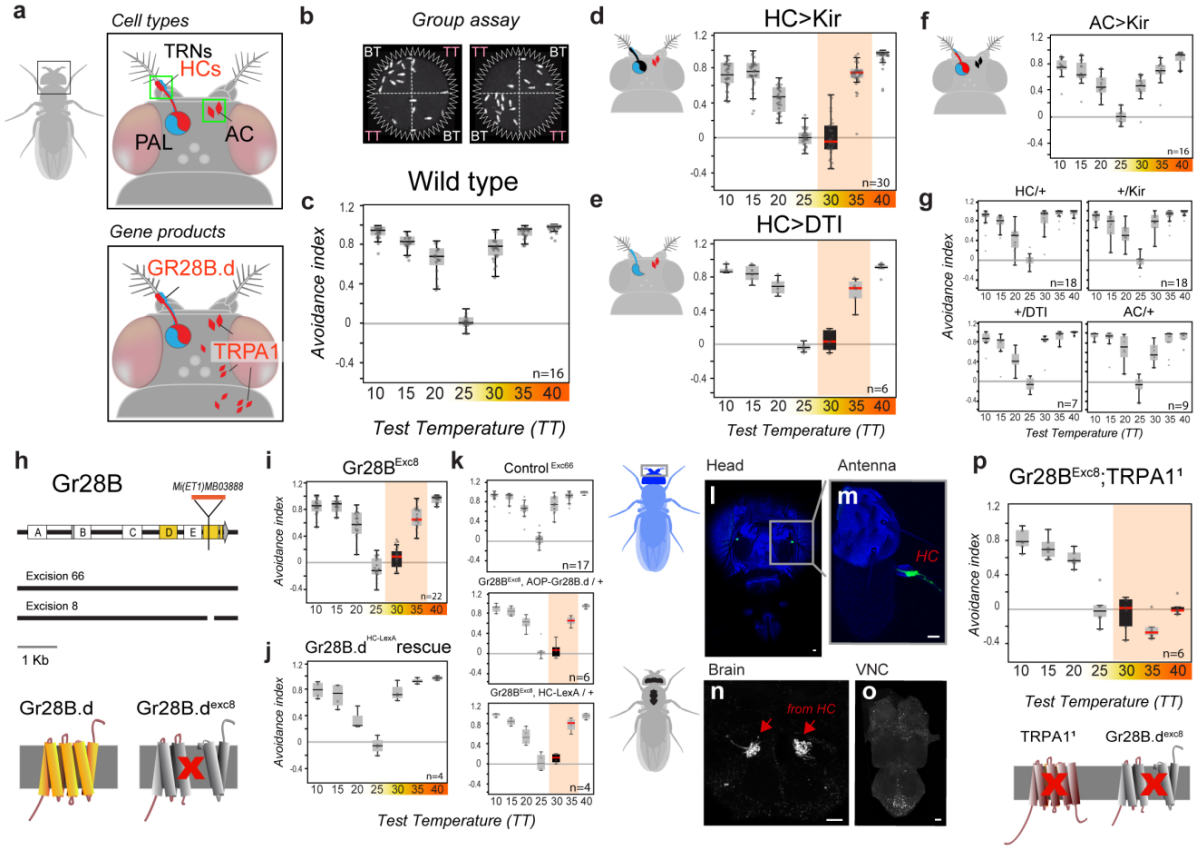

Figure 2.1. Noxious and innocuous heat sensing together mediate heat avoidance in Drosophila. **a.** Schematic representation of the cell types and gene products involved in heat sensing in adult Drosophila (TRNs: temperature receptor neurons, AC: anterior cells, PAL: posterior antennal lobe). **b-c.** Two-choice assay for temperature preference. **b.** Groups of flies are given a choice between a Base Temperature (BT, 25°C) and a variable test temperature (TT; a single video frame is shown). **c.** Temperature preference is quantified as an avoidance index for the various test temperatures (wild type is shown). **d.** Genetic silencing(by expression of Kir2.1, a hyperpolarizing agent) or **e** ablation (by Diphteria toxin, DTI, a cell killing toxin -under the control of HC-Gal4)of hot TRNs of the arista abolishes avoidance of 30°C and reduces avoidance of 35°C. **f.** Genetic silencing of AC (in AC-Gal4>UAS-Kir2.1) has no effect on avoidance. **g.** Control genotypes (drivers and effectors). **h.** Creation of a GR28B null mutant (by Alessia Para). Schematics of the Gr28B genomic locus, Minos insertion, genomic excisions produced for this work and effect of excisions on the predicted protein. **i.** An excision in one of the common exons (Exc8) abolishes avoidance of 30°C and reduces avoidance of 35°C. **j.** Targeting expression of a GR28B.d cDNA to hot activated TRNs (by HC-LexA) completely rescues avoidance defects.

Figure 2.1. **k.** Controls. **l-o.** HC-LexA expression visualized by GFP (in HC-LexA>Aop-GFP animals). **l-m.** Confocal stacks from head/antennae (blue= cuticle autofluorescence, green = GFP expression in Hot TRNs of the arista; scalebars = 20μm). **n-o.** 2-photon stacks of brain and ventral nerve chord (VNC), showing (**n**) hot TRNs axon terminals in the brain, and (**o**) no labeling in the VNC (scalebars, 20μm). **p.** Gr28B^{Exc8} , TRPA1^{1} double mutants display no heat avoidance, but normal cold avoidance. In all boxplots, the edges of the boxes are the first and third quartiles, a solid line marks the median, and whiskers delimit the data range; A solid red median line denotes a significant interaction between experimental and control animals (two way ANOVA, P<0.001), a black box denotes avoidance indexes not significantly different from zero (t test,P <0.05).$P_{HC\text{-}Kir30}$ = 3.78e-12, $P_{HC\text{-}Kir35}$ = 6.74e-4; $P_{HC\text{-}DTI30}$ = 1.73e-7, $P_{HC\text{-}DTI35}$ = 2.74e-5; $P_{HC,AC\text{-}Kir30}$ = 1.39e-11, $P_{HC,AC\text{-}Kir35}$ = 4.67e-6; $P_{Exc8\text{-}30}$ =8.12e-18, $P_{Exc8\text{-}35}$ = 3.8e-7; $P_{Exc8AOP\text{-}30}$ = 5.06e-9; $P_{Exc8AOP\text{-}35}$ = 8.01e-6; $P_{Exc8lexA\text{-}30}$ = 9.59e-8; $P_{Exc8lexA\text{-}35}$ = 6.28e-3; $P_{Exc8Df\text{-}30}$ = 4.22e-12 ,$P_{Exc8Df\text{-}35}$ = 4.14e-6; $P_{GR28TRPA1\text{-}30}$= 2.42e-18, $P_{GR28TRPA1\text{-}35}$ = 1.87e-27, $P_{GR28TRPA1\text{-}40}$ = 1.95e-25, $P_{HC\text{-}Kir30}$ = 0.44; $P_{HC\text{-}DTI30}$ =0.25; $P_{Exc8\text{-}30}$ =0.06; $P_{Exc8Df\text{-}30}$ =0.24; $P_{GR28TRPA1\text{-}30}$ = 0.50, $P_{GR28TRPA1\text{-}40}$ = 0.80. Emanuela Zaharieva and Leah Vinson also helped collect this data. Since analysis of group behavior had been done previously in the lab, an existing MATLAB script was used for tracking and AI calculation (the only analysis script used in this work that I did not write).

of the Gr28B.d protein variant exclusively in arista hot cells (under the control of a selective HC-LexA line, Figure 2.1h-k; and see Figure 2.1l-o for this driver's expression pattern).

Together, these results demonstrate an essential role for the hot-activated TRNs of the arista in the avoidance of innocuous heat and suggest that Gr28B (and Gr28B.d in particular) functions as the main heat receptor for this cell type [**7**].

(2) In the adult, the broadly conserved nociceptor TRPA1 mediates noxious heat responses by sensing H_2O_2/ROS produced as a result of heat damage [**5**]. As such, a prominent effect of TRPA1 loss is a stark reduction of heat avoidance in the noxious range ($\geq$35°C [**5**]). Strikingly, a Gr28B-TRPA1 double-mutant completely eliminated heat avoidance, including to 40°C, a temperature that can be quickly lethal to D. melanogaster (Figure 2.1p).

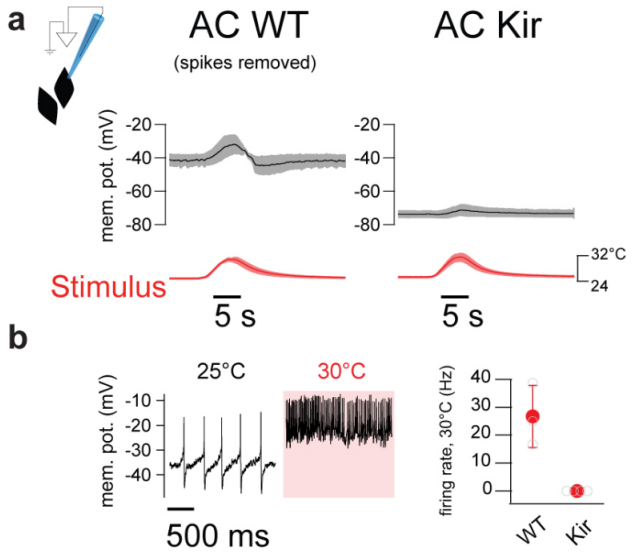

Figure 2.2. Kir2.1 effectively silences AC neurons. Whole-cell current clamp recordings show genetic silencing of AC by Kir2.1 expression is effective. **a.** Filtered membrane potential traces (spikes removed) from wild type AC neurons and from AC expressing Kir2.1. Kir2.1 expression hyperpolarizes AC cells and prevents the response to a ∼5°C hot stimulus (red trace below; traces are average ± SEM from 5 cells/5 repeats per cell). **b.** Representative raw traces (left) recorded from a wild-type AC neuron showing increased firing in response to a temperature stimulus, and (right) quantification of firing rates from unfiltered recordings from wild type and Kir2.1 expressing AC neurons (plot is average ± STD; 5 cells/5 repeats per cell). This recording was performed by Michael Alpert.

We conclude that, while the arista heat-activated TRNs play a dominant role in the avoidance of innocuous heat (<35°C), the response to noxious temperature engages an additional cellular system — distinct from AC neurons, that uses TRPA1 as the main transducer.

It is worth noting that all of the genetic and cellular manipulations affecting heat sensing — even the apparently entirely heat-insensitive Gr28B-TRPA1 double mutants — retained normal temperature preference in the "cold" range (i.e., below the preferred temperature of 25°C, Figure 2.1). In agreement with past studies, this evidence shows that the processing of temperature preference can function quite independently in the hot vs cold range [**11, 67, 68, 69**].

Our results so far demonstrate how both noxious and innocuous signals play a role during rapid heat avoidance, but do not help explain how they may guide the rapid navigational decisions that determine thermotaxis.

2.4. High resolution analysis of heat avoidance

To address this question, we modified our assay by recording with higher spatial and temporal (30Hz) resolution and tracked the trajectories of individual flies as they navigate between the base (25°C) and test temperatures in the two-choice arena (Figure 2.3a — see Appendix for details on fly tracking).

This single-fly assay recorded robust avoidance of both hot and cold temperatures (Figure 2.3b), with avoidance scores comparable to the ones obtained in the group assays. Consistent with the fact that the antennae contain both hot and cold receptors [**11, 70**], bilateral antennae ablation resulted in a complete loss of avoidance for innocuous temperatures both below the preferred 25°C (the "cold" range: 15°C, 20°C) and above it (30°C; Figure 2.3b).

Strikingly, ablation of both antennae did not reduce noxious heat avoidance (Figure 2.3b; 35°C, 40°C, green arrowhead). However, tracking of single flies revealed that control and antenna-ablated flies used significantly different strategies to achieve heat avoidance in the noxious temperature range. Whenever control animals encounter the cool/hot boundary within the arena, they perform sharp turns ("U-turns") and immediately return to the 25°C quadrant. This behavior is frequently observed at the 25°C/30°C boundary (Figure 2.3c, asterisk; —and see Figure 2.3e for quantification), and becomes prevalent at the 25°C/40°C one, such that control flies appear completely confined to the 25°C quadrant as if contained by an invisible border wall.

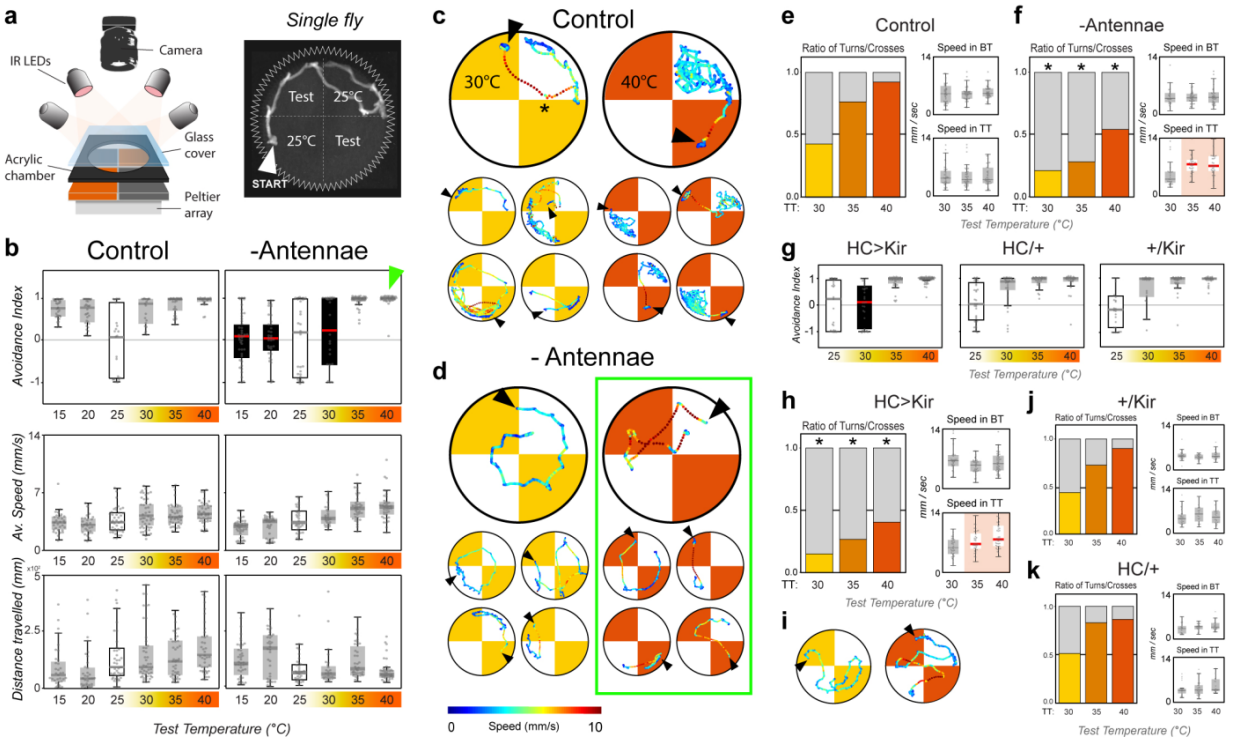

Figure 2.3. Thermosensory neurons of the arista guide rapid navigation during thermotaxis. **a.** Schematic representation of the singly fly 2-choice assay for temperature preference. (Test= test temperature). **b.** Avoidance indexes and locomotory parameters of (left) single wild-type control flies and (right) single flies in which the antennae had been surgically removed at eclosion. (Top row) Avoidance indexes. Antenna ablated flies display no avoidance for test temperatures ranging from 15° to 30°C (a solid red median line denotes a significant difference between experimental and controls, ANOVA, $P<0.001$; a black box denotes avoidance indexes not different from zero, t test, $P<0.05$). (Center and bottom row) Quantification of locomotor parameters shows that antenna ablation does not produce major defects in motility (WT: $N_{15}= 27$, $N_{20}= 26$, $N_{25}=43$, $N_{30}= 55$, $N_{35}= 53$, $N_{40}= 55$, Ablated: $N_{15}= 43$, $N_{20}= 36$, $N_{25}=32$, $N_{30}=26$, $N_{35}= 38$, $N_{40}= 38$). **c,d.** Single representative tracks from control and antenna-ablated flies. **c.** Control flies avoid hot quadrants by producing sharp U-turns at cool/hot boundaries (asterisk; note that in all panels arrowheads denote the position of each fly at the start of heating, and that tracks are color-coded by speed). **d.** Antenna ablated flies fail to systematically produce sharp U-turns and instead frequently invade the hot quadrants. **e-f.** Quantification of the ratio of U-turns/border crosses at the cool/hot boundaries and associated locomotor parameters. **e.** In control flies the ratio of U-turns/border crosses increases as a function of the temperature on the hot side, until (for test temperature =40°C) most border interactions result in U-turns.

Figure 2.3. **f.** Antenna-ablated flies display significantly smaller fractions of U-turns at the border in all conditions, but instead display a higher speed for traversals of the 35°C and 40°C hot quadrants (highlighted in the lower right panel in **f**, BT=base temperature, TT=test temperature). **g-i.** Genetic silencing of hot-activated TRNs of the arista results in phenotypes in the hot range very similar to antenna ablation (HC/Kir: N_{25} = 29, N_{30} =33 , N_{35} =36 , N_{40} =46 , HC/+: N_{25} =27, N_{30} = 22, N_{35} =29 , N_{40} =26 , Kir/+: N_{25} = 35, N_{30} =32 , N_{35} =26 , N_{40} =26). **j,k.** Control genotypes (drivers and effectors). In all boxplots, the edges of the boxes are the first and third quartiles, a solid line marks the median, and whiskers delimit the data range; In **e-k**, a solid red median line denotes a significant interaction between experimental and control animals (ANOVA, P<0.001), a black box denotes avoidance indexes not significantly different from zero (t test, P<0.05). Asterisks in **f** and **h** denote significant differences in turn/cross ratios from the appropriate controls (GLMM, Wald test, P<0.05). (ANOVA: P_{15} = 1.1e-7, P_{20} = 3.7e-6, P_{30} = 2.3e-2). (GLMM, Wald test: vs Control P_{30} = 3.3e-2, P_{35} = 6.4e-11, P_{40} = 6.5e-6), (ANOVA, P_{35} = 2.1e-5, P_{40} = 5.1e-6). (2-way ANOVA: P_{30} = 1.3e-3) (2-Way GLMM, Wald Test: P_{30} = 2.3e-3, P_{35} = 1.6e-6, P_{40} = 3.0e-2), (2-way ANOVA, P_{35} = 3.6e-2, P_{40} = 1.2e-3, see controls **h-k**)

Antenna-ablated flies appear unable to efficiently produce such U-turns, and instead often invade the hot quadrants (Figure 2.3d,f). Interestingly, while this failure to turn away appears to have little consequence in the 25°C/30°C condition (resulting in no avoidance for 30°C), invasion of the 35°C or 40°C quadrants produces faster movement (Figure 2.3d,f), which ultimately results in escape from heat and in an overall high avoidance index for the noxious temperatures (Figure 2.3b).

Remarkably, the differential effect on the avoidance of 30°C vs 35°C and 40°C in antenna-ablated is reminiscent of what was observed when silencing heat-activated TRNs of the arista (see Figure 2.1). Indeed, when subjected to this single-fly assay, animals in which heat-activated TRNs had been genetically silenced displayed a remarkably similar phenotype to that of antenna-ablated flies: no avoidance for 30°C but high avoidance for 35°C and 40°C, and a reduced fraction of U-turns at the 25°C/hot borders accompanied by increased speed in the hot quadrants (Figure 2.3h,i, see Figure 2.3j,k for controls).

Taken together, our results suggest that the heat-activated TRNs of the arista play a key role in the avoidance of both noxious and innocuous heat by allowing flies to produce sharp turns away from hot boundaries to efficiently escape both aversive and dangerous conditions. In the absence of the antennae (or when signaling from the heat-activated TRNs is impaired), flies are unable to effectively produce U-turns away from heat. However, while they appear indifferent to innocuous conditions (30°C), they still react to noxious heat by increasing their speed. The fact that this increase in speed does not require the antenna (Figure 2.3), together with our results on Gr28B-TRPA1 double mutants (which appear completely insensitive to both noxious and innocuous heat, Figure 2.1) suggest that this effect is likely mediated by TRPA1-expressing nociceptors in the fly head and/or body. Hence, heat-activated TRNs of the arista are essential to control the thermotactic responses that allow flies to efficiently steer away from aversive and potentially dangerous heat. But how are the signals from TRNs used to chart a trajectory that quickly puts the fly out of harm's way? To address this question, we next reconstructed the profile of the temperature gradient that flies encounter when crossing the border between cool (25°C) and hot quadrants.

2.5. Analysis and modeling of behavioral arena

First, we used a thermal imaging system equipped with a macro lens to ensure that the border between 25°C and hot floor tiles was reasonably sharp and homogeneous (Figure 2.4a,b). Taking into consideration the physical dimensions of the chamber, the thermal conductivity of air, the heat transfer coefficient of the materials used, and the potential impact of convection (see methods for details), we produced a realistic, high-resolution, 3-dimensional simulation of temperature distribution within the arena in the various experimental conditions (Figure 2.4c,d and Figure 2.5).

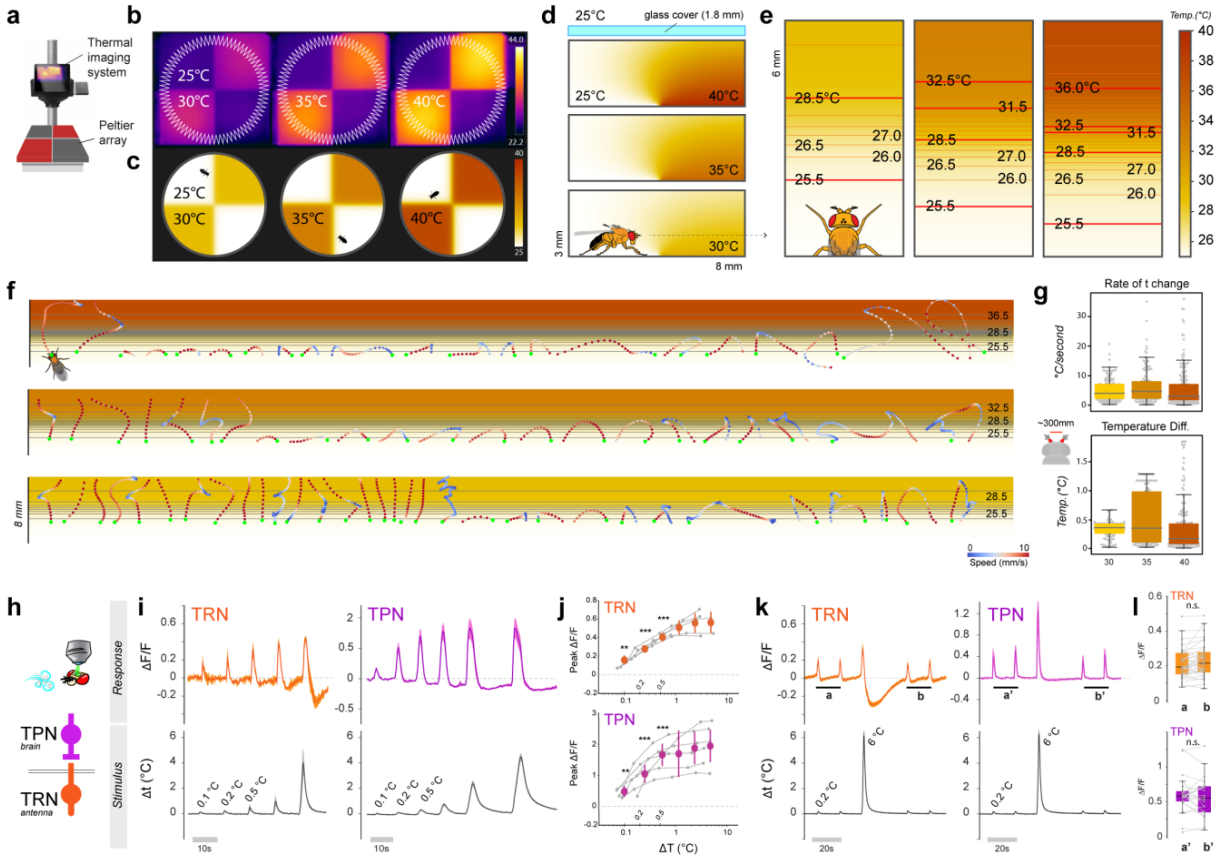

Figure 2.4. A 3-dimensional simulation of the thermal environment reveals small temperature differences are salient stimuli. **a.** Schematic representation of the thermal imaging system. **b.** Thermal images of the arena in the three experimental conditions, and **c**, at the same scale, thermal conditions predicted by the simulation (see scale bars for temperature). **d.** Side view of a 3x8mmsection of the experimental chamber, centered on the interface between floor tiles set at 25° /30° , 25° /35° and 25° /40°C, respectively, and showing the predicted thermal conditions (note that the glass cover on top is not to scale). **e.** Top view of the simulated thermal gradients the fly encounters at the cool/hot boundary, produced by slicing the 3D model at the height of the antennae ($\sim 700 \mu m$; note that the 3 panels are not aligned; scalebar: temperature in °C). **f.** Representative fly trajectories overlaid atop the gradients in **e**. Tracks are color-coded by translational speed (see scalebar). Each dot represents the position of the fly head (acquired at 30Hz). A green dot indicates the fly head position upon entry in the boundary region. **g.** Maximum rate of temperature change (top) and maximum inter-antennal temperature difference (bottom) experienced by flies traversing the border in the 3 experimental conditions. **h.** Schematic representation of the 2-photon calcium imaging setup and of the cell types targeted for recording (temperature receptor neurons, TRN and second-order projection neurons, TPN).

Figure 2.4. **i.** Average stimuli (bottom) and response traces (top) recorded from TRN axon terminals (orange trace, left) and TPN (purple trace, right) each separately targeted by transgenic expression of G-CaMP7f (traces represent average ±STD of N_{TRN} =5, N_{TPN} =6 from 6 flies). **j.** Orange and purple dots,peak fluorescence averages from data in **i**, ± STD (bin width starting at 0.1°C and doubling in size for each consecutive bin; asterisk= significantly different from zero, t test, P<0.05; t-test TRN: $P_{0.1}$ = 3.5e-3, $P_{0.2}$ = 1.5e-6, $P_{0.5}$ = 4.1e-4; TPN: $P_{0.1}$ = 2.1e-3, $P_{0.2}$ =1.5e-4, $P_{0.5}$ =9.0e-5). **k,l.** Exposure to a larger heat stimulus does not lead to sensitization to smaller stimuli. **k.** Average stimuli (bottom) and responses (top) ± STD. **l.** Average peak signal recorded before (a,a') and after (b,b') a 6°C stimulus are not different (n.s.= not significant; paired T-tests;**k** and **l** are from N_{TRN} =18, N_{TPN} =12 from 7 and 6 animals, respectively; note that the twin peaks in a, a', b and b' are considered independently in **l**).

To better understand the thermal landscape experienced by the fly as it navigates within the arena, we developed a detailed simulation of the temperature conditions within the chamber, based on the thermal properties of air (and of the chamber's materials) and well-established fluid dynamics and heat transfer principles [**71**]. Our simulation used the Boussinesq approximation for the Navier Stokes equations, which were nondimensionalized to the form:

$$\frac{\partial \mathbf{u}}{\partial t} + \mathbf{u} \cdot \nabla \mathbf{u} = -\nabla P + \sqrt{\frac{Pr}{Ra}} \nabla^2 \mathbf{u} + \hat{k} T \tag{2.1}$$

$$\nabla \cdot \mathbf{u} = 0 \tag{2.2}$$

$$\frac{\partial T}{\partial t} + \mathbf{u} \cdot \nabla T = \frac{1}{\sqrt{PrRa}} \nabla^2 T \tag{2.3}$$

where **u**, P, and T nondimensionalized velocity, pressure, and temperature. Pr and Ra are the well known Prandtl and Rayleigh numbers, respectively, and $\hat{k}$ is the vertical unit vector. No-slip boundary conditions (i.e., $u = 0$) were used for the walls of the cavity, and the sides were treated as insulating. We used Dirichlet boundary conditions for the Peltier plates

lining the bottom of the chamber:

$$T|_{\text{cold plate}} = -0.5, \quad T|_{\text{hot plate}} = 0.5 \tag{2.4}$$

and the Robin condition for the glass barrier that encloses the chamber at the top:

$$\frac{\partial T}{\partial n} = -\lambda(T - T_0) \tag{2.5}$$

where $T_0 = -0.5$ and λ is a dimensionless coefficient often referred to as the Biot number. The problem was solved numerically using a Chorin projection scheme [**72**] written using the FEniCS finite element package in Python [**73**] (here, we treated inertial terms explicitly and the viscous terms semi-implicitly using a Crank-Nicolson approach [**74**]). Finite elements in the velocity and and pressure meshes were implemented using a Taylor-Hood scheme, with quadratic elements for velocity and linear elements for pressure [**75**]. The temperature mesh was also implemented using linear elements. For the velocity, pressure, and temperature components, we denote the test functions as v, Q, and τ, respectively.

Each iteration of the Chorin "fractional" step scheme begins with the calculation of a predicted fluid velocity, $\tilde{u}$,

$$\begin{aligned}\int_\Omega \frac{\tilde{u} - u_n}{\Delta t} v dx + \int_\Omega (u_n \cdot \nabla u_n) v dx + \int_\Omega \sqrt{\frac{Pr}{Ra}} \frac{\nabla(\tilde{u} + u_n)}{2} \cdot \nabla v dx = \\ \int_{\partial\Omega} \sqrt{\frac{Pr}{Ra}} \frac{(\nabla(\tilde{u} + u_n)}{2} \cdot n) v ds + \int_\Omega \hat{k} T_n v dx.\end{aligned} \tag{2.6}$$

Next, a pressure update is calculated using

$$\int_\Omega \nabla P \cdot \nabla Q dx = -\int_\Omega \frac{1}{\Delta t} (\nabla \cdot \tilde{u}) Q dx, \tag{2.7}$$

Followed by a correction step to get the velocity u

$$\int_\Omega u \cdot v dx = -\Delta t \int_\Omega \nabla P \cdot v dx + \int_\Omega \tilde{u} \cdot v dx. \tag{2.8}$$

Finally, we perform a temperature step to solve for T

$$\begin{aligned} &\int_\Omega \frac{T - T_n}{\Delta t} \tau dx + \int_\Omega \Big[u \cdot \nabla \Big(\frac{3T_n - T_{n-1}}{2} \Big) \Big] \tau dx = \\ &-\frac{1}{\sqrt{PrRa}} \int_\Omega \nabla\theta \cdot \nabla\tau dx - \frac{1}{\sqrt{PrRa}} \int_{\Gamma_{top}} \kappa(\theta + 0.5)\tau ds, \end{aligned} \tag{2.9}$$

and then iterate this procedure to advance the simulation in time. The method was benchmarked as in Christon, Gresho and Sutton [**76**]. As an additional test, we performed direct temperature measurements (using a thermocouple, Physitemp) above both the hot and cool side of the arena, and at both sides of the glass cover in all experimental conditions; the measured temperature matched simulations predictions within ± 0.1°C data not shown).

We note that, as predicted, our simulations show a small convective cell ($\sim$1 mm wide) centered at the interface between the cool and hot floor plates (Figure 2.5). This cell is expected to cause a very localized horizontal air flow at the interface boundary between tiles, with a local maximum flow velocity of $\sim$1 mm/s over $\sim$1 mm. The fly's average walking speed in this region is significantly higher ($\sim$5 mm/sec, max 10 mm/sec) and therefore this air flow is unlikely to independently influence behavior in the boundary region (see also [**77**]). Given the small spatial scales involved the heat transfer process equilibrated very rapidly ($\sim$0.5 seconds), hence our further analysis considers steady-state temperature profiles.

Note that, for this work, we do not account for potential delays produced by the diffusion of hot/cold stimuli from the external environment to the temperature receptors within the

arista. To understand the impact of this approximation, we determined the time for temperature to diffuse to the hot cells taking into consideration the known thermal properties of chitin [**78**]. Since the base of the arista is covered in an approximately $2\mu m$ layer of chitin [**79**], the average diffusion time across this boundary layer is likely negligible:

$$t_d = \frac{L^2}{\alpha} = \frac{(2 \times 10^{-6} m)^2}{1 \times 10^{-7} m^2/s} \approx 4 \times 10^{-5} s \tag{2.10}$$

(where α is the thermal diffusivity of chitin).

Next, we "sliced" this 3D volume at the height of the fly antenna ($\sim 700\mu m$) and produced 2-dimensional models representing the steep thermal gradient that is expected to form at the border between 25°C and hot floor tiles (Figure 2.4e). Finally, we overlaid the dynamic trajectories that flies performed in our assays as a result of encounters with the border (Figure 2.4f), and derived the temperature values at each antenna at any given time-point during a border interaction (i.e., based on a simple rigid model of the fly body, in which the antennae protrude from the head and are separated by $300\mu m$).

We also tested the potential impact of a different estimate of the height of the antennae on our 2-dimensional temperature models (Figure 2.4e). We find that key temperature gradient parameters are rather similar for a wide range of antennal heights ($\sim$500-900μm , Figure 2.5). Here, we use an antenna height of 700 μm (consistent with our in-house measurements from pictures of standing flies).

Our simulation reveals a number of interesting features of the sensory landscape the fly encounters at the quadrant border. As flies can move quite rapidly across the border region ($\sim$cm/sec), they are expected to experience a significant rate of temperature change, with many interactions in the $\sim$1 to 10 degrees per second range (Figure 2.4g). In addition,

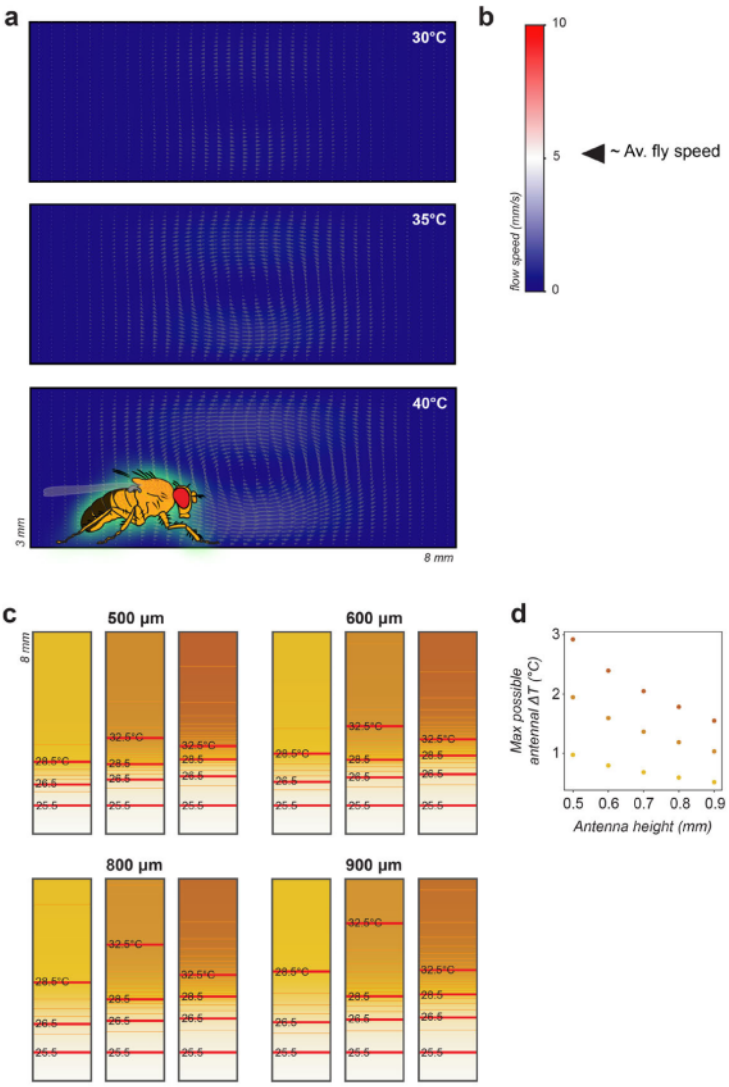

Figure 2.5. 3D simulation of the thermal environment: impact of convection and sensitivity of 2D models to height. **a.** A simulation of the thermal conditions inside the arena predicts a small convective cell centered at the interface between the cool and hot floor plates. This cell is expected to cause a localized horizontal air flow (represented by arrows) above the interface boundary between cool and hot tiles. Flow velocity is represented by color (see scale bar in **b**; note that the arrow length in a is also proportional to flow velocity). The fly's average walking speed in this region is ∼5 mm/sec (max ∼10 mm/sec), and is also indicated on the scale bar in **b** for comparison. Because of the limited localization and speed of this air flow, we considered it unlikely to independently influence behavior in the boundary region.

Figure 2.5. **c.** Predicted thermal gradient at different heights relative to the chamber floor (e.g., for different estimates of the height of the antennae). **d.** Maximum possible temperature differential between the antennae given the parameters in c (colors represents experimental conditions, yellow =25°C vs 30°C, orange =25°C vs 35°C, brown =25°C vs 40°C).

considering the spatial separation of the antennae (and accounting for the steep gradient that our simulation predicts at the border region), the temperature at the aristae at any given point often differs by nearly 1°C (Figure 2.4g; note that, because of their tiny mass and the good thermal conductivity of chitin [**80**], the aristae are expected to match the external temperature nearly instantaneously — see methods for a simple calculation illustrating this point).

2.6. The role of the innocuous thermosensors in steering

Do flies use differential temperature readings from the antennae to chart the trajectory of U-turns away from heat? Many larger animals (e.g., owls [**81**], rodents [**82**], humans [**83**], etc.) are well-known to use readings from bilaterally symmetrical sensory organs to orient in the environment, and both fly larvae and adult flies can use left-right asymmetries in the activity of olfactory neurons to orient towards an odor source [**84, 85, 86**].

Whether similar mechanisms are used during thermotaxis is not known. Our simulation now makes it possible to address this question in highly controlled experiments in Drosophila, despite the small spatial scales involved. We set out to address the following questions: (1) can the thermosensory neurons of the antenna reliably detect the small temperature differences (0.1-1°C) that would determine the direction of U-turns at hot/cool thermal boundaries? And is this information transmitted to upstream circuits within the brain? (2) Do asymmetries in the thermal stimuli at each antenna correlate with the left/right orientation

of U-turns? And can experimental manipulation in the symmetry of TRN activation result in predictable left/right-turn bias?

To test the limits of sensitivity of the antennal TRNs, we utilized a preparation that allows one to challenge the antennae with highly controlled thermal stimuli [**11**], designed to be as similar as possible to what the fly would encounter leading up to a U-turn at the border (see Figure 2.6 for a direct comparison). At the same time, we measured responses in the axon terminals of antennal hot TRNs using Calcium imaging and 2-photon microscopy (i.e., by targeted expression of the transgenic Calcium indicator G-CaMP7f [**87**], Figure 2.4h-l).

Our observations suggest that, indeed, hot-activated TRNs of the arista can reliably respond to temperature stimuli as small as 0.1°C (Figure 2.4i,j). Moreover, imaging second-order thermosensory projection neurons (TPNs, by expressing G-CaMP under the control of VT46265 [**15**]) demonstrated that these cells are also reliably activated by such stimuli (Figure 2.4i,j). This result shows that the response to small thermal stimuli is faithfully transmitted across the first central synapse to drive activity in central thermosensory circuits. Interestingly, in this range (ΔT $<\sim$5°C), the responses to thermal stimuli scaled with the magnitude of the stimulus for both TRNs and TPNs, and showed no sensitization following exposure to a larger stimulus (Figure 2.4k-l; note that we will return to this point further below).

Next, we tested the idea that flies may use the differential activation of antennal TRNs to chart an effective trajectory away from heat. In the simplest scenario, a fly approaching the hot/cool boundary head-on is expected to experience minimal differential activation of the antennae and is therefore likely to turn either left or right with equal probability. In contrast, a fly approaching the boundary from the left (i.e., forming an acute angle of approach with

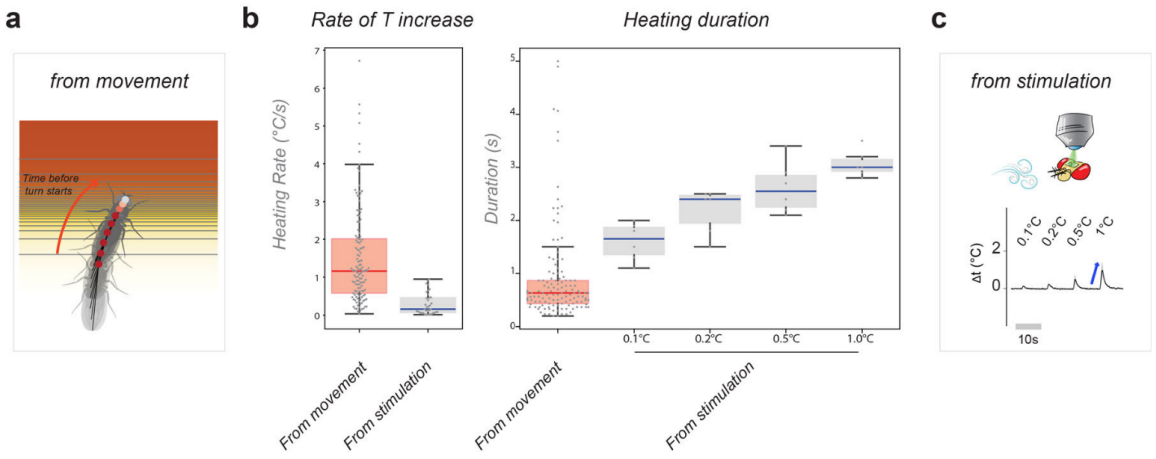

Figure 2.6. Comparison of stimulus parameters in 2-choice experiment and 2-photon imaging. **a.** Diagram of fly moving through the thermal gradient -magnitude and duration of heating were estimated from the point of entry into the gradient to the starting point of a turn (see methods for details). **b.** Heating rate and duration experienced by flies leading up to a turn (red boxes, $N_{movement} = 129$ from 28 flies) shown for comparison next to the stimuli used during 2-photon microscopy experiments (grey boxes, $N_{stim} = 36$ from 6 animals). **c.** Representation of a typical 2-photon microscopy experiment -rate and duration of heating were measured from baseline to peak temperature (blue arrow). In all boxplots, the edges of the boxes are the first and third quartiles, a solid line marks the median, and whiskers delimit the data range.

the boundary) would experience greater heat activation of the left antenna, and therefore may be more likely to turn right to escape the heat (Figure 2.7a).

Our data suggest that, when considering the first turning maneuver a fly performs at the hot/cool boundary, this prediction indeed bears true: flies approaching the boundary head-on turn equally likely to the left or right; flies approaching from the left overwhelmingly turn right to escape the heat, and flies approaching from the right overwhelmingly turn left (Figure 2.7b). Interestingly, an estimate of the temperature difference between antennae during those first turns (based on the simulation described above) suggests that temperature differentials as small as 0.1-0.2°C are sufficient to predict turn direction (Figure 2.7c).

To further test the idea that asymmetric activation of the antennae may determine turn direction, we ran our assays on flies from which either the right or left antenna had been surgically removed. Removal of the left antenna produced flies that, when approaching the hot/cool boundary, overwhelmingly turned left to escape — irrespective of the direction of approach.

Conversely, removal of the right antenna produced flies that, when approaching the hot/cool boundary, overwhelmingly turned right (Figure 2.7d,f). Importantly, left/right turn probability was not biased in these animals at constant 25°C (Figure 2.8). Together, these results suggest that flies may interpret lack of input from the lesion side to indicate cooler conditions, and chart their escape turns towards the lesion side accordingly. As an additional control, removal of both antennae completely abolished left/right turning bias producing flies that turned either left or right with comparable frequency, no matter the angle of approach (Figure 2.7c, but note that antenna-less flies perform U-turns much less frequently and — as a result — are more likely to invade the hot quadrants, see Figure 2.3).

Next, we tested the extent to which the hot receptors of the arista may contribute to this left-right turn signal. We engineered flies in which transient activation of a FLP recombinase (i.e., under the control of a heat shock promoter [**88**]) leads to stochastic but permanent loss of the Gal4 inhibitor Gal80 in embryonic precursor cells that will eventually contribute to the adult body. In our set-up, clonal loss of Gal80 results both in genetic silencing (by expression of Kir2.1) and fluorescent labeling (by GFP) of cells that also express HC-Gal4 (i.e., hot TRNs of the arista). Because of early induction of the clones, the Gal80+ and Gal80- territories represent large areas of the body of mosaic animals, including flies in which TRNs are silenced in the left but not in the right antenna (Figure 2.7g).

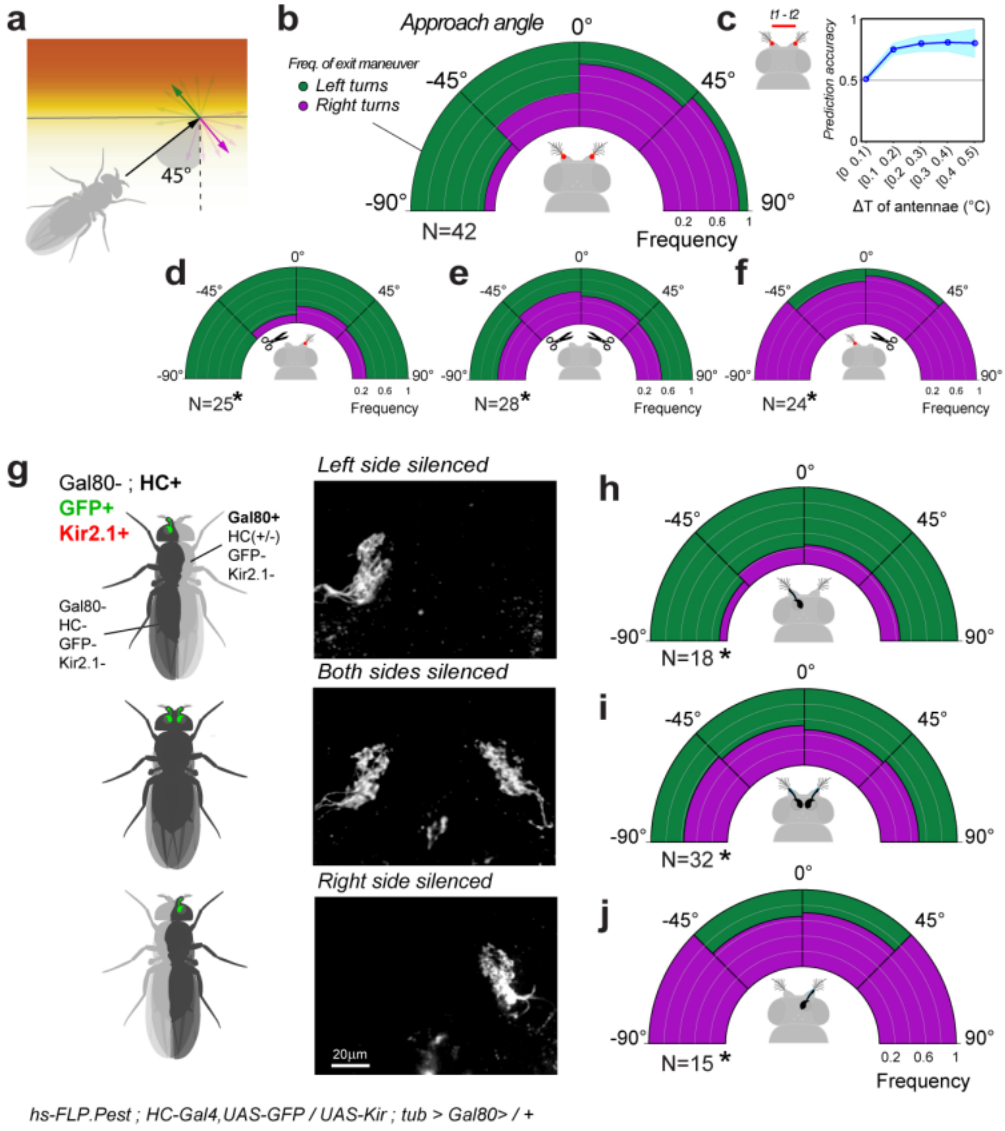

Figure 2.7. Differences in antennal input determine the direction of escape turns during thermotaxis. **a-c.** For border interactions, the angle of heading is predictive of the angle of escape. **a.** Schematic of the analysis. The heading angle is quantified in relation to the isothermal lines of the cool/hot boundary while the escape turn is categorized as "left" (green) or "right" (purple). **b.** Distribution of left/right escape turns (binned in 45° intervals) as a function of initial heading angle. **c.** Inter-antennal differences >0.1°C are predictive of escape turn direction.

Figure 2.7. **d-f.** Surgical removal of the left (**d**) or right (**f**) antenna biases escape turn direction towards the side of the lesion (GLMM, Wald Test, P_{left} = 6.3e-5, P_{right} =9.3e-4), while removal of both antennae (**e**) abolishes left/right bias (GLMM, Wald Test, P_{both} = 2.1e-4). **g.** Stochastic loss of the Gal4 inhibitor Gal80 produces flies in which either the left or right hot TRNs of the arista are genetically silenced and, at the same time, labeled by GFP expression (representative 2-photon stacks of TRN axon terminals are shown to the right). **h-j.** Stochastic silencing of either left or right hot TRNs (or both), produces a distribution of turning angles similar to that obtained from surgical ablation (**i** is the control genotype with bi-lateral silencing, see corresponding panel in **g**) (In all panels N denotes the number of animals, GLMM, Wald test, P_{left} = 9.0e-6,P_{right} = 2.1e-2; P_{both} = 2.5e-5). Note that mosaicism was determined by post-facto dissection and imaging. Peixiong Zhao assisted in the engineering of mosaic flies.

For this experiment, we ran ∼200 putative mosaic flies in our behavioral assay, and selected 33 asymmetrically silenced individuals for analysis by post-facto dissection and imaging (Figure 2.7g-h,j). As a control, we used flies that did not express Gal80, and in which therefore hot TRNs of both antennae had been silenced (Figure 2.7g,i). The results of asymmetric silencing of hot TRNs (Figure 2.7h,j) line up remarkably well with those obtained by surgical removal of either the left or right antenna. Silencing the hot TRNs of the left antenna produced flies that overwhelmingly turned left to escape the heat, while silencing the hot TRNs of the right antenna produced flies that escaped to the right (Figure 2.7h,j; and see Figure 2.8 for additional controls). Together, these results demonstrate that creating an artificial asymmetry in the input from hot TRNs of the arista is sufficient to predictably bias turn direction at the hot/cool boundaries towards the silenced or ablated side.

2.7. A vehicle model of *Drosophila* sensorimotor transformation

Our results so far suggest that, upon encountering a hot/cool boundary, the fly uses differential information from the antennae to compute an efficient turn trajectory away

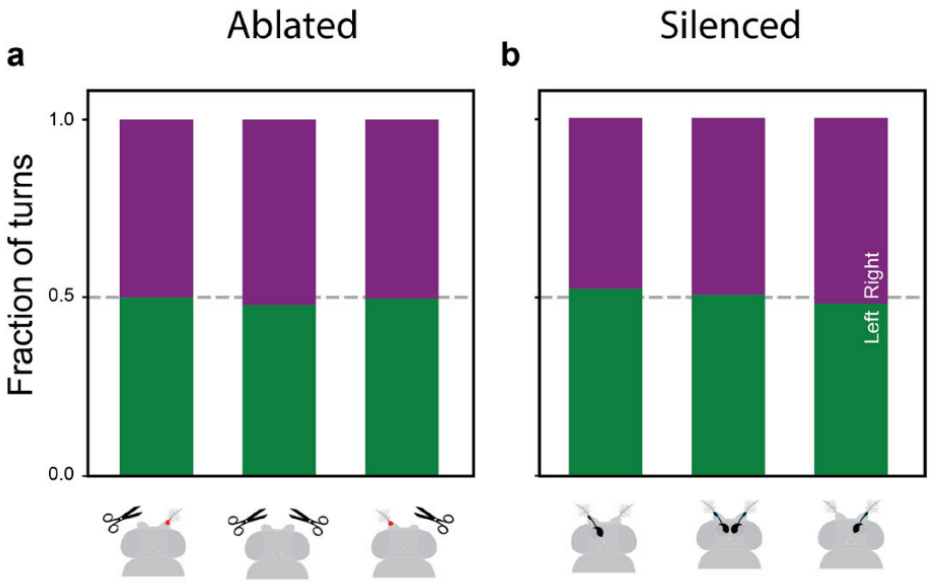

Figure 2.8. Ablation of the antennae does not bias turning direction at 25°C. **a.** Physical ablation of the right antenna, both antennae, or of the left antenna does not bias turning direction at 25°C ($N_{Lablated} = 32$, $N_{L+Rablated} = 38$, $N_{Rablated} = 27$). **b.** Similar results are obtained for genetic silencing of hot receptor neurons (by HC>Kir2.1; see Figure 2.4, $N_{Lsilenced} = 33$, $N_{L+Rsilenced} = 36$, $N_{Rsilenced} = 23$). Plots show ratio of left/right turns at 25°C.

from heat. This is reminiscent of the behavior of a "Braitenberg Vehicle" [**23**], one of the simplest theoretical models of sensorimotor transformation, in which differential activity at two symmetrical detectors produces turns away from the source of a stimulus by controlling the speed of two symmetrical motors.

To what extent can the fly's turning responses be explained by that of a simple "Braitenberg Vehicle" hard wired for aversion? We reasoned that comparing the behavior of the fly to that of a simple vehicle model may reveal indications of plasticity and/or decision making that are not immediately obvious from analyzing fly behavior alone.

Towards this goal, we created an in silico vehicle scaled to the physical dimensions of the fly (e.g. with the same height and distance between the antennae, antennae and legs/motors,

etc.) and used an evolutionary algorithm to optimize eight free parameters (Figure 2.9a-c, Figure 2.10a,b and see methods for details), selecting at each generation vehicles that, when tested in the simulated chamber, best matched the fly's behavior in 4 key areas: probability of "spontaneous" turns at 25°C; avoidance index for the 3 challenge temperatures; fraction of U-turns/crosses at the border between 25° and 30° , 35° and 40°C, and sensitivity to left/right temperature differences between the antennae (i.e., by matching the probability of a left/right turn given antennal temperature difference at turn start, see Figure 2.7c). Amongst the free parameters that determine vehicle responses, two were used to define a simple sensory transformation, and two parameters specified the amplitude and time constant for each independent noise function (on sensor and motor output); we also added independent weights to the ipsi-lateral and contra-lateral sensor-to-motor connections (Figure 2.9a, and see methods for details).

2.7.1. Mathematical formulation of vehicles

We used an evolutionary algorithm to develop a "Braitenberg" vehicle-inspired model [**23**] that could reproduce fly navigational responses in our arena. The vehicle model is intended to "navigate" a realistic virtual arena, with a thermal landscape derived from our simulation (described above), and was therefore developed to be consistent with the physical dimensions of a real fly.

We considered a 2-wheeled description of movement dynamics of the form:

$$\begin{bmatrix} x' \\ y' \\ \theta' \end{bmatrix} = \begin{bmatrix} \frac{1}{2}(v_L + v_R)\cos(\theta) \\ \frac{1}{2}(v_L + v_R)\sin(\theta) \\ \frac{1}{d}(v_R - v_L) \end{bmatrix} \tag{2.11}$$

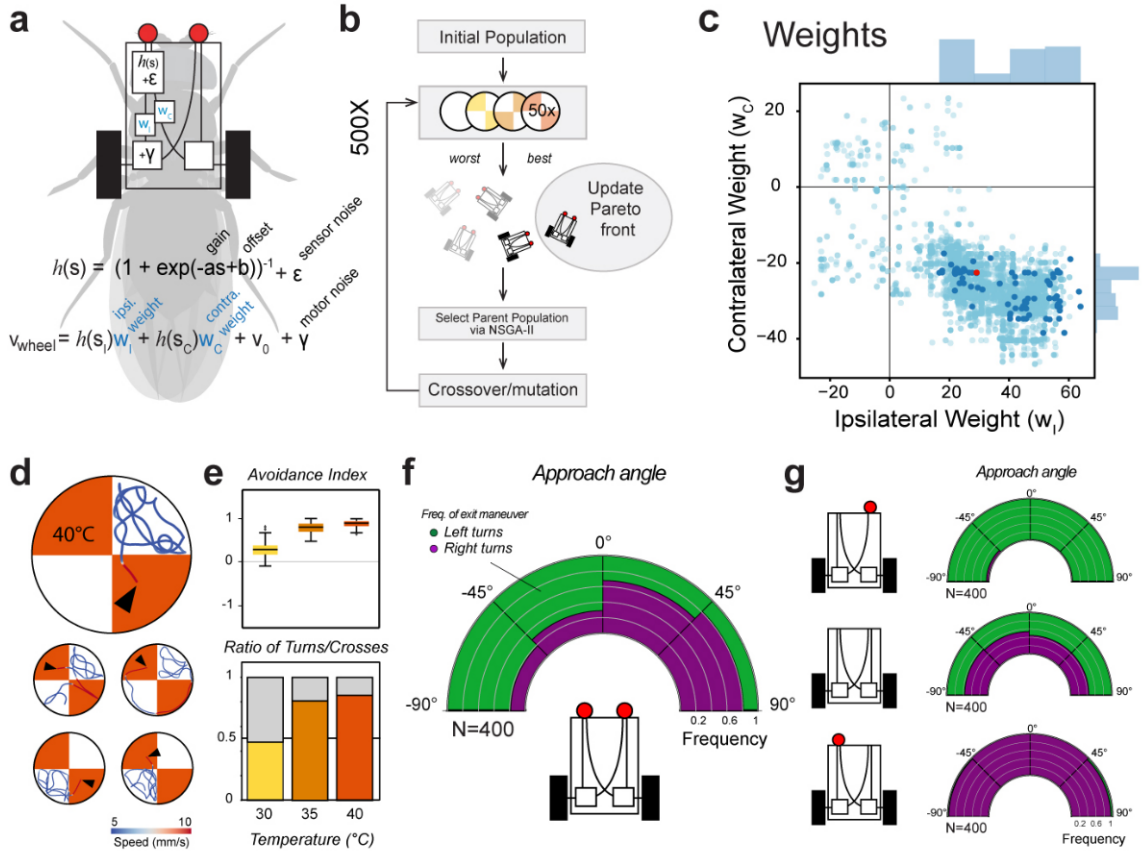

Figure 2.9. An evolved "Braitenberg vehicle" nearly reproduces fly thermotaxis. **a.** An in silico "Braitenberg vehicle" model matching the dimensions of a fly, with key parameters used as substrate for evolution (s = sensory input, v=velocity; parameters: a=gain, b=offset ϵ, γ = noise (2 evolved parameters each, see methods), w_1, w_2 = weights of ipsi-and contra-lateral connections). **b.** Schematic of the evolutionary process used to optimize the parameters. **c.** Connectivity weights (W_c = contralateral, W_I = ipsilateral). Note that the best performing vehicles preserve both ipsi- and contra-lateral connectivity, and that ipsilateral weights are exclusively positive (excitatory) while contralateral weights are exclusively negative(inhibitory). **d-f.** An evolved vehicle nearly reproduces fly thermotactic behavior in a simulated arena. **d.** Traces from a top-performing vehicle in the simulated arena (see Figure 2.10 and methods for details; arrowhead = start). **e,f.** Vehicle performance in the simulated chamber (N=400 simulations). **g.** Vehicle responses are not robust to perturbation. "Ablation" of a single sensor produces vehicles that, entering the cool/hot boundary, invariably turn to the side of the lesion, irrespective of the direction of approach (mid-panel: as a control, removal of both sensors abolishes directional responses; N=400 simulations each).

Where x and y are the positions of the centroid and θ is the orientation. The wheels are independently driven, but fixed in their orientation relative to the body axis of the vehicle. Here, v_L and v_R are the velocities of the left and right motor, respectively, while d is the distance between the two wheels (set to 750 μm, reasonably close to a fly's width). The speed of the motors is controlled by two symmetrical sensors, with positions:

$$(x_{LA}, y_{LA}) = (x + \frac{BL}{2}\cos(\theta) - \frac{AD}{2}\sin(\theta), y + \frac{BL}{2}\sin(\theta) + \frac{AD}{2}\cos(\theta)) \tag{2.12}$$

$$(x_{RA}, y_{RA}) = (x + \frac{BL}{2}\cos(\theta) + \frac{AD}{2}\sin(\theta), y + \frac{BL}{2}\sin(\theta) - \frac{AD}{2}\cos(\theta)) \tag{2.13}$$

where BL (body length) = 3mm and AD (antennal distance) = 300μm (so that the sensors are located 300 μm apart at the front of the vehicle, and the motors 1.5 mm along the body axis separated by d). The base velocity v_0 was set to 5mm/sec. BL, AD, sensor position and d were chosen to be reasonably close to a fly's.

The sensory input used in the model derives from our temperature simulation of the behavioral arena (described above) and is additively modulated with time correlated noise generated by an Ornstein-Uhlenbeck model:

$$\tau_s d\epsilon = -\epsilon dt + \sigma_s dW \tag{2.14}$$

where τ_s is a time constant for the process, σ_s is a parameter that defines amplitude of the noise, dW denotes the Wiener process. Temporal integration of the differential equation was performed using the Euler-Maruyama method. Effective sensory input is given as

$$s_L = s_{L0} + \epsilon_L \tag{2.15}$$

$$s_R = s_{R0} + \epsilon_R \tag{2.16}$$

where s_{L0}, s_{R0} are the temperatures at the left and right sensor, respectively, and ϵ_L, ϵ_R are the noise values at each sensor (note that noise is not correlated between L and R sensors). Another Ornstein-Uhlenbeck process was used to describe motor noise γ

$$\tau_m d\gamma = -\gamma dt + \sigma_m dW \tag{2.17}$$

where τ_m is a time constant for the motor noise process, and σ_m is a parameter that defines amplitude of the noise. The velocities of the wheels are linear combinations of sensory input (s_L, s_R) processed through a logistic nonlinearity $h(s)$ at the two symmetric sensors and additively combined with the motor noise γ:

$$v_L = f_L(s_L, s_R) = h(s_L)w_{L,L} + h(s_R)w_{L,R} + v_0 + \gamma \tag{2.18}$$

$$v_R = f_R(s_L, s_R) = h(s_L)w_{R,L} + h(s_R)w_{R,R} + v_0 - \gamma. \tag{2.19}$$

Note that the effect of the motor noise is anti-correlated for L and R wheel speeds in order to impact turning bias without altering overall speed. The weights:

$$W = \begin{bmatrix} w_{L,L} & w_{L,R} \\ w_{R,L} & w_{R,R} \end{bmatrix} \tag{2.20}$$

relay the transformation of sensory input into left and right wheel speeds (note that the vehicle wiring is symmetric, as W is symmetric and $W_{L,L} = W_{R,R}$). $h(s)$ is a transformation of the sensory input defined by the logistic function $h(s) = \frac{1}{1+\exp(-as+b)}$. To prevent the vehicle from getting stuck on the external border wall of the simulated chamber we specified

that, upon collision with the wall, the orientation of the vehicle would be reflected about the wall normal vector and reversed as in a simple ballistic collision.

2.7.2. Evolutionary optimization of vehicles

Multi-objective optimization of the vehicles was performed via an evolutionary strategy using the Non-dominated Sorting Genetic Algorithm II (NSGA-II) method available in DEAP Python package [**89, 90**]. We optimized the vehicles to best match four objectives (i.e., by minimizing the Euclidean distance between the performance of the vehicle and fly for each objective): (1) the avoidance index and (2) turn-cross ratio at each of the three test temperatures, (3) the probability of a left/right turn given antennal temperature difference at turn start, and (4) the "spontaneous" rate of turns per distance walked. Optimization was performed over an 8 dimensional space, $z = \{W_I, W_C, \tau_s, \sigma_s, a, b, \tau_m, \sigma_m\}$ containing the ipsilateral and contralateral weights W_I and W_C), sensory noise parameters (τ_s, σ_s) , nonlinearity parameters (a, b), and motor noise parameters (τ_m, σ_m).

At each new generation, the algorithm either "crossed" or "mutated" (each with probability 0.5) individuals from the previous round. For "crossing", the two-point crossover operation was used, which creates children c_1, c_2 by mixing the features of two parents, z_1, z_2. This process is intended to be similar to chromosomal crossover during meiosis, and for random $n_1, n_2 \in \{1, 2, \ldots 8\}, n_1 \leq n_2$ can be written as

$$c_1[1 : n_1] = z_1[1 : n1] \tag{2.21}$$

$$c_1[n_1 : n_2] = z_2[n_1 : n_2] \tag{2.22}$$

$$c_1[n_2 : 8] = z_1[n2 : 8] \tag{2.23}$$

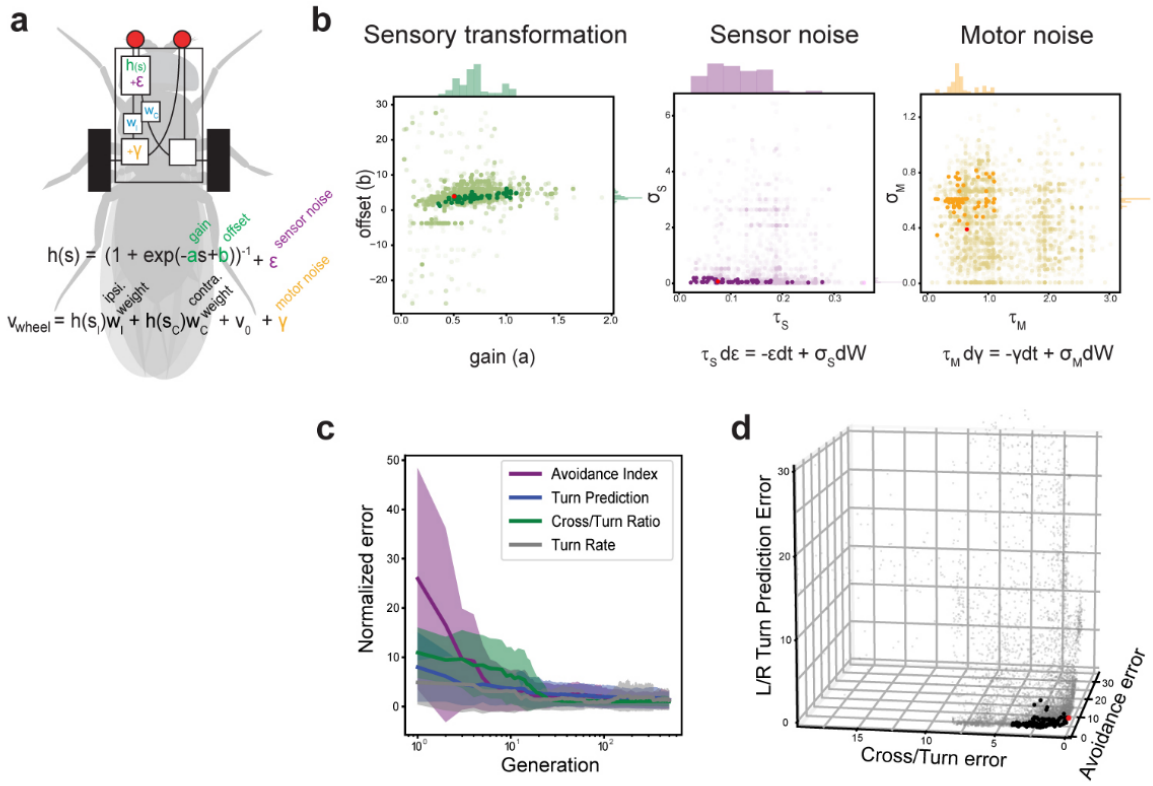

Figure 2.10. Parameter space explored during vehicle evolution. **a.** Schematic of the vehicle model, indicating some of the functions and parameters used for evolution. **b.** Parameter space explored by six of the eight variables allowed to change during 500 generations of evolution (see main figure for ipsilateral and contralateral weight). Light-color points represent all vehicles tested during evolutionary optimization (N=42042), dark-color points are from all-time best performers in all four objective functions (see methods for details; N=102), red point represents the best performing vehicle chosen for comparison with flies. Left panel (sensory transformation), a,b = evolved variables. Center panel, sensor noise ϵ, σ_S and τ_S = evolved variables. Right panel, motor noise γ, σ_M and τ_M = evolved variables. **c.** The error in each of the four objective functions converges following evolution (median ± median absolute deviation; error values are from each generation's Pareto front vehicles, the error of each vehicle is normalized by the median error of the final Pareto front vehicles) **d.** 3D scatter plot showing the error space for 3 key objectives of all vehicles tested (grey), the all-time best performing vehicles after 500 generations (black), and the top performing vehicle (red). X-axis = Crossover/U-turn ratio error, Y-axis = avoidance index error, Z-axis = Left/Right turn predictability error.

for child c_1, where the colon operator specifies the Python indexing convention (i.e., second number is not included). An analogous procedure generates child c_2. Mutation was accomplished by adding a randomly generated number from a zero-mean normal distribution ϵ_n to each coordinate with probability 0.25. We can write this as

$$c_i[n] = \begin{cases} z_i[n] + \epsilon_n, & \text{if} \qquad \Gamma_n < 0.25 \\ z_i[n], & \text{else} \end{cases} \tag{2.24}$$

where the Γ_n are random numbers drawn from a uniform distribution on the interval $[0, 1]$.

The best performing individuals based on 200 trial simulations (comprised of 50 simulations of 25°/25°C, 25°/30°C, 25°/35°C, and 25° /40°C, each) were then selected using the nondominated sorting genetic algorithm II (NSGA-II) method. In this approach, an individual z can be said to dominate another individual $\hat{z}$ if it (a) does no worse than $\hat{z}$ on all objectives and (b) outperforms $\hat{z}$ on at least one objective. Any individual that is not dominated by any others is optimal in a multi-objective sense, often referred to as Pareto optimal. The set of all such points is often called the Pareto "front". By removing all points in this group and finding the non-dominated set of the remaining set, we can define a secondary "front". Iteration of this procedure allows for determination of remaining "fronts".

In addition to nondominated selection, NSGA-II includes an explicit diversity preserving mechanism, called the "crowding distance", which sums the total distance between neighboring points for each individual, over all objectives. This helps prevent oversampling of the search space and potential convergence to local minima.

Combining these two measurements, NSGA-II establishes a partial-ordering $\prec_n$ of all individuals such that $i \prec_n j$ if ($i_{rank} < j_{rank}$) or ($i_{rank} = j_{rank}$ and $i_{cd} > j_{cd}$), where the

subscripts denote the rank and crowding distance, respectively. This allows for unambiguous selection of top candidates for further evolution.

After 500 generations of evolution (each with 112 individuals) we observed strong convergence of the error in each performance criterion among members of the Pareto front (Figure 2.10c, here, we consider the error in each objective of a particular vehicle,e_i, normalized by the median error in that objective of all final Pareto front members, γ_i, such that $\text{Error}_i = e_i/\gamma_i$). Following evolution, we compared the 102 alltime best performing vehicles in all four criteria (members of the final Pareto front that had no error greater that 4X the median error for any objective). The top performing vehicle, defined as the vehicle with highest minimum rank across the four objectives (ranking according to magnitude of error in the objective), was used for comparisons with flies (see Figure 2.11; W_I [mm/s] =29.1, W_C [mm/s] =-22.5, τ_s [s] =0.75, σ_S =0.0067, a [1/°C] =0.5, b =3.9, τ_M [s] =0.65, σ_M =0.39). However, we note that all of the 102 best performing vehicles performed similarly well (Figure 2.9 and Figure 2.10).

Our simulation assessed the performance of 42,042 vehicles over 500 generations of evolution. The final group of all-time best performers (the Pareto front), contained 559 vehicles, and 102 of those were chosen for further analysis based on good performance in all four criteria (the dark points in Figure 2.9c and Figure 2.10b,d represent parameters from these vehicles). We finally chose the best performing vehicle to compare to fly behavior (but note that all 102 vehicles in the final group performed similarly, as shown by convergence of the four loss functions, Figure 2.10c,d).

Despite their inherent simplicity, after 500 generations our vehicles matched the performance of flies in the arena remarkably well (Figure 2.9d,e and see Movie S1 in our paper [**60**]). This included the distribution of U-turn left/right choices at the border (Figure 2.9f),

an objective not explicitly included in our selection process. We note that all top vehicles resulting from our evolutionary process retained both ipsi- and contra-lateral connectivity (i.e., the connectivity weights settled on non-zero values, see Figure 2.9c). This suggests that coordination between left and right motors may be advantageous even in these very simple conditions.

2.8. Comparison of vehicle and fly behavior in the 2-choice experiment

Interestingly, while recapitulating well the fly's turning responses at the border, the vehicle model failed to capture distinctive aspects of fly navigational behavior — ranging from the obvious to the more intriguing.

First, flies appeared better than vehicles at adapting to a change in sensory input state — i.e., as a result of removal of the left or right antenna/sensor. Like flies, sensor-ablated vehicles had a significant turning bias at cool/hot boundaries and overwhelmingly turned towards the side of the lesion when encountering heat (Figure 2.9g). Yet, occasional entries in the hot region trapped the vehicles in a state of continuous spinning, a behavior not seen in flies (Movie S2 in our paper [**60**]). This effect was also observed in homogeneous heat conditions: unlike flies, sensor-ablated vehicles were unable to cope with uniform heat and remained trapped in continuous spins (Figure 2.11a-c). Antenna-ablated flies initially turned towards the side of the lesion when exposed to homogeneous heating (Figure 2.12), but adapted their behavior to produce less stereotypical trajectories in constant heat (see Figure 2.11b).

In addition to being less robust to new conditions, as may be expected, the vehicle's maneuvers at the boundary appeared much more stereotyped than those of flies. As our algorithm does not directly select for stopping frequency, the vehicles did not perform the

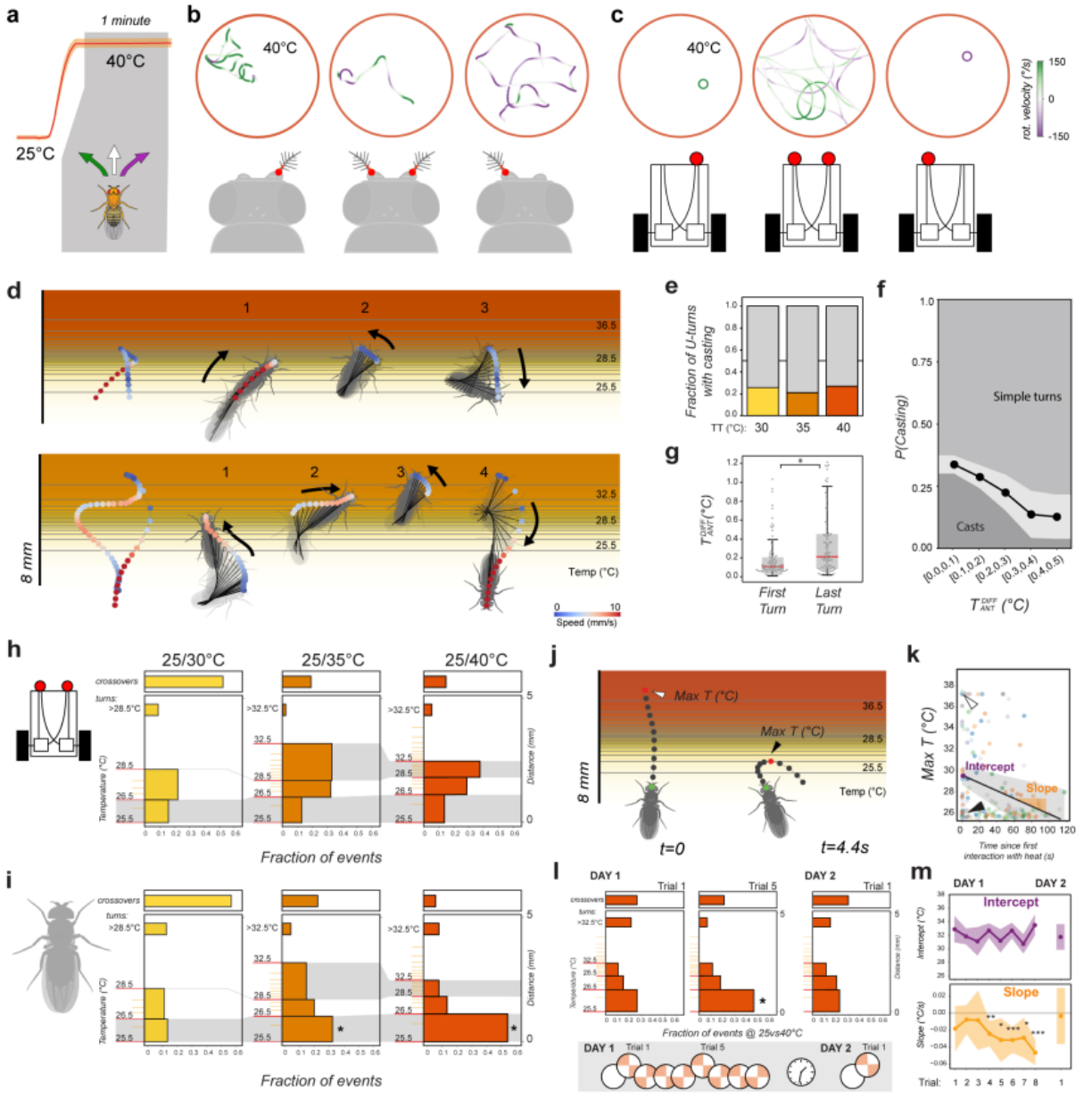

Figure 2.11. Comparison of thermotaxis in flies and vehicles reveals latent robustness and plasticity in fly behavior. **a-c.** Under uniform heat conditions, fly behavior following antenna ablation is less stereotypical that vehicle behavior following sensor ablation. **a.** Schematic of constant-heat experiment. **b-c.** Representative tracks from (**b**) antenna ablated and control flies and (**c**) sensor ablated and control vehicles. Track color represents rotational speed (green=leftward rotation, purple=rightward rotation). Unlike flies, sensor-ablated vehicles rotate in place in uniform heat.

Figure 2.11. **d-g**. When navigating the cool/hot boundary, fly behavior is also less stereotypical than that of vehicles. Unlike vehicles, in a fraction of border interactions, flies perform "casting" (defined as at least two changes in direction in close succession) before escaping. **d.** Two examples of casting behavior. **e.** Fraction of escape turns that contain at least one casting event, plotted by experimental condition (N_{30} =67/28, N_{35} =114/30, N_{40} =191/39 turns/animals). **f.** Probability of casting is highest when the approach angle results in a small temperature difference between the antennae (N=341 interactions from 95 flies; bins = 0.1°C intervals, grey shading = ± STD, GLMM with Wald Test, P = 1.5e-2, Coefficient = -3.12). **g.** The last turn of a casting sequence is often characterized by a larger temperature difference between the antennae, compared with the first turn (box edges = first and third quartiles, solid line = median, whiskers = data range; N=92 casts from 55 animals, LMM, ANOVA, P = 2.2e-4). **h-m.** Fly heat avoidance also displays hallmarks of rapid learning. **h, i.** Compared to vehicles, flies display a disproportionate fraction of early turns (turns in the <26.5°C region, lower grey shading) in the 25°/35°C and 25°/40°C experimental conditions. Histograms represent fraction of U-turns in different regions of the temperature gradients for (**h**) vehicles and (**i**) flies (left y axis = temperature (°C), right y axis = distance (mm); grey shading = similar temperature range across conditions; crossover frequencies are shown at the top; asterisks in **i** = GLMM, Wald Test, P_{35} =1.2e-7, P_{40} =1.1e-26; **h**: N_{30} =138/29, N_{35} =131/25, N_{40} =181/29 events/flies; **i**: N=2493, 3087, 3109 events/400 vehicle simulations each). **j-m.** The dynamics of appearance of early turns suggests an underlying learning process. **j.** Representative tracks showing a border crossing followed by an "early turn" (t = time from first border interaction; arrowheads = maximum temperature at the antennae, Max T, capped at 37°C for crossings). **k.** Border crossings and deep turns (leading to exposure to high heat) decrease during the course of an experiment in favor of early turns (LMM ANOVA, P = 1.3e-4; grey shading = 95% confidence interval; arrowheads in **k** correspond to events in **j**; N=28 flies). **l.** When naïve flies are subjected to consecutive trials, early turns are significantly increased after 5 trials (plots as in **h,i**; asterisk = GLMM, Wald test, P = 1.3e-2, N= 55 flies, N_{events}: N_{D1T1} =238, N_{D1T5} =264, N_{D2T1} =79). Early turn frequency returns to naïve levels after 24h (right panel). **m.** When considering the maximum temperature experienced at each border interaction, the initial exposure to heat remains constant across trials (intercept, top panel), but, after trial 4, flies rapidly resort to early turns as a strategy to escape heat (negative slope, bottom panel). This effect is reversed after 24 hours of rest. Here, max temperature data was extracted and plotted as in **j, k** (points = coefficient from maximum likelihood estimation LMM, shading = 95% confidence interval from parametric bootstrap; asterisks = LMM ANOVA, P_4 =1.4e-3, P_5 =1.7e-2, P_6 =5.5e-5, P_7 =1.7e-2, P_8 =1.4e-9; in **l,m**: N_{day1} =55 flies,N_{events} : N_1 =108, N_2 =268, N_3 =71, N_4 =338, N_5 =105, N_6 =280, N_7 =103, N_8 =268, N_{day2} =13 flies, N_{events} = 71).

spontaneous stop-and-go's that are typical of fly locomotor behavior. In particular, real flies in the arena slowed down considerably within the cool/hot boundaries, often coming nearly

to a stop and performing side to side swings (reminiscent of "casting" [**65, 86, 91**]) before performing a sharp turn, and speeding up again to escape the heat (Figure 2.11d and see technical methods for details of trajectory segmentation).

This was not seen in vehicles, whose turns instead efficiently minimize the time spent within the hot area (i.e., by speeding up as the heat increases) and exhibit no modulation of motor output (i.e., changes in spontaneous turning frequency) at the hot/cool boundary. We propose that this fly "casting" behavior may represent an information gathering step that leads to a better informed turning decision. This idea is supported by two lines of evidence:

(1) casting occurred in ∼25% of U-turns (Figure 2.11e), and was more likely in cases in which the initial border approach resulted in a small temperature differential between the antennae (perhaps reflecting initial uncertainty on escape direction; Figure 2.11f).

(2) A casting sequence may comprise multiple side-to-side swings (see Figure 2.11d for an example), but the last turn of the sequence (the one leading to escape) generally started from a position characterized by a larger temperature differential between the antennae, compared to the first turn (Figure 2.11g). Hence, the casting sequence often resulted in reduced uncertainty on the direction of escape.

Finally, we analyzed turning frequencies at the boundary as a function of temperature, and compared the results from flies and vehicles. The data revealed that flies resort remarkably rapidly to learned responses, even in this simple behavioral assay.

Our detailed simulation demonstrates that, at the height of the antennae, the cool/hot boundary is characterized by different temperature gradients in each of the 3 experimental

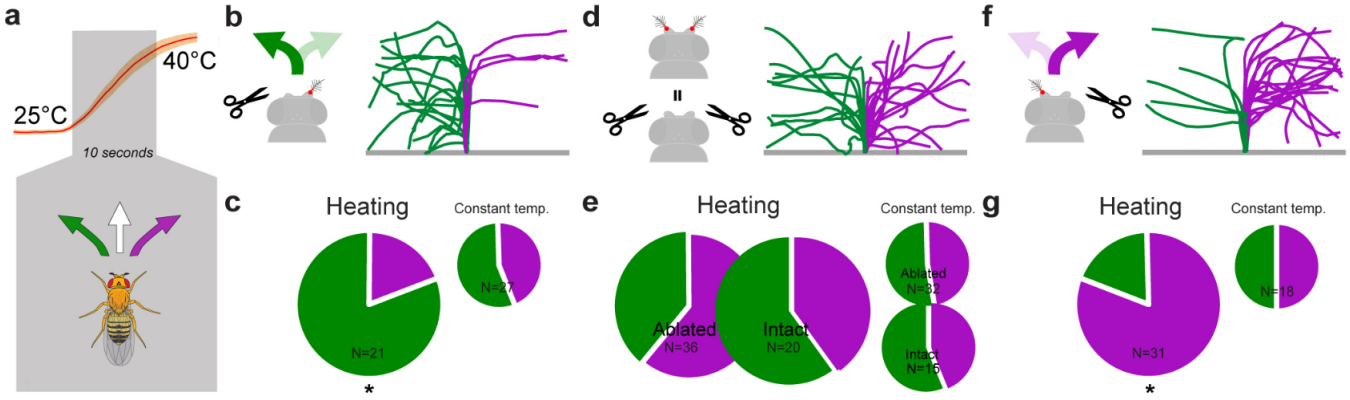

Figure 2.12. The behavior of antenna-ablated flies during uniform heating. **a.** Experiment schematic. **b-g.** Analysis of the direction of the first turn performed by intact and antenna-ablated flies under uniform heating. **b,c.** Left antenna ablated. **d,e.** Both antennae ablated. **f,g.** Right antenna ablated. **b,d,f.** Fly tracks that include the first turn a fly performed upon heating (green=left turn, purple=right turn). **c,e,g.** Quantification of left/right turning frequencies in antenna-ablated flies (left/right turning frequency at constant 25°C is shown as a control; N=number of flies tested; asterisks denote a difference from the expected control distribution of 1:1, Chi-Squared test, P_{left} = 4.6e-3, P_{right} = 1.6e-4).

conditions (25° /30°C, 25° /35°C and 25/40°C). For example, while the gradient in the 25.5-26.5°C thermal range is very similar across the 3 conditions (lower grey shading in Figure 2.11h,i), the 28.5-32.5°C gradient is much steeper within the 25/40°C than in the 25/35°C boundary (upper grey shading in Figure 2.11h,i).

As a result of a very similar initial gradient, the vehicle's turning frequency is comparable across conditions in the 25.5-26.5°C region (lower grey box in Figure 2.11h). Beyond this point, vehicle turning frequency becomes higher in hotter regions (e.g., in the 25/35°C condition) or in correspondence of the steepest gradient (25/40°C, upper grey box in Figure 2.11h).

Surprisingly, this was not the case for fly behavior. Flies' turning frequencies appeared disproportionately high in the 25.5-26.5°C initial region compared to vehicles' turning frequencies, in particular in the 25/35°C and 25/40°C conditions. In fact, the fly's propensity to perform "early turns" (turns in the initial part of the gradient) seemed to increase as a function of the test temperature (i.e., the frequency of early turns was higher in the 25/40°C than in 25/35°C experiments; lower grey box in Figure 2.11i).

Moreover, one or more "early turns" often followed a "deep turn" (a turn that lead to exposure to higher temperatures) or a border crossing (Figure 2.11j), and a quantification of all border interactions in the 25/40°C condition demonstrates that "deep turns" and border crossings were significantly reduced over the course of a single experiment (i.e., within-trial, Figure 2.11k). Hence, the frequency of early turns appears to increase following interactions with more intense heat (>35°C).

We reasoned that this phenomenon could be explained either by sensitization (exposure to intense heat may boost the subsequent responses to mild heat) or as a result of more complex plasticity. For example, flies could rapidly learn to associate a temperature increase with the exposure to "dangerous" heat that follows it, and turn early within the gradient.

As noted before, we observed no sensitization in the neural responses to heat in TRNs and TPNs (using 2-photon microscopy, see Figure 2.4), but this observation alone is not sufficient to exclude potentially sensitized responses further downstream.

To directly test the possibility that rapid learning may indeed explain the appearance of early turns, we designed the following experiment: rather than exposing flies to a full sequence of temperature choices as in previous runs, we exposed a cohort of "naïve" flies to 8 consecutive presentations of the choice between 25 and 40°C (as usual in alternating spatial configuration, see schematics in Figure 2.11l). Indeed, naïve flies behave more like

the "hard wired" vehicles, and only after ∼5 trials did we observe a significant increase in the fraction of early turns (Figure 2.11l). This effect was reversible: allowing individual flies to recover for 24 hrs in fly food vials restored the behavior to its naïve state (flies seemed to have forgotten what they learned, Figure 2.11l).

Intriguingly, the dynamic restructuring of turning behavior following heat exposure could again be observed within trial, but the effect of heat exposure appeared to depend on prior experience. When considering all border interactions as a function of temperature, both naïve and experienced flies responded similarly to each new presentation of the stimulus (i.e., performed deep turns and border crosses at the beginning of each new trial; Figure 2.11m, intercept). Yet, unlike naïve flies, experienced flies rapidly adopted early turns as a strategy to minimize heat exposure (Figure 2.11m, negative slopes; intercepts and slopes were calculated from data plotted as in Figure 2.11k). These complex dynamics, together with the fact that we observed no sensitization in the responses to heat in TRNs and TPNs (see above), lead us to conclude that learning, rather than neural sensitization, is likely to explain the difference in the frequency of early turns we observed between flies and the "hard wired" vehicle. Hence, even in this simple assay, flies rapidly deploy learned programs to better adapt behavior to the specific features of the thermal environment.

2.9. Conclusion

Together, our results demonstrate how even a small poikilotherm such as the fruit fly possesses sophisticated mechanisms to navigate the thermal environment.

We show that, much like the more studied sensory systems of larger animals, fly thermosensation leverages input differences between symmetrical sensors (the antennal thermosensory neurons) to estimate the direction of change of a salient stimulus (increasing

temperature). Rather than using this information to localize a prey [**81**] or to move up an olfactory plume [**84**], this differential reading is used to quickly draft an efficient escape trajectory away from dangerous thermal conditions.

While the fly's ability to discern temperature differences as small as $0.1°C$ using sensors placed only 0.3mm apart may seem surprising, this is not the first example of spatial comparison of sensory information in invertebrates. As early as 1907, W.M. Barrows performed single antenna ablation experiments and observed that flies subjected to uniform fermented banana odor walk in a circular motion, with a bias towards the direction of the ablation [**92**]. In 1933, Wigglesworth and Gillett showed that single antennal resection could drive biased turning behavior upon exposure to heat (albeit in the opposite direction) in the blood-sucking parasite *Rhodnius prolixus* [**93**].

More recent studies of *Drosophila* olfactory navigation have shown that bilateral sensory input is essential to odor tracking [**84**]. Importantly, differential activation across antennae has been shown to drive asymmetric neurotransmitter release, thought to enable rapid turning in the direction of an attractive odor [**85**].

Since we know diffusion dynamics govern both olfactory and thermal stimuli, it is not unreasonable to expect that the sensory processing of each may follow similar rules. One key difference is the nature of the stimulus. Thermal stimuli away from the fly's preferred 25°C are exclusively aversive, whereas olfactory stimuli can be either attractive or aversive.

Additionally, it is worth noting that the generation of large thermal differences over small spatial scales is not restricted to the experimental conditions described. Large thermal differences often accumulate at the interface between materials of different specific heat or reflectance properties (e.g., asphalt vs grass), as well as at the boundaries of turbulent flows [**94**].

This work parallels efforts to produce quantitative models of sensory-motor transformations in C.elegans [**95**], the fly larva [**65, 96, 97, 98**] and adult [**38**], as well as in vertebrate model systems such as zebrafish [**99, 100**]. It remains an open question to what extent, even in these relatively simple systems, sensory-motor transformations remain flexible, rather than being strictly determined by a combination of stimulus parameters.

A 3D simulation of the thermal landscape put us in the unique position to create a realistic virtual arena in which to evolve a "Braitenberg-inspired" vehicle model, directly testing the notion that fly heat avoidance may be controlled by a combination of simple hard-wired responses.

We note that the Braitenberg formulation is an intentionally simplistic one. Our sensor parameters are not designed to match what we know about thermosensory neurons, and our "circuit" formulation is rather simple compared to the complexity of the fly nervous system.

Nevertheless, after evolution of a number of key parameters, our Braitenberg-inspired vehicles performed remarkably well in the simulated arena, matching many of the characteristic features of fly thermotaxis. This suggests that the basic navigational responses to a hot front may be indeed controlled by a relatively simple set of transformations.

Yet, our vehicles appeared less robust to a sudden change in input (e.g., from sensor ablation) and fly-vehicle comparisons revealed features of fly thermotaxis that suggest an information gathering/decision-making process, as well as an unexpectedly rapid emergence of learned responses. Together, our results reveal additional layers of complexity within this seemingly simple insect behavior.

Animal navigation continues to be an essential source of inspiration for work involving autonomous robots and vehicles. Our approach shows that the reverse can also be true: comparing an intentionally bare vehicle-model to real animal responses can reveal aspects of

natural behavior that defy reduction to a combination of fixed action patterns and hard-wired responses.

CHAPTER 3

Egocentric and allocentric processing in Drosophila thermotaxis

3.1. Forward

This chapter constitutes a step towards a more global understanding of the processing required for thermotaxis, examining a novel context in which temperature changes occur over sufficiently large scales that inter-antennal temperature differences are negligible. Analysis of fly behavior in this setting and comparison with the steep gradients of the two-choice assay allows us to explore key components of the thermosensory circuit required for heat avoidance in each condition. This work is ongoing and will eventually be supplemented by additional experimental study of relevant processing circuitry. As in the previous chapter, this work is the product of a close collaboration with José Miguel Simões of the Gallio lab, who recorded the behavior of both control and mutant flies, while I analyzed the raw data and developed quantitative methods to study navigation.

3.2. Introduction

In nature, animals encounter diverse sensory cues over a wide range of spatial and temporal scales. Confronted with this input, animals must extract key information from noisy and ambiguous signals to determine a course of action. This task is fundamental to all motile animals, and underlies behaviors from rapid reflexes to months-long migrations.

Here, we show that elements of both egocentric and allocentric processing enable robust thermotaxis across contexts in adult *Drosophila melanogaster*. Following the previous chapter, in which we describe how flies use small temperature differences between their antennae to chart the direction of escape turns away from heat, our first objective is to identify the sensors required for navigation of shallow thermal gradients, where inter-antennal temperature differences are negligible. Our next goal is to identify and study the sensory processing circuitry required for successful thermotaxis in this context, and how it may differ from that used for the navigation of steep gradients (described in Chapter 2).

Temperature constitutes one of the most fundamental sensory cues. While responses to intense and noxious thermal stimuli are often most salient, such dramatic thermal landscapes represent only part of the temperature environment. In response to such diverse sensory information, animals have developed a host of strategies to ensure they remain in a suitable thermal environment, but we generally know little about the sensory processing required for these behaviors. To address this question, we again consider the fruit fly *Drosophila melanogaster*.

As poikilotherms, flies must navigate the environment to regulate their body temperature, and are particularly sensitive to heat. In laboratory conditions, flies navigate to regions of approximately 25°C, away from cooler and warmer positions in the landscape [**13, 11**]. As described in the previous chapter, adult flies demonstrate avoidance of temperatures above 25°C, with robust avoidance of innocuous heat (25-35°C) and very strong avoidance of noxious heating (> 35°C) [**11, 60**].

Though the steep thermal gradients studied in the previous chapter constitute an important navigational challenge, shallow temperature gradients are also likely to be common, particularly at the spatial scales of the body of a fly. Indeed, fruit flies, which measure about

3 mm in length and have temperature sensors positioned approximately 300 μm apart, are far too small to measure temperature differences between their antennae in non-steep thermal gradients. Yet, flies are known to successfully navigate over large distances in complex, multi-sensory environments[**101**].

As described in Chapter 1, flies are thought to process sensory information in the central complex (CX) in order to guide many aspects of navigation. In particular, a group of allocentric "compass" neurons (also known as EPGs) are thought to maintain a robust estimate of current heading angle in the ellipsoid body (EB) using both proprioceptive and external sensory cues [**46, 50, 102, 53, 103**]. These cells are required for consistent traveling at an arbitrary angle with respect to environmental landmarks, also known as menotaxis [**51, 52**].

Considerable evidence suggests that the fan-shaped body (FB) region of the brain may also play a significant role in navigation [**59, 49**]. For example, a class of neurons targeting the FB (ventral PFNs, or PFNvs) are thought to egocentrically encode external airflow velocity and are required for corrective turning and proper orientation to flow direction [**58**]. More recent research has shown that they may also represent backwards translational velocity (even in the dark), and thus may integrate both self and external cues [**57, 56**].

Despite our knowledge of the molecular and cellular temperature sensors possessed by the fly, we know little about the role of each of these sensors in different types of thermal environments, much less how downstream neurons process this information to ensure robust navigation in each context.

3.3. The role of heat sensors in navigating a thermal gradient

To further develop our understanding of how thermal input is processed into navigation responses, we used a linear gradient assay to study both control and mutant flies. Importantly, we chose the physical dimensions of the assay to minimize thermal differences between antennae. Using Peltier thermal elements applied to either side of a 35 cm aluminum sheet (more than 100 times the length of a fly), we obtained a reproducible linear thermal gradient (as measured with a thermal imaging camera, see Figure 3.1a,b).

For our experiments, flies were started in an insertion chamber on the hot side of the stage and allowed to freely navigate the behavioral arena (Figure 3.1c). For up to 15 minutes following departure from the start chamber, we recorded navigational maneuvers until the fly reaches its preferred temperature (approximately 25°C, or 90% of the length of the behavioral stage — see Appendix for details on fly tracking).

To estimate the sensory input received by flies in our assay, we used a simple model of heat diffusion (see below for details) to simulate the temperature landscape in three dimensions (Figure 3.1d). As before, we extracted the temperature profile at the height of the antennae (about 700 μm, Figure 3.1e,h).

3.3.1. Modeling the thermal landscape

Specifically, we solve the steady-state heat equation in the arena

$$0 = \frac{\partial T}{\partial t} = \nabla^2 T, \tag{3.1}$$

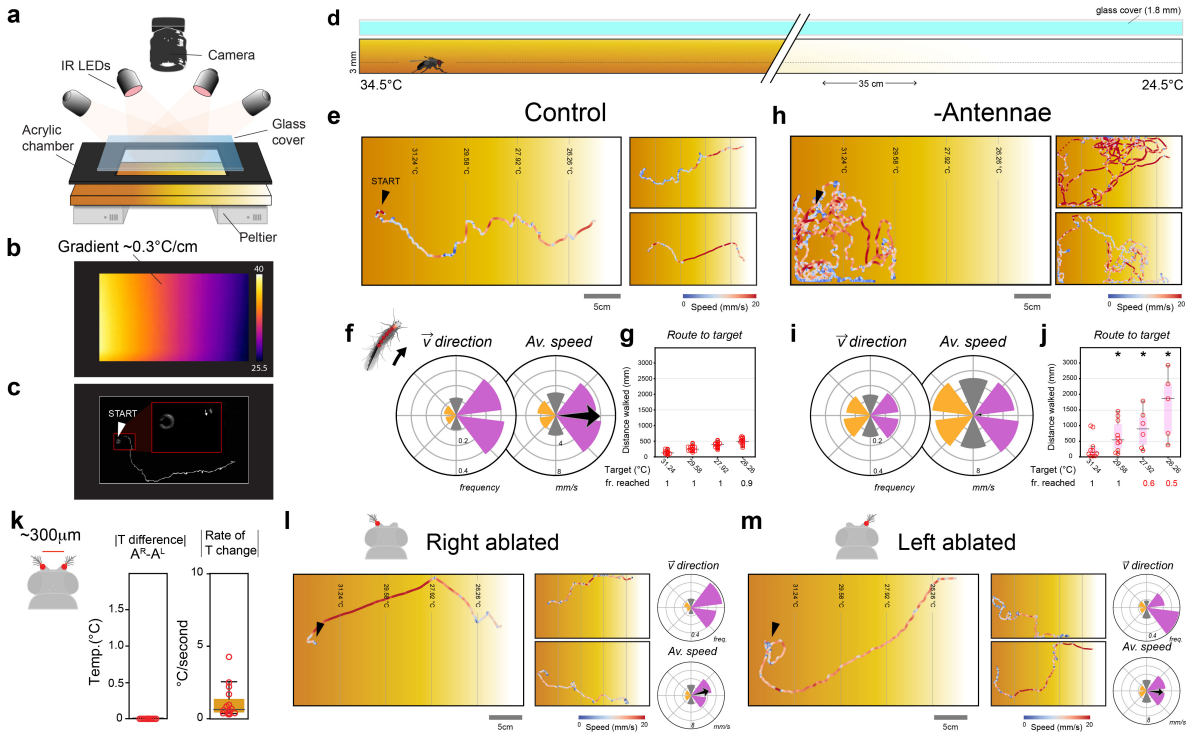

Figure 3.1. The antennae are required for thermotaxis. **a.** Schematic of linear gradient behavioral assay and recording **b.** Thermal images of the experimental stage, and **c.** maximum projection of an example trajectory from a trial. **d.** Side view of the 3mm x 35cm chamber, showing temperature profile predicted by thermal model, with fly for scale (note the break in the diagram, indicating a spatial jump of 30cm.) **e,h.** Representative walking trajectories from control and antenna-ablated flies. **f,i.** Fraction of time spent walking in direction, and average speed in each direction, with overall average speed shown in with the black arrow (shown as 3X the true average). **g,j.** Distance walked to reach each isothermal line (positioned at increments of 20% of stage length; P_{Ablated} = n.s.,0.0061,0.0036,0.00080), as shown in **e,h**, and below, the fraction of flies reaching each line (P_{Ablated} = n.s.,n.s,0.011,0.054). **k**. Maximum temperature difference between antenna and maximum instantaneous rate of change predicted by model among control flies. **l,m**. Example trajectories and walking direction and speed graphs for animals with right and left antenna ablated, respectively. Arrowheads indicate the start position of flies in each trial.

where T is the air temperature. The sides of the chamber are treated as insulating, and we use the Dirichlet boundary condition on the bottom

$$T_{bottom}(x) = T_{max} - x\frac{T_{max} - T_{min}}{L}, \tag{3.2}$$

where L is the length of the plate (35 cm), $T_{max} = 34.5°\text{C}$, and $T_{min} = 24.5°\text{C}$. This linear function $T_{bottom}(x)$ closely matches our measurements of the plate (all points within 0.1°C). Finally, we also include the the Robin condition on the top

$$\frac{\partial T}{\partial n} = -\lambda(T - T_0) \tag{3.3}$$

where $T_0 = 25°\text{C}$ is the environmental temperature and λ is a dimensionless coefficient from Newton's Law of Cooling. For numerical implementation, we used a similar finite element approach as in the previous chapter, albeit with a simpler model (the pressure differences are now more gradual and negligible fluid flow is expected). Linear elements were again used for the temperature mesh. In variational form, we can write this as

$$\int_\Omega \nabla T \cdot \nabla \tau dx = -\int_{\Gamma_{top}} \lambda(T - T_0)\tau ds, \tag{3.4}$$

where τ is a test function and Ω and Γ_{top} are the domain and top boundary, respectively. Since this problem is expected to be invariant in the y-coordinate, we simplified by solving the 2D problem in x and z and extrapolating across y.

3.3.2. Observations in the assay

When tested in the heat assay, control flies rapidly descend the thermal gradient, walking predominantly and most rapidly in directions corresponding to cooling (Figure 3.1e,f), and robustly reach their preferred temperature of 25°C (Figure 3.1g). In contrast, flies without antennae demonstrate no clear directional bias (Figure 3.1h,i), only arriving at the cooler parts of the arena after significantly more walking, and with decreased frequency (Figure

3.1j). Importantly, this suggests that the antennae are required for thermotaxis in the shallow gradient, in which inter-antennal temperature differences are negligible, but heating and cooling of the sensors can be achieved by moving about the chamber (Figure 3.1k).

To study the relative importance of differential input (i.e., inter-antennal temperature difference) based steering and more complex processing, we tested the navigation of flies with a single antenna ablated in our assay. Remarkably, these flies showed a movement bias in the direction of the ablation (note that flies were started facing the direction of temperature ascent), yet remained capable of robust navigation down the gradient (Figure 3.1l,m). Interestingly, this suggested that antenna-guided navigation is robust and likely requires complex processing beyond inter-antennal comparison.

Next, we sought to identify the role of known cellular and molecular heat sensors (Figure 3.2a) in this directed navigation behavior. Our findings provide support that antennal heat sensors are required for thermotaxis:

(1) Mutation of the molecular sensor Gr28B.d led to a decrease in descent-biased walking, and only a small fraction of mutant flies reached the cool region of the gradient (Figure 3.2b-d and see Figure 3.3a-c for control behavior).

(2) Transgenic silencing of the heat activated TRNs (HCs) in the arista resulted in a phenotype similar to both antenna ablated and Gr28B mutant flies (Figure 3.2e-g and see Figure 3.3d-i for control behavior).

(3) Similar to our results in the two-choice experiment (Chapter 2), silencing of the AC neurons did not impair directed navigation. AC/Kir flies rapidly navigated down the gradient, comparable to controls (Figure 3.2h-j and see Figure 3.3d-f,j-l for control behavior).

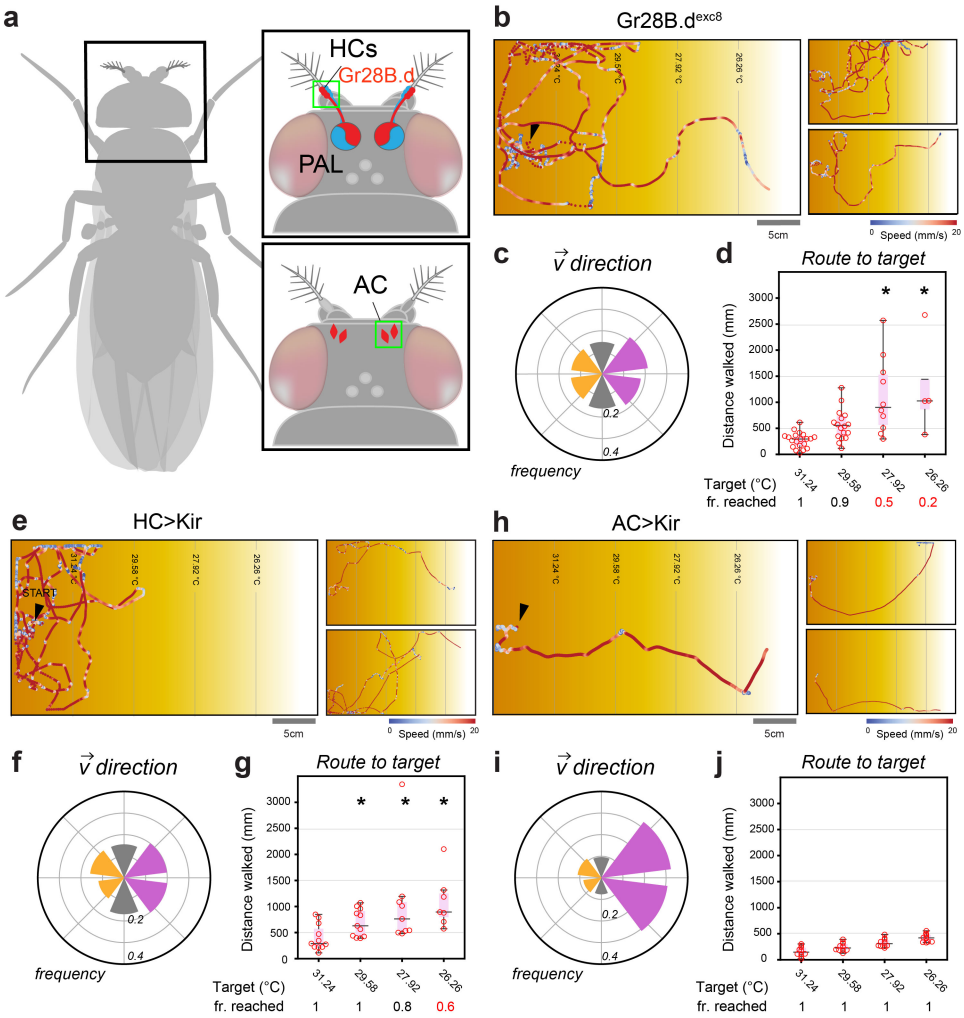

Figure 3.2. Innocuous arista heat sensors are required for navigation, while internal AC neurons modify search directness. **a.** Schematic representation of the cell types involved in innocuous heat sensing the adult *Drosophila* (HCs: hot cells, PAL: posterior antennal lobe, AC: anterior cells). **b,e,h.** Representative walking trajectories from mutant flies. **c,f,i.** Fraction of time spent walking in direction. **d,g,j.** Distance walked to reach each isothermal line($P_{Gr28B.dexc8}$ = n.s.,n.s,0.0068,0.020;$P_{HC/Kir}$ = n.s.,0.011,0.039,0.010), and below, the fraction of flies reaching each line ($P_{Gr28B.dexc8}$ = n.s.,n.s,1.4e-4,3.1e-5;$P_{HC/Kir}$ = n.s.,n.s,n.s.,0.061).

3.4. Sensorimotor processing underlying rapid thermotaxis

Although our results to this point demonstrate the importance of innocuous heat sensing in the antennae, they do not provide insight on the nature of the processing involved in rapid

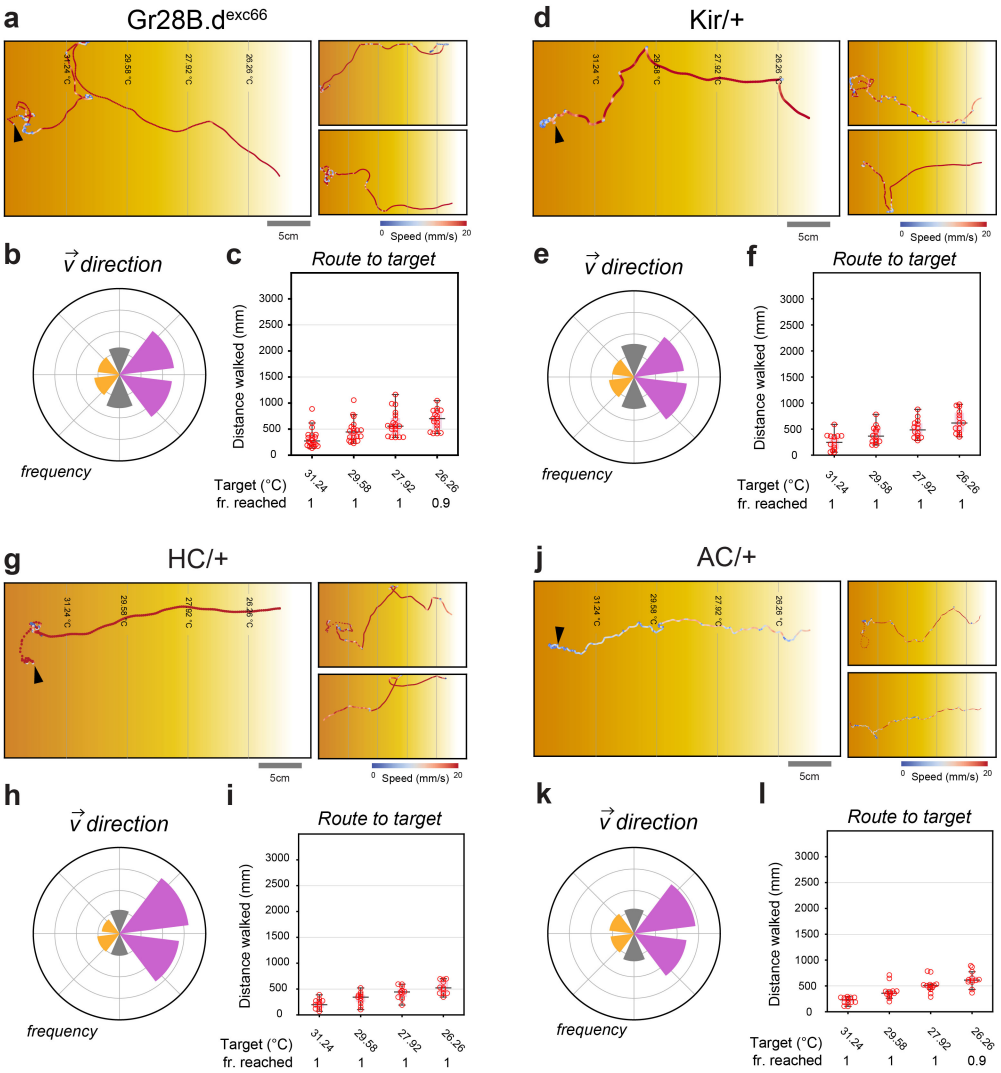

Figure 3.3. Control animals for sensor mutant and silencing experiments. **a,d,g,j.** Representative walking trajectories from control flies. **c,f,i.** Fraction of time spent walking in each direction (grouped into six bins). **d,g,j.** Distance walked to each line, and fraction of flies reaching each line.

thermotaxis. To tackle this question, we again considered our fly-sized *in silico* vehicle model with two hard-wired symmetrical sensors and motors (a "Braitenberg" vehicle), which uses differential input at each sensor to drive directed motion [**23, 60**]. Although an optimized vehicle can reproduce key aspects of fly heat avoidance in a steep thermal gradient (as shown

in Chapter 2), this requires significant thermal differences between sensors (positioned $300\mu m$ apart to match the fly) to drive turning, which are intentionally made negligible in our assay (Figure 3.1k).

Using our simulation of the linear thermal gradient, we studied the behavior of a hard-wired ("naive") vehicle, with parameters matching those of the "top performer" from Chapter 2. As expected, the "naive" vehicle model fails to navigate successfully (Figure 3.4). The vehicle displays swirling trajectories (Figure 3.4b), minimal bias in walking direction (Figure 3.4c — note that some bias is expected since trials are terminated upon arrival at the preferred temperature), and longer distances are traveled to reach the cool side of the gradient (Figure 3.4d).

These findings further suggest that successful navigation in the shallow gradient requires processing beyond inter-antennal comparison. However, it is unclear how this is achieved in flies.

3.5. A "compass" modulated vehicle

So how do flies integrate sensory information over time to navigate in shallow gradients? And how might this processing be related to the inter-antennal difference computation involved in navigation of steep gradients?

Inspired by recent work on the allocentric "compass" direction system of the fly, we aimed to incorporate a simple type of spatio-temporal memory as a modulator of the "hard-wired" sensorimotor transformation of our vehicle model (Figure 3.5a, denoted by green text). As in Chapter 2, our approach is not intended to capture the true biophysical complexity involved in the underlying computation of heading direction. Rather, we wished to form a minimal adaptation of the vehicle that captures key features of fly navigation in the shallow gradient.

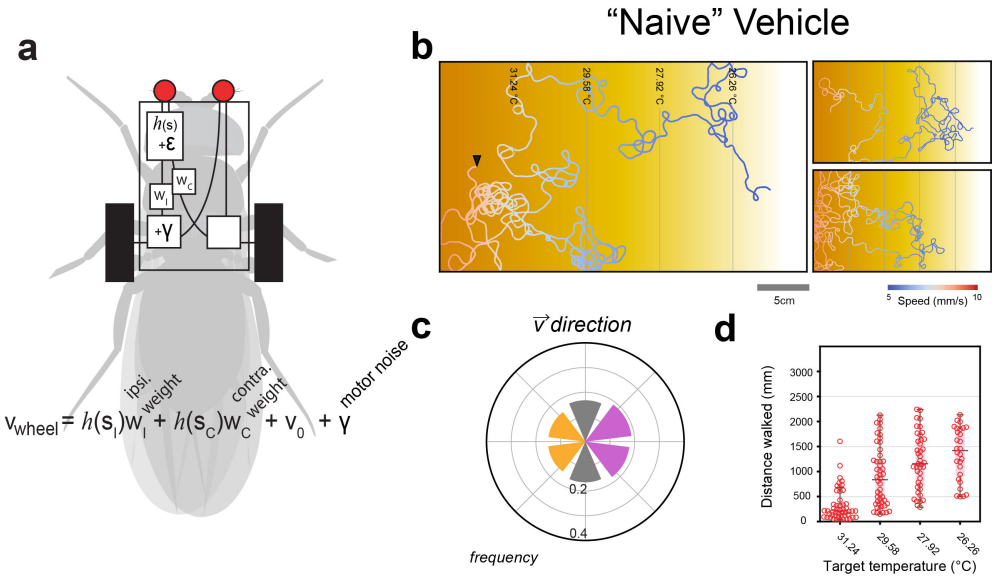

Figure 3.4. Inter-antennal comparison is not sufficient to achieve rapid thermotaxis. **a.** Schematic representation of the "Naive" Vehicle **b.** Representative trajectories of vehicles. **c.** Fraction of time spent walking in each direction bin. **d.** Distance traveled to each isothermal line exceeds that of control flies.

Our adaptation of the model aims to encode fundamental aspects of compass-guided navigation in flies, namely, (1) discordance between the current heading and the goal heading leads to an increase in turning frequency (possibly in an effort to realign with the goal heading), as reported in recent work studying optogenetic perturbations of the compass [**52**]. Also, (2) the compass acts as a modulator of steering, which in the fly brain may be achieved through privileged connections to descending neurons [**104**], or through connections to the FB [**105**].

Our goal is to determine if the incorporation of a simple heading/goal-direction circuit in our vehicle model is sufficient to achieve robust navigation down the gradient. In particular, we aim to study how navigational efficiency in the shallow gradient may depend both on this circuit as well as other key parameters of the vehicle model, especially sensor and motor noise.

3.5.1. Formulation of a generalized vehicle

As in the previous chapter, we use a model of 2-wheel movement dynamics

$$\begin{bmatrix} x' \\ y' \\ \theta' \end{bmatrix} = \begin{bmatrix} \frac{1}{2}(v_L + v_R)\cos(\theta) \\ \frac{1}{2}(v_L + v_R)\sin(\theta) \\ \frac{1}{d}(v_R - v_L) \end{bmatrix} \tag{3.5}$$

where x, y are the positions of the centroid and θ is the orientation. Wheels are driven independently and oriented along the long axis of the vehicle. We again allow v_L and v_R to be the velocities of the left and right wheel, respectively, and d is the distance between the two wheels (chosen to be 750 μm, approximately the width of a fly).

In contrast with our previous approach, we consider a more general formulation of the sensorimotor transformation, in which additional modulation is introduced by an arbitrary function $m(S_L, S_R, X, Y, \Theta)$ such that S_L, S_R, X, Y, Θ contain all sensory, position, and orientation data up to the current time point. This results in the form

$$v_L = m(S_L, S_R, X, Y, \Theta)\Big[h(s_L)w_{L,L} + h(s_R)w_{L,R}\Big] + v_0 + \gamma \tag{3.6}$$

$$v_R = m(S_L, S_R, X, Y, \Theta)\Big[h(s_L)w_{R,L} + h(s_R)w_{R,R}\Big] + v_0 - \gamma, \tag{3.7}$$

where base velocity v_0, sensorimotor transformation weight parameters, W, and motor noise, γ, are defined as in Chapter 2. For our "naive" vehicle, the modulating function $m(S_L, S_R, X, Y, \Theta)$ was chosen to be unity (i.e., $m(S_L, S_R, X, Y, \Theta) = 1$), corresponding to no modulation of the sensorimotor transformation.

3.5.2. Computation of a heading/goal direction filter

Our next objective was to develop a modulating function $m(S_L, S_R, X, Y, \Theta)$, in which sensory information could be integrated over time to bias the direction of movement. Since the neural processing involved in this computation remains poorly understood, we propose a simple, purely computational method to estimate a goal heading in order to study how the corresponding neural circuit may play a role in navigation.

To do so, we note that for a diffusive process, the relationship between previously experienced temperature, position, and a direction of descent/ascent, ϕ, can be described locally by the linear approximation

$$T_{-i} = \langle(\cos(\phi), \sin(\phi)), x_{-i}\rangle\beta + T_0 + \epsilon_{-i}, \tag{3.8}$$

where T_{-i} and x_{-i} represent previously experienced temperatures (taken as the average of the temperature — including sensory noise — at each of the two sensors) and head positions, T_0 is an intercept, β is the slope of the gradient, and ϵ_{-i} describes model error. Determination of ϕ can then be written as a least squares optimization problem using data from the preceding N_I timepoints

$$\hat{\phi} = \arg\min_{\phi} \left\{ \min_{\beta \leq 0} \sum_{i=0}^{N_I} ||T_{-i} - \langle(\cos(\phi), \sin(\phi)), x_{-i}\rangle\beta + T_0||^2 \right\}. \tag{3.9}$$

Although it is unlikely this is how flies compute a goal direction, this problem specifies a goal heading, which can be used to design a filter to modulate the prominence of inter-antennal difference based steering relative to straight-line walking. In order to bias walking

in the goal direction as observed in flies, this filter should inhibit steering while heading in a direction of maximal thermal descent, and should be robust to conditions with negligible signal (where variation is purely due to sensory noise). One way this can be done is by comparing the error of a model optimized in direction θ, relative to a null model

$$G(\theta) = \frac{\mathrm{RSS}_0 - \mathrm{RSS}_\theta}{\mathrm{RSS}_\theta}, \tag{3.10}$$

where $\mathrm{RSS}_\theta = \min_\beta \sum_{i=0}^{N_I} ||T_{-i} - \langle(\cos(\theta), \sin(\theta)), x_{-i}\rangle\beta + T_0||^2$, and RSS_0 is the null residual (i.e., $\beta = 0$). We note that this function should be large if θ specifies a direction of thermal change (i.e., RSS_θ is small relative to RSS_0), and goes to zero when the null model performs as well as the alternative. In order to incorporate this into the vehicle, we form the filter

$$m(S_L, S_R, X, Y, \Theta) = 1 - \frac{G(\theta)H(-\beta(\theta))}{\hat{G}}, \tag{3.11}$$

where $\beta(\theta)$ is the slope of the best fit line along angle θ, H denotes the Heaviside operator ($H(x) = \mathbb{1}_{x>0}$), and $\hat{G}$ is a normalizing factor, chosen as the maximum value of $G(\theta)$ over all $\theta \in [0, 2\pi)$. Importantly, this function goes to zero at $\hat{\phi}$ (i.e., the estimated descent direction), leading to a loss of sensor guided turning when heading in that direction, and is equal to 1 when heading in a non-descent direction. We note that similar results are achieved using a wrapped Gaussian filter centered about the estimated descent direction $\hat{\phi}$, but this requires the choice of additional model parameters. While neither filter captures the true biophysical complexity involved in the calculation of goal direction in the fly brain (which likely requires complex neural processing), they provide an analogous mechanism to modulate sensor guided steering.

3.5.3. Model behavior in thermal gradient

When we added this new component to the "naive" vehicle (using a memory of the 30 previous timepoints, sampled at 30 Hz), we found that inclusion of the heading/goal direction module was not sufficient to achieve efficient navigation down the gradient. Tests on vehicles simulated with a longer memory (i.e., larger N_I) did not demonstrate improved navigation. However, after noting that flies show a decrease in spontaneous turning relative to the 2-choice behavioral assay, we probed the role of motor noise in the vehicle model. Remarkably, we found that decreasing the amplitude of the motor noise, σ_M, was sufficient to achieve successful navigation (Figure 3.5b-d, and note that it did not do so in the "naive" vehicle). As a result, we defined a scaling parameter μ of the noise, such that $\sigma_M = \mu\sigma_{M_0}$, where σ_{M_0} is the motor noise amplitude parameter of the "naive" vehicle (see Figure 3.6 for a sweep over noise parameter μ). For values of μ roughly 0.25 and lower, vehicles demonstrated efficient descent of the gradient, comparable to control flies. This suggests that attenuation of spontaneous turning behavior may be necessary during navigation of shallow thermal gradients in order for ensure robust travel in a direction of temperature descent. Importantly, the modified vehicles continued to exhibit key features of fly-like behavior in the 2-choice assay (i.e., similar to the "naive" vehicle), confirming that inter-antennal comparison can still guide navigation in this combined model (Figure 3.5e-h).

Our results so far suggest that, for both flies and vehicles, successful navigation of the linear gradient requires complex processing of information received by the innocuous heat sensors. In particular, a compass/goal circuit is sufficient to enable robust navigation in the shallow gradient in a generalized vehicle, but requires decreased spontaneous turning, reminiscent of control fly walking trajectories (Figure 3.1). Importantly, our results indicated

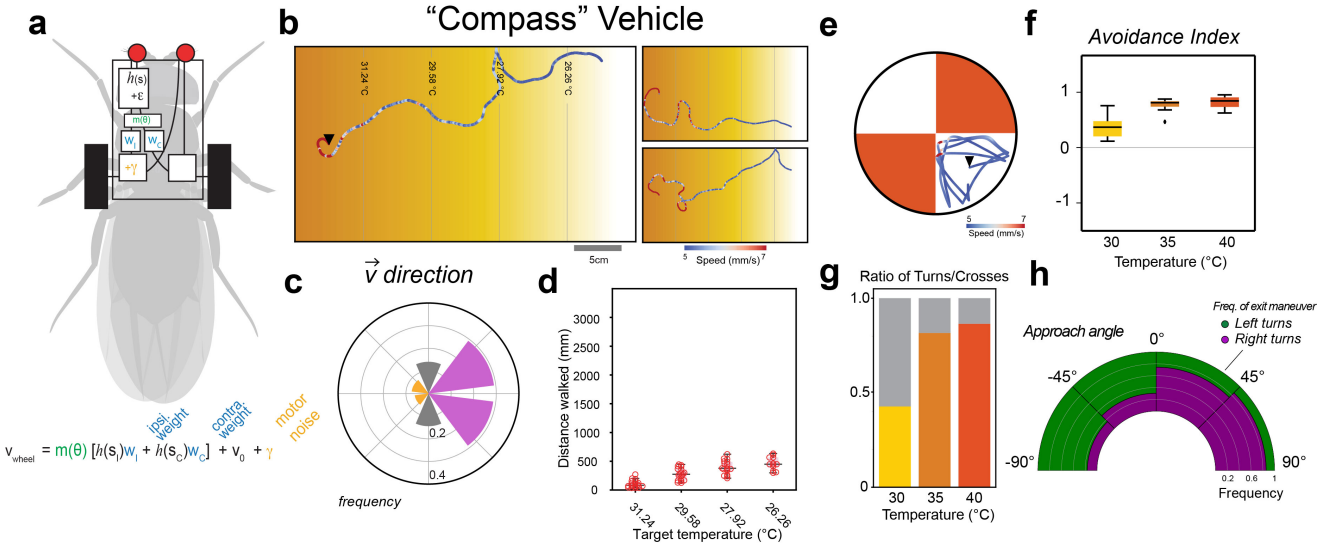

Figure 3.5. Integrating sensory input over time enables biased movement in a simple model. **a.** Schematic representation of generalized vehicle model. **b.** Example trajectories of vehicles with $\mu = 0.25$. **c.** Travel direction frequency and **d.** distances walked to each isothermal line. **e-h.** Modified vehicle maintains normal performance in simulated two-choice experiments. **e.** Example trajectory. **f.** Avoidance index for each test temperature. **g.** Fraction of turns vs crosses at the hot-cold boundary. **h.** Polar plot showing relationship of incoming angle to turn direction.

that although compass-like processing can drive successful navigation of the shallow gradient, it may play a negligible role in steep thermal gradients. As such, by analyzing navigation of real flies in both steep and shallow gradients, we may be able to separately target egocentric and allocentric processing.

3.6. Neural circuitry required for robust navigation across contexts

To what extent does this *in silico* vehicle model, using an estimate of goal heading direction, help us understand the role of a central sensory integrator in modulating fly turning behavior? Do analogous neural circuits govern fly navigation in steep and shallow thermal gradients?

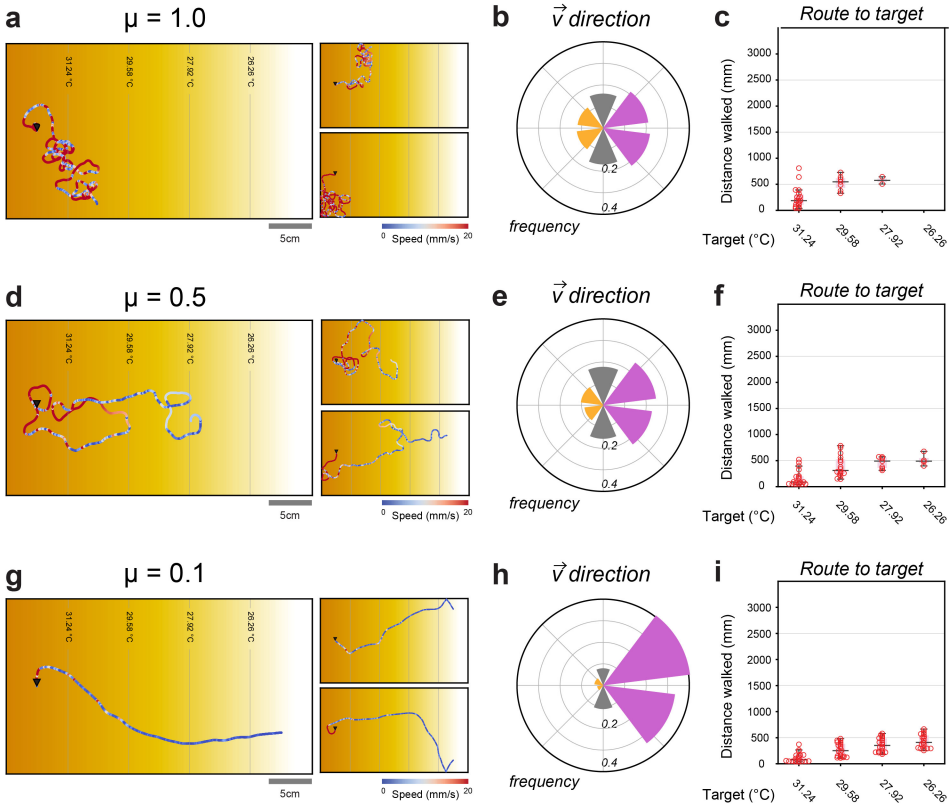

Figure 3.6. Sweep over possible values of noise parameter μ. **a,d,g.** Example vehicle trajectories. **b,e,h.** Polar plots show increasing down gradient bias with decreasing μ. **c,f,i.** Distances traveled upon successful arrival at specified isothermal lines, 15 simulated trials per parameter value. Note that for larger values of μ, very few of the models reach the cool side of the gradient.

To answer these questions, we started by studying the behavior of flies with transgenically silenced "compass" (EPG) neurons. In line with the our "naive" vehicle, compass-silenced flies tested in the linear gradient spent more time walking in non-descent directions, more frequently failed to navigate down gradient, and among successful flies, required a longer walking distance to descend the gradient (Figure 3.7a-c). We then evaluated the role of the compass in steep gradients — which our vehicle model would suggest is not required — by testing EPG-silenced flies in our 2-choice temperature assay. Interestingly, these flies still perform U-turns at the boundary, and appear contained within the heat boundary

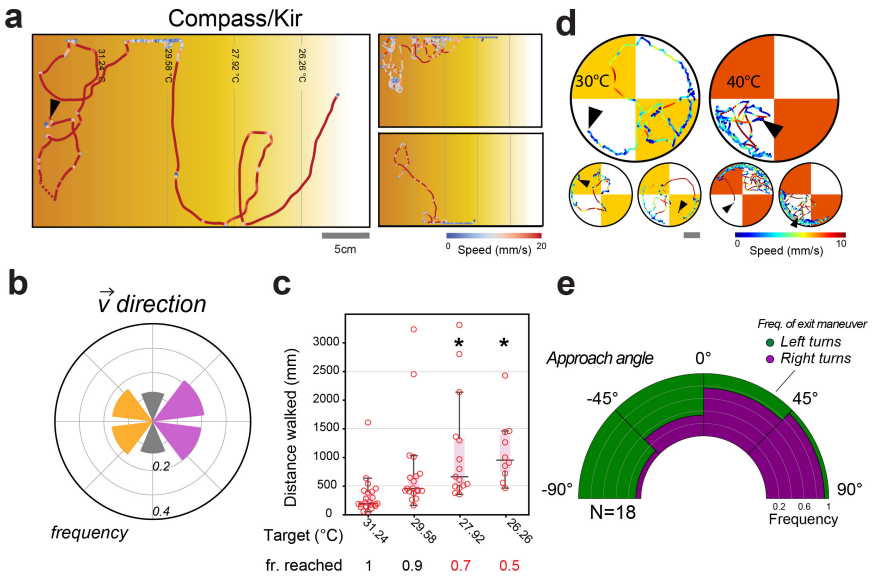

Figure 3.7. Compass silenced flies display decreased descent efficiency, but maintain differential steering. **a.** Example walking trajectories of compass silenced flies. **b,c.** Directional frequency plot, distances walked to isothermal lines (P=n.s,n.s., 0.045,0.028), and frequency of arrival at each line (P=n.s,n.s., 8.1e-3,7.4e-5). **d.** Example trajectories of compass-silenced flies in the two-choice assay. Grey scale bar represents 5 mm in large plots, and 1 cm in small plots. **e.** Polar plot of turn direction depending on approach angle is comparable to controls.

(particularly at 40°C, Figure 3.7d). Similar to the behavior of the "naive" vehicle, approach angle remains a strong predictor of turn direction (Figure 3.7e), suggestive of inter-antennal temperature difference guided turning.

In parallel, we studied flies with transgenically silenced PFNv cells in both experimental contexts. In the shallow linear gradient, PFNv-silenced flies display navigation comparable to control animals (Figure 3.8a-c). But, when tested in the 2-choice assay, these flies often struggle to turn at the hot-cold boundary, resulting in flies remaining near the boundary (Figure 3.8d). Strikingly, unlike controls, these flies demonstrate a marked decrease in

turning bias as a function of approach angle (Figure 3.8e). This indicated that the PFNv cells may be important for directional responses at a steep thermal boundary.

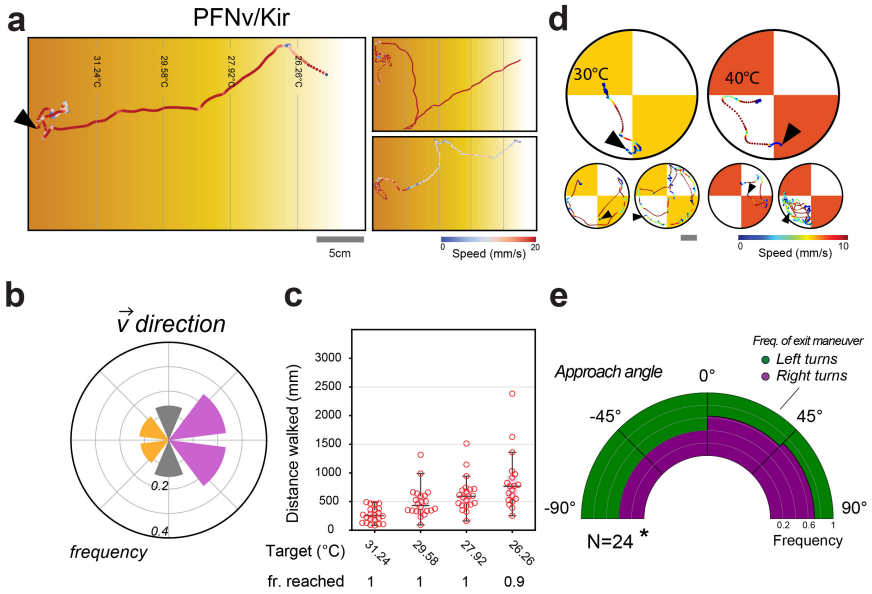

Figure 3.8. PFNv silencing only disturbs thermotaxis in the two-choice assay. **a.** Example walking trajectories of PFNv-silenced flies. **b,c.** Directional frequency plot, walking distances to isothermal lines, and success frequency are comparable to controls. **d.** Example trajectories of compass-silenced flies in the two-choice assay. Grey scale bar represents 5 mm in large plots, and 1 cm in small plots. **e.** Polar plot of turn direction depending on approach angle shows a decrease in bias from controls (P= 0.043).

Together, this suggests that the compass is involved in processing of diffuse thermal cues (i.e., without discrete landmarks), and is required for robust navigation of the gradient. In the shallow linear gradient, the navigational phenotype is comparable to silencing the antennae, suggesting that the compass may be a key processing center of temperature information. This navigational deficiency is particularly apparent when considering the heading index (sometimes called "drift efficiency"),

$$\mathrm{HI} = \frac{1}{T}\int_0^T \cos(\theta(t))dt \tag{3.12}$$

where $\theta(t)$ is the heading direction (Figure 3.9).

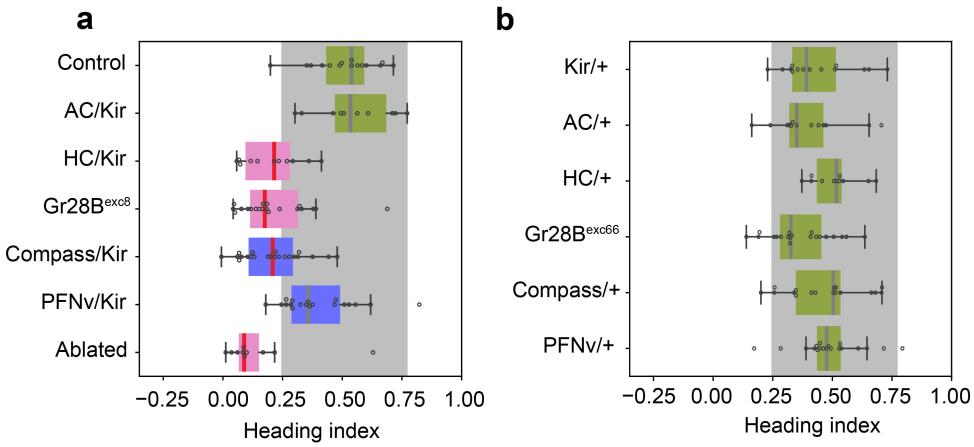

Figure 3.9. Compass-silenced flies show comparable descent efficiency to HC mutant flies. **a.** Heading index for control and mutants (grey region indicates 95% confidence interval for WT - green=no perturbation to HCs or CX, pink=HC mutants, blue=CX mutant; $P_{HC/Kir} = 0.0024$, $P_{Gr28Bexc8} = 0.0018$, $P_{Compass/Kir} = 0.010$, $P_{Ablated} = 8.0e\text{-}6$). Red medians indicate significant difference from appropriate controls. **b.** Heading index for additional controls.

On the other hand, strong directional responses in the steep gradient among compass-silenced flies suggest that separate processing may be required for turning based on temperature differentials between the antennae. Indeed, PFNv neurons appear to be involved in charting the direction of rapid escape turns at the boundary, but are not required for navigation in the shallow gradient.

3.7. Hot input to the central complex

While it is clear that both the EB and FB play key roles in goal-directed navigation, we know little about how heat signals are relayed there. Fortunately, the release of the EM "hemibrain" connectome enabled us to study possible paths in detail [**17**]. This network includes annotation of approximately 25,000 neurons of the fly brain, along with about 20 million chemical synapses between them.

Shortest path analysis of the connectome using Dijkstra's method [**106**] uncovered a handful of privileged routes from the HCs to the EPG neurons, including a series of paths through the Extrinsic Ring (ExR) neurons. Though they were identified more than 30 years ago, these neurons have been the subject of relatively little study, and are named for their "ring-like arborizations around the ellipsoid body canal" and "extensive arborization outside of the ellipsoid body" [**107, 108**]. Four cells of type ExR1 (all of the ExR1 cells in the hemibrain annotation), also known as "helicon" cells due to their spiral morphology [**109**], are of particular interest as they may provide directional input to the compass. Each of these cells receives synaptic input from an uncharacterized third order thermosensory neuron, denoted SMP based on its location in the brain (Figure 3.10a, and see 3.10b for neuron morphologies).

A similar approach targeting the PFNv cells uncovered a path via a class of known fast-adapting hot TPNs [**15**], which are well suited to detecting rapid changes in the sensory input (Figure 3.9c and see 3.10d for neuron morphologies). This path also includes an octopaminergic neuron, VPM3, which is presynaptic to the PFNvs.

The role of these cells in thermotaxis is the subject of ongoing experimental analysis.

3.8. Discussion

Our results suggest that flies are capable of rapid and robust thermotaxis across diverse thermal environments, requiring separate yet interacting neural processing circuitry.

This work directly builds upon our results from the previous chapter, and parallels similar forms of allocentric processing studied in rats [**43, 110**] and birds [**111**]. However, rather than using this information to navigate a maze or travel home, flies perform rapid aversive maneuvers to navigate to a safe region of the thermal environment.

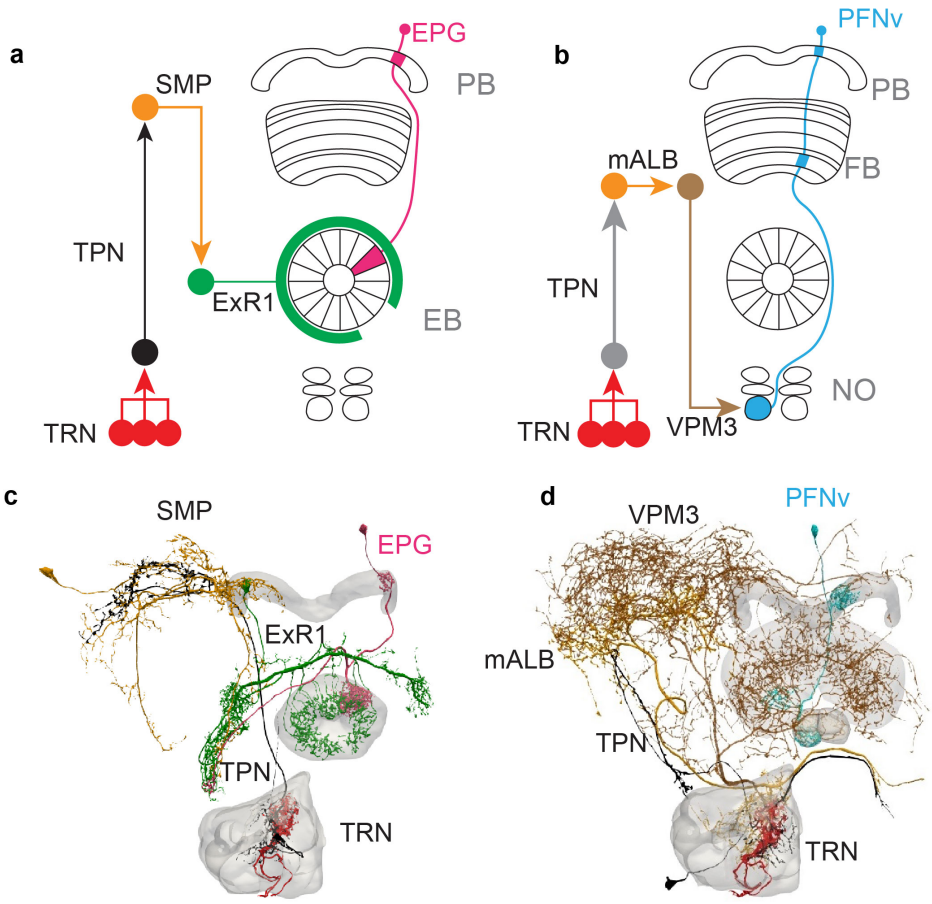

Figure 3.10. Relays to the central complex. **a,b.** Schematics of relays from HCs to EPG (compass) and PFNv neurons. Neuron names are in black, brain region names are shown in grey. **c.** Morphology of proposed relay from TRNs (hot cells) to the EPG cells. Names of neurons in the relay are shown in black. Antennal lobe, ellipsoid body and protocerebral bridge are shown in grey. **d.** Morphology of proposed relay to the PFNv cells. Antennal lobe, noduli, fan-shaped body, and protocerebral bridge are shown in grey.

Following our analysis of heat avoidance described in Chapter 2, we were in the unique position to investigate the differences in neural processing required for navigation of two extreme thermal landscapes, a steep and a shallow gradient. This highlighted a tradeoff between egocentric inter-antennal difference based steering and compass-based, allocentric navigation.

We found that, in a shallow thermal gradient, the antennal sensors and their molecular hot sensor Gr28B.d are required for rapid descent to the preferred temperature of 25°C. However, since the instantaneous temperature difference between antennae is negligible, flies employ a separate strategy in this environment.

Inspired by recent evidence of compass-guided navigation in the fly, we adapted our existing hard-wired vehicle model, incorporating a compass-like module that was sufficient to restore fly-like rapid descent of the thermal gradient. Though this model is intentionally simple, it performs remarkably well across both experimental contexts, suggesting navigational responses to hot stimuli may indeed be approximated by a series of simple computations.

Like the "naive" vehicles, compass-silenced flies demonstrated a navigation phenotype comparable to heat sensor mutants in the shallow gradient, but retained the ability to make turns on the basis of approach angle to the boundary in the steep gradient. Oppositely, silencing experiments targeting the ventral PFN neurons demonstrated control-like behavior in the shallow gradient. However, in the steep gradient we observed decreased bias in directed turning as a function of approach angle, suggesting that the PFNv cells are involved in determining the direction of escape turns at the boundary. Together, these results suggest that these two pathways are used for distinct forms of navigation, but work together to ensure robust thermotaxis over a wide range of sensory landscapes.

The study of animal navigation is a key source of inspiration for improving the strategies that guide autonomous robots and vehicles. Our model-driven approach, combined with detailed analysis of neural circuitry reveals possible shortcomings of relying on a single strategy for navigation, and suggests that robust navigation across contexts may require separate yet interacting guidance programs.

CHAPTER 4

Conclusion

Since the days of T.H. Morgan's legendary fly room, *Drosophila melanogaster* has reigned as one of the most powerful model organisms. Despite measuring only a few millimeters in length, flies possess a central brain with around 100,000 neurons, and demonstrate a wide range of complex behaviors. They have laid the foundation for modern biology, and continue to inspire discovery.

The work in this dissertation has sought to develop quantitative frameworks for the study of fly behavior by combining a range of experimental and mathematical approaches. A central theme of this work is the use of a simple "Braitenberg" vehicle, which appears to reproduce key characteristics of fly thermotaxis. However, it was actually critical differences between our hard-wired model and real flies that allowed us to identify unexpectedly complex behavior involved in fly thermotaxis. In particular, we found that flies demonstrate key features of plasticity, learning, and robustness during heat avoidance. By analyzing both vehicle and fly navigation in two extreme thermal landscapes, we were able to isolate distinct forms of neural processing, as well as corresponding circuitry, required for navigation across a broad range of environmental contexts.

These two chapters represent the first ever high-resolution characterization of fly thermotaxis, taking an important step beyond identification of relevant sensors to understand their functional role in guiding navigation. We extracted many of our key findings from dedicated

analysis of the walking trajectories of freely moving flies, which allowed us to capture realistic responses to thermal stimuli. Though were able to uncover large amounts of information using this approach, further progress may require new types of data and additional tools for unbiased analysis of behavior.

Systems neuroscience (and biology in general) has entered into an age of massive data collection. In parallel, the techniques for studying individual neurons continue to gain in accuracy and specificity, and descriptors of behavior are becoming more robust and data-driven. Over the past few years, massive projects like the the flyEM connectome [**17**] have greatly aided our ability to discuss the organization and structure of the fly brain, and methods like DeepLabCut [**112**] and LEAP [**113**] have made it orders of magnitude easier to track the positions of individual animal body parts.

Accordingly, a key avenue for future work in the field will be combining domain specific knowledge with computational analysis of these rich sources of data, in order to make sense of the many neurons in the brain and their role in neural processing and behavior. The study of behavior has historically dealt in largely qualitative descriptions, and an important step will be to continue to develop quantitative frameworks (like [**114**]) to study behavior and the brain with minimal user bias. This will be particularly useful for research on sensory navigation, allowing researchers to identify relevant neural circuitry and behaviors that underlie decision-making and locomotion with unprecedented precision.

I believe that data-driven mathematical approaches hold the key to developing the language and theory to more deeply understand the connections between the brain and behavior. Although this requires leaps of faith into unknown fields (for both mathematicians and neuroscientists), I've found that submersing myself in experimental collaboration has allowed me to see new aspects of scientific problems, and has led to a host of exciting new questions

to study. In my own future work, I plan to take a similar approach, starting with rigorous measurements of key biological phenomena, followed by the development of quantitative, physics/data-driven frameworks for analysis.

References

[1] Bernd Nilius and Grzegorz Owsianik. The transient receptor potential family of ion channels. *Genome Biology*, 12(3), 2011.

[2] D. J. Cosens and Aubrey Manning. Abnormal electroretinogram from a Drosophila mutant. *Nature*, 224(5216):285–287, 1969.

[3] Michael J. Caterina, Mark A. Schumacher, Makoto Tominaga, Tobias A. Rosen, Jon D. Levine, and David Julius. The capsaicin receptor: A heat-activated ion channel in the pain pathway. *Nature*, 389(6653):816–824, 1997.

[4] Makoto Tominaga. *TRP Ion Channel Function in Sensory Transduction and Cellular Signaling Cascades*. CRC Press, 9 2006.

[5] Oscar M. Arenas, Emanuela E. Zaharieva, Alessia Para, Constanza Vásquez-Doorman, Christian P. Petersen, and Marco Gallio. Activation of planarian TRPA1 by reactive oxygen species reveals a conserved mechanism for animal nociception. *Nature Neuroscience*, 20(12):1686–1693, 2017.

[6] W. Daniel Tracey, Rachel I. Wilson, Gilles Laurent, and Seymour Benzer. painless, a Drosophila gene essential for nociception. *Cell*, 113(2):261–273, 4 2003.

[7] Lina Ni, Peter Bronk, Elaine C. Chang, April M. Lowell, Juliette O. Flam, Vincent C. Panzano, Douglas L. Theobald, Leslie C. Griffith, and Paul A. Garrity. A gustatory receptor paralogue controls rapid warmth avoidance in Drosophila. *Nature*, 500(7464):580–584, 2013.

[8] Koji Sato, Kana Tanaka, and Kazushige Touhara. Sugar-regulated cation channel formed by an insect gustatory receptor. *Proceedings of the National Academy of Sciences of the United States of America*, 108(28):11680–11685, 7 2011.

[9] Jie Liu, Alex Ward, Jingwei Gao, Yongming Dong, Nana Nishio, Hitoshi Inada, Lijun Kang, Yong Yu, Di Ma, Tao Xu, Ikue Mori, Zhixiong Xie, and X. Z.Shawn Xu. C. elegans phototransduction requires a G protein-dependent cGMP pathway and a taste receptor homolog. *Nature Neuroscience*, 13(6):715–722, 6 2010.

[10] Aditi Mishra, Autoosa Salari, Benton R. Berigan, Kayla C. Miguel, Marzie Amirshenava, Abbey Robinson, Benjamin C. Zars, Jenna L. Lin, Lorin S. Milescu, Mirela Milescu, and Troy Zars. The Drosophila Gr28bD product is a non-specific cation channel that can be used as a novel thermogenetic tool. *Scientific Reports*, 8(1):901, 12 2018.

[11] Marco Gallio, Tyler A. Ofstad, Lindsey J. Macpherson, Jing W. Wang, and Charles S. Zuker. The coding of temperature in the Drosophila brain. *Cell*, 144(4):614–624, 2011.

[12] Joseph B. Duffy. GAL4 system in Drosophila: A fly geneticist's Swiss army knife. *Genesis*, 34(1-2):1–15, 9 2002.

[13] Omer Sayeed and Seymour Benzer. Behavioral genetics of thermosensation and hygrosensation in Drosophila. *Proceedings of the National Academy of Sciences of the United States of America*, 93(12):6079–6084, 1996.

[14] Fumika N. Hamada, Mark Rosenzweig, Kyeongjin Kang, Stefan R. Pulver, Alfredo Ghezzi, Timothy J. Jegla, and Paul A. Garrity. An internal thermal sensor controlling temperature preference in Drosophila. *Nature*, 454(7201):217–220, 2008.

[15] Dominic D. Frank, Genevieve C. Jouandet, Patrick J. Kearney, Lindsey J. MacPherson, and Marco Gallio. Temperature representation in the Drosophila brain. *Nature*, 519(7543):358–361, 2015.

[16] Anthony M. Zador. A critique of pure learning and what artificial neural networks can learn from animal brains. *Nature Communications*, 10(1), 2019.

[17] Louis K. Scheffer, C. Shan Xu, Michal Januszewski, Zhiyuan Lu, Shin Ya Takemura, Kenneth J. Hayworth, Gary B. Huang, Kazunori Shinomiya, Jeremy Maitin-Shepard, Stuart Berg, Jody Clements, Philip M. Hubbard, William T. Katz, Lowell Umayam, Ting Zhao, David Ackerman, Tim Blakely, John Bogovic, Tom Dolafi, Dagmar Kainmueller, Takashi Kawase, Khaled A. Khairy, Laramie Leavitt, Peter H. Li, Larry Lindsey, Nicole Neubarth, Donald J. Olbris, Hideo Otsuna, Eric T. Trautman, Masayoshi Ito, Alexander S. Bates, Jens Goldammer, Tanya Wolff, Robert Svirskas, Philipp Schlegel, Erika R. Neace, Christopher J. Knecht, Chelsea X. Alvarado, Dennis A. Bailey, Samantha Ballinger, Jolanta A. Borycz, Brandon S. Canino, Natasha Cheatham, Michael Cook, Marisa Dreher, Octave Duclos, Bryon Eubanks, Kelli Fairbanks, Samantha Finley, Nora Forknall, Audrey Francis, Gary Patrick Hopkins, Emily M. Joyce, Sungjin Kim, Nicole A. Kirk, Julie Kovalyak, Shirley A. Lauchie, Alanna Lohff, Charli Maldonado, Emily A. Manley, Sari McLin, Caroline Mooney, Miatta Ndama, Omotara Ogundeyi, Nneoma Okeoma, Christopher Ordish, Nicholas Padilla, Christopher Patrick, Tyler Paterson, Elliott E. Phillips, Emily M. Phillips, Neha Rampally, Caitlin

Ribeiro, Madelaine K. Robertson, Jon Thomson Rymer, Sean M. Ryan, Megan Sammons, Anne K. Scott, Ashley L. Scott, Aya Shinomiya, Claire Smith, Kelsey Smith, Natalie L. Smith, Margaret A. Sobeski, Alia Suleiman, Jackie Swift, Satoko Takemura, Iris Talebi, Dorota Tarnogorska, Emily Tenshaw, Temour Tokhi, John J. Walsh, Tansy Yang, Jane Anne Horne, Feng Li, Ruchi Parekh, Patricia K. Rivlin, Vivek Jayaraman, Marta Costa, Gregory S.X.E. Jefferis, Kei Ito, Stephan Saalfeld, Reed George, Ian A. Meinertzhagen, Gerald M. Rubin, Harald F. Hess, Viren Jain, and Stephen M. Plaza. A connectome and analysis of the adult drosophila central brain. *eLife*, 9:1–74, 9 2020.

[18] Kohei Shimono, Azusa Fujimoto, Taiichi Tsuyama, Misato Yamamoto-Kochi, Motohiko Sato, Yukako Hattori, Kaoru Sugimura, Tadao Usui, Ken Ichi Kimura, and Tadashi Uemura. Multidendritic sensory neurons in the adult Drosophila abdomen: Origins, dendritic morphology, and segment- and age-dependent programmed cell death. *Neural Development*, 2009.

[19] Steven M. Reppert and Jacobus C. de Roode. Demystifying Monarch Butterfly Migration. *Current Biology*, 28(17):1009–1022, 9 2018.

[20] Avalon C.S. Owens and Sara M. Lewis. The impact of artificial light at night on nocturnal insects: A review and synthesis, 11 2018.

[21] A W Carter, R T Paitz, K E Mcghee, and R M Bowden. Turtle hatchlings show behavioral types that are robust to developmental manipulations. *Physiology & Behavior*, 155:46–55, 2015.

[22] P. Bedard and C. J. Pycock. 'Wet-Dog' shake behaviour in the rat: A possible quantitative model of central 5-hydroxytryptamine activity. *Neuropharmacology*, 16(10):663–670, 10 1977.

[23] Valentino. Braitenberg. *Vehicles, experiments in synthetic psychology*. MIT Press, Cambridge, Mass., 1984.

[24] Carlos Ribeiro and Barry J. Dickson. Sex peptide receptor and neuronal TOR/S6K signaling modulate nutrient balancing in Drosophila. *Current Biology*, 20(11):1000–1005, 6 2010.

[25] M. Florencia Camus, Chun Cheng Huang, Max Reuter, and Kevin Fowler. Dietary choices are influenced by genotype, mating status, and sex in Drosophila melanogaster. *Ecology and Evolution*, 8(11):5385–5393, 6 2018.

[26] Yong Kyu Kim, Mathias Saver, Jasper Simon, Clement F. Kent, Lisha Shao, Mark Eddison, Pavan Agrawal, Michael Texada, James W. Truman, and Ulrike Heberlein. Repetitive aggressive encounters generate a long-lasting internal state in Drosophila

melanogaster males. *Proceedings of the National Academy of Sciences of the United States of America*, 115(5):1099–1104, 1 2018.

[27] Lily Kahsai and Troy Zars. Learning and memory in drosophila: Behavior, genetics, and neural systems. In *International Review of Neurobiology*, volume 99, pages 139–167. Academic Press Inc., 1 2011.

[28] W. G. Quinn, W. A. Harris, and S. Benzer. Conditioned behavior in Drosophila melanogaster. *Proceedings of the National Academy of Sciences of the United States of America*, 71(3):708–712, 1974.

[29] Howard C. Berg. Motile behavior of bacteria. *Physics Today*, 2000.

[30] Kazuo Funabiki, Go Ashida, and Masakazu Konishi. Computation of interaural time difference in the owl's coincidence detector neurons. *Journal of Neuroscience*, 31(43):15245–15256, 10 2011.

[31] Agenor Mafra-Neto and Ring T. Cardé. Fine-scale structure of pheromone plumes modulates upwind orientation of flying moths. *Nature*, 369(6476):142–144, 1994.

[32] Bert Holldobler and Edward O. Wilson. *The Ants*. Harvard University Press, 1990.

[33] Jennifer A. Mather. Navigation by spatial memory and use of visual landmarks in octopuses. *Journal of Comparative Physiology A*, 168(4):491–497, 1991.

[34] Russell A. Epstein, Eva Zita Patai, Joshua B. Julian, and Hugo J. Spiers. The cognitive map in humans: Spatial navigation and beyond, 11 2017.

[35] Timothy A. Currier and Katherine I. Nagel. Multisensory control of navigation in the fruit fly, 10 2020.

[36] Massimo Vergassola, Emmanuel Villermaux, and Boris I. Shraiman. 'Infotaxis' as a strategy for searching without gradients. *Nature*, 445(7126):406–409, 1 2007.

[37] Lauren M. Miller, Yonatan Silverman, Malcolm A. MacIver, and Todd D. Murphey. Ergodic Exploration of Distributed Information. *IEEE Transactions on Robotics*, 2016.

[38] Floris Van Breugel and Michael H. Dickinson. Plume-tracking behavior of flying drosophila emerges from a set of distinct sensory-motor reflexes. *Current Biology*, 24(3):274–286, 2 2014.

[39] John C. Tuthill and Rachel I. Wilson. Mechanosensation and Adaptive Motor Control in Insects, 10 2016.

[40] Eve Marder and Dirk Bucher. Central pattern generators and the control of rhythmic movements. *Current Biology*, 11(23):R986–R996, 11 2001.

[41] Salil S. Bidaye, Christian Machacek, Yang Wu, and Barry J. Dickson. Neuronal control of Drosophila walking direction. *Science*, 344(6179):97–101, 2014.

[42] Clarissa Goldsmith, Nicholas Szczecinski, and Roger Quinn. Drosophibot: A Fruit Fly Inspired Bio-Robot. In *Lecture Notes in Computer Science (including subseries Lecture Notes in Artificial Intelligence and Lecture Notes in Bioinformatics)*, volume 11556 LNAI, pages 146–157. Springer Verlag, 7 2019.

[43] Edward C. Tolman. Cognitive maps in rats and men. *Psychological Review*, 55(4):189–208, 7 1948.

[44] Norman M. White and Robert J. McDonald. Multiple parallel memory systems in the brain of the rat. *Neurobiology of Learning and Memory*, 77(2):125–184, 3 2002.

[45] Andrej Bicanski and Neil Burgess. Neuronal vector coding in spatial cognition. *Nature Reviews Neuroscience*, 21(9):453–470, 2020.

[46] Johannes D. Seelig and Vivek Jayaraman. Neural dynamics for landmark orientation and angular path integration. *Nature*, 521(7551):186–191, 2015.

[47] Roland Straussa and Martin Heisenberg. A Higher Control Center of Locomotor Behavior in the Drosophila Brain. *The Journal of Neuroscience*, 13(5):1852–891, 1993.

[48] Adrienn G. Varga, Nicholas D. Kathman, Joshua P. Martin, Peiyuan Guo, and Roy E. Ritzmann. Spatial navigation and the central complex: Sensory acquisition, orientation, and motor control, 1 2017.

[49] Anna Honkanen, Andrea Adden, Josiane Da Silva Freitas, and Stanley Heinze. The insect central complex and the neural basis of navigational strategies. *Journal of Experimental Biology*, 222, 2 2019.

[50] Jonathan Green, Atsuko Adachi, Kunal K. Shah, Jonathan D. Hirokawa, Pablo S. Magani, and Gaby Maimon. A neural circuit architecture for angular integration in Drosophila. *Nature*, 546(7656):101–106, 2017.

[51] Ysabel Milton Giraldo, Katherine J. Leitch, Ivo G. Ros, Timothy L. Warren, Peter T. Weir, and Michael H. Dickinson. Sun Navigation Requires Compass Neurons in Drosophila. *Current Biology*, 28(17):2845–2852, 9 2018.

[52] Jonathan Green, Vikram Vijayan, Peter Mussells Pires, Atsuko Adachi, and Gaby Maimon. A neural heading estimate is compared with an internal goal to guide oriented navigation. *Nature Neuroscience*, 22(9):1460–1468, 2019.

[53] Tatsuo S. Okubo, Paola Patella, Isabel D'Alessandro, and Rachel I. Wilson. A Neural Network for Wind-Guided Compass Navigation. *Neuron*, 107(5):924–940, 2020.

[54] Daniel Turner-Evans, Stephanie Wegener, Hervé Rouault, Romain Franconville, Tanya Wolff, Johannes D. Seelig, Shaul Druckmann, and Vivek Jayaraman. Angular velocity integration in a fly heading circuit. *eLife*, 6, 5 2017.

[55] Thomas Stone, Barbara Webb, Andrea Adden, Nicolai Ben Weddig, Anna Honkanen, Rachel Templin, William Wcislo, Luca Scimeca, Eric Warrant, and Stanley Heinze. An Anatomically Constrained Model for Path Integration in the Bee Brain. *Current Biology*, 27(20):3069–3085, 10 2017.

[56] Cheng Lyu, L F Abbott, and Gaby Maimon. A neuronal circuit for vector computation builds an allocentric traveling- direction signal in the Drosophila fan-shaped body. *bioRxiv*, 2020.

[57] Jenny Lu, Elena A Westeinde, Lydia Hamburg, Paul M Dawson, Cheng Lyu, Gaby Maimon, Shaul Druckmann, and Rachel I Wilson. Transforming representations of movement from body- to world-centric space. *bioRxiv*, page 2020.12.22.424001, 12 2020.

[58] Timothy A Currier, Andrew MM Matheson, and Katherine I Nagel. Encoding and control of orientation to airflow by a set of Drosophila fan-shaped body neurons. *eLife*, 9, 12 2020.

[59] Joshua P. Martin, Peiyuan Guo, Laiyong Mu, Cynthia M. Harley, and Roy E. Ritzmann. Central-complex control of movement in the freely walking cockroach. *Current Biology*, 25(21):2795–2803, 2015.

[60] José Miguel Simões, Joshua I. Levy, Emanuela E. Zaharieva, Leah T. Vinson, Peixiong Zhao, Michael H. Alpert, William L. Kath, Alessia Para, and Marco Gallio. Robustness and plasticity in Drosophila heat avoidance. *Nature Communications*, 12(1):2044, 12 2021.

[61] David P. Robinson, Mohammed Y. Jaidah, Steffen S. Bach, Christoph A. Rohner, Rima W. Jabado, Rupert Ormond, and Simon J. Pierce. Some like it hot: Repeat migration and residency of whale sharks within an extreme natural environment. *PLoS ONE*, 2017.

[62] Timothy A. Currier and Katherine I. Nagel. Multisensory Control of Orientation in Tethered Flying Drosophila. *Current Biology*, 2018.

[63] Timothy L. Warren, Ysabel M. Giraldo, and Michael H. Dickinson. Celestial navigation in Drosophila. *The Journal of Experimental Biology*, 222(Pt Suppl 1), 2019.

[64] Quentin Gaudry, Katherine I. Nagel, and Rachel I. Wilson. Smelling on the fly: sensory cues and strategies for olfactory navigation in Drosophila. *Current Opinion in Neurobiology*, 22(2):216–22, 4 2012.

[65] Linjiao Luo, Marc Gershow, Mark Rosenzweig, Kyeongjin Kang, Christopher Fang-Yen, Paul A. Garrity, and Aravinthan D T Samuel. Navigational decision making in Drosophila thermotaxis. *The Journal of Neuroscience*, 30(12):4261–72, 3 2010.

[66] R. B. Huey, W. D. Crill, J. G. Kingsolver, and K. E. Weber. A Method for Rapid Measurement of Heat or Cold Resistance of Small Insects. *Functional Ecology*, 6(4):489, 1992.

[67] Leah A. Pogorzala, Santosh K. Mishra, and Mark A. Hoon. The cellular code for mammalian thermosensation. *Journal of Neuroscience*, 2013.

[68] Chen Ran, Mark A. Hoon, and Xiaoke Chen. The coding of cutaneous temperature in the spinal cord. *Nature Neuroscience*, 2016.

[69] David A. Yarmolinsky, Yueqing Peng, Leah A. Pogorzala, Michael Rutlin, Mark A. Hoon, and Charles S. Zuker. Coding and Plasticity in the Mammalian Thermosensory System. *Neuron*, 92(5):1079–1092, 12 2016.

[70] Michael H. Alpert, Dominic D. Frank, Evan Kaspi, Matthieu Flourakis, Emanuela E. Zaharieva, Ravi Allada, Alessia Para, and Marco Gallio. A Circuit Encoding Absolute Cold Temperature in Drosophila. *Current Biology*, 30(12):2275–2288, 6 2020.

[71] L. Gary Leal. *Advanced Transport Phenomena*. Cambridge University Press, Cambridge, 2007.

[72] Alexandre Joel Chorin. Numerical solution of the Navier-Stokes equations. *Mathematics of Computation*, 22(104):745–745, 13 1968.

[73] Martin S Alnaes, Jan Blechta, Johan Hake, August Johansson, Benjamin Kehlet, Anders Logg, Chris Richardson, Johannes Ring, Marie E Rognes, and Garth N Wells. The FEniCS Project Version 1.5. *Archive of Numerical Software*, 3(100):9–23, 12 2015.

[74] J. Crank and P. Nicolson. A practical method for numerical evaluation of solutions of partial differential equations of the heat-conduction type. *Mathematical Proceedings of the Cambridge Philosophical Society*, 43(1):50–67, 1947.

[75] C. Taylor and P. Hood. A numerical solution of the Navier-Stokes equations using the finite element technique. *Computers and Fluids*, 1(1):73–100, 1 1973.

[76] Mark A. Christon, Philip M. Gresho, and Steven B. Sutton. Computational predictability of time-dependent natural convection flows in enclosures (including a benchmark solution). *International Journal for Numerical Methods in Fluids*, 40(8):953–980, 11 2002.

[77] Suzuko Yorozu, Allan Wong, Brian J. Fischer, Heiko Dankert, Maurice J. Kernan, Azusa Kamikouchi, Kei Ito, and David J. Anderson. Distinct sensory representations of wind and near-field sound in the Drosophila brain. *Nature*, 458(7235):201–5, 3 2009.

[78] Junko Morikawa, Meguya Ryu, Gediminas Seniutinas, Armandas Balčytis, Ksenia Maximova, Xuewen Wang, Massimiliano Zamengo, Elena P. Ivanova, and Saulius Juodkazis. Nanostructured Antireflective and Thermoisolative Cicada Wings. *Langmuir*, 32(18):4698–703, 2016.

[79] Shubha R. Shanbhag, K Singh, and R. Naresh Singh. Fine structure and primary sensory projections of sensilla located in the sacculus of the antenna of Drosophila melanogaster. *Cell and Tissue Research*, 282(2):237–249, 11 1995.

[80] Seong Soo Kim, Seon Jeong Kim, Yoon Duk Moon, and Young Moo Lee. Thermal characteristics of chitin and hydroxypropyl chitin. *Polymer*, 35(15):3212–3216, 7 1994.

[81] A. Moiseff and M. Konishi. Neuronal and behavioral sensitivity to binaural time differences in the owl. *The Journal of Neuroscience*, 1(1):40–48, 1 1981.

[82] Raghav Rajan. Rats Smell in Stereo. *Science*, 311(5761):666–670, 2 2006.

[83] Philip X. Joris and Marcel van der Heijden. Early Binaural Hearing: The Comparison of Temporal Differences at the Two Ears. *Annual Review of Neuroscience*, 42(1):433–457, 7 2019.

[84] Brian J. Duistermars, Dawnis M. Chow, and Mark A. Frye. Flies Require Bilateral Sensory Input to Track Odor Gradients in Flight. *Current Biology*, 19(15):1301–1307, 8 2009.

[85] Quentin Gaudry, Elizabeth J. Hong, Jamey Kain, Benjamin L. De Bivort, and Rachel I. Wilson. Asymmetric neurotransmitter release enables rapid odour lateralization in Drosophila. *Nature*, 493(7432):424–428, 1 2013.

[86] Alex Gomez-Marin, Greg J. Stephens, and Matthieu Louis. Active sampling and decision making in Drosophila chemotaxis. *Nature Communications*, 2(1):441, 9 2011.

[87] Hod Dana, Yi Sun, Boaz Mohar, Brad K. Hulse, Aaron M. Kerlin, Jeremy P. Hasseman, Getahun Tsegaye, Arthur Tsang, Allan Wong, Ronak Patel, John J. Macklin, Yang Chen, Arthur Konnerth, Vivek Jayaraman, Loren L. Looger, Eric R. Schreiter, Karel Svoboda, and Douglas S. Kim. High-performance calcium sensors for imaging activity in neuronal populations and microcompartments. *Nature Methods*, 16(7):649–657, 7 2019.

[88] Aljoscha Nern, Barret D. Pfeiffer, Karel Svoboda, and Gerald M. Rubin. Multiple new site-specific recombinases for use in manipulating animal genomes. *Proceedings of the National Academy of Sciences*, 108(34):14198–14203, 8 2011.

[89] Kalyanmoy Deb, Amrit Pratap, Sameer Agarwal, and T. Meyarivan. A fast and elitist multiobjective genetic algorithm: NSGA-II. *IEEE Transactions on Evolutionary Computation*, 6(2):182–197, 4 2002.

[90] Felix Antoine Fortin, Francois Michel De Rainville, Marc Andre Gardner, Marc Parizeau, and Christian Gagne. DEAP: Evolutionary algorithms made easy. *Journal of Machine Learning Research*, 13:2171–2175, 2012.

[91] J. S. Kennedy. Zigzagging and casting as a programmed response to wind-borne odour: a review. *Physiological Entomology*, 8(2):109–120, 6 1983.

[92] William Morton Barrows. The reactions of the Pomace fly, Drosophila ampelophila loew, to odorous substances. *Journal of Experimental Zoology*, 4(4):515–537, 10 1907.

[93] V. B. Wigglesworth and J. D. Gillett. The Function of the Antennae in Rhodnius prolixus (Hemiptera) and the Mechanism of Orientation to the Host. *Journal of Experimental Biology*, 11(2):120–139, 4 1934.

[94] Amayu W. Gena, Conrad Voelker, and Gary S. Settles. Qualitative and quantitative schlieren optical measurement of the human thermal plume. *Indoor Air*, 30(4):757–766, 7 2020.

[95] Linjiao Luo, Nathan Cook, Vivek Venkatachalam, Luis A. Martinez-Velazquez, X. Zhang, Ana C. Calvo, Josh Hawk, Bronwyn L. MacInnis, Michelle Frank, Jia Hong Ray Ng, Mason Klein, Marc Gershow, Marc Hammarlund, Miriam B. Goodman, D. A. Colon-Ramos, Yun Zhang, and A. D. T. Samuel. Bidirectional thermotaxis in Caenorhabditis elegans is mediated by distinct sensorimotor strategies driven by the AFD thermosensory neurons. *Proceedings of the National Academy of Sciences*, 111(7):2776–2781, 2 2014.

[96] Alex Davies, Matthieu Louis, and Barbara Webb. A Model of Drosophila Larva Chemotaxis. *PLoS computational biology*, 11(11):e1004606, 11 2015.

[97] Tihana Jovanic, Casey Martin Schneider-Mizell, Mei Shao, Jean-Baptiste Masson, Gennady Denisov, Richard Doty Fetter, Brett Daren Mensh, James William Truman, Albert Cardona, and Marta Zlatic. Competitive Disinhibition Mediates Behavioral Choice and Sequences in Drosophila. *Cell*, 167(3):858–870, 10 2016.

[98] Jane Loveless, Konstantinos Lagogiannis, and Barbara Webb. Modelling the mechanics of exploration in larval Drosophila. *PLOS Computational Biology*, 15(7):e1006635, 7 2019.

[99] Martin Haesemeyer, Drew N Robson, Jennifer M Li, Alexander F Schier, and Florian Engert. A Brain-wide Circuit Model of Heat-Evoked Swimming Behavior in Larval Zebrafish. *Neuron*, 98(4):817–831, 5 2018.

[100] Eva A. Naumann, James E. Fitzgerald, Timothy W. Dunn, Jason Rihel, Haim Sompolinsky, and Florian Engert. From Whole-Brain Data to Functional Circuit Models: The Zebrafish Optomotor Response. *Cell*, 167(4):947–960, 2016.

[101] Katherine J. Leitch, Francesca V. Ponce, William B. Dickson, Floris Van Breugel, and Michael H. Dickinson. The long-distance flight behavior of Drosophila supports an agent-based model for wind-assisted dispersal in insects. *Proceedings of the National Academy of Sciences of the United States of America*, 118(17), 4 2021.

[102] Yvette E. Fisher, Jenny Lu, Isabel D'Alessandro, and Rachel I. Wilson. Sensorimotor experience remaps visual input to a heading-direction network. *Nature*, 576(7785):121–125, 2019.

[103] Daniel B. Turner-Evans, Kristopher T. Jensen, Saba Ali, Tyler Paterson, Arlo Sheridan, Robert P. Ray, Tanya Wolff, J. Scott Lauritzen, Gerald M. Rubin, Davi D. Bock, and Vivek Jayaraman. The Neuroanatomical Ultrastructure and Function of a Biological Ring Attractor. *Neuron*, 108(1):145–163, 2020.

[104] Aleksandr Rayshubskiy, Stephen Holtz, Isabel D'Alessandro, Anna Li, Quinn Vanderbeck, Isabel Haber, Peter Gibb, and Rachel Wilson. Neural circuit mechanisms for steering control in walking Drosophila. *bioRxiv*, 7 2020.

[105] Hiroshi M. Shiozaki, Kazumi Ohta, and Hokto Kazama. A Multi-regional Network Encoding Heading and Steering Maneuvers in Drosophila. *Neuron*, 106(1):126–141, 4 2020.

[106] E. W. Dijkstra. A note on two problems in connexion with graphs. *Numerische Mathematik*, 1(1):269–271, 12 1959.

[107] U. Hanesch, K. F. Fischbach, and M. Heisenberg. Neuronal architecture of the central complex in Drosophila melanogaster. *Cell and Tissue Research*, 257(2):343–366, 1989.

[108] Jaison Jiro Omoto, Bao Chau Minh Nguyen, Pratyush Kandimalla, Jennifer Kelly Lovick, Jeffrey Michael Donlea, and Volker Hartenstein. Neuronal constituents and putative interactions within the drosophila ellipsoid body neuropil. *Frontiers in Neural Circuits*, 12, 11 2018.

[109] Jeffrey M. Donlea, Diogo Pimentel, Clifford B. Talbot, Anissa Kempf, Jaison J. Omoto, Volker Hartenstein, and Gero Miesenböck. Recurrent Circuitry for Balancing Sleep Need and Sleep. *Neuron*, 97(2):378–389, 1 2018.

[110] J. S. Taube, R. U. Muller, and J. B. Ranck. Head-direction cells recorded from the postsubiculum in freely moving rats. I. Description and quantitative analysis. *Journal of Neuroscience*, 10(2):420–435, 2 1990.

[111] Gustav Kramer. Experiments On Bird Orientation. *Ibis*, 94(2):265–285, 4 2008.

[112] Alexander Mathis, Pranav Mamidanna, Kevin M. Cury, Taiga Abe, Venkatesh N. Murthy, Mackenzie Weygandt Mathis, and Matthias Bethge. DeepLabCut: markerless pose estimation of user-defined body parts with deep learning. *Nature Neuroscience*, 21(9):1281–1289, 9 2018.

[113] Talmo D. Pereira, Diego E. Aldarondo, Lindsay Willmore, Mikhail Kislin, Samuel S.H. Wang, Mala Murthy, and Joshua W. Shaevitz. Fast animal pose estimation using deep neural networks. *Nature Methods*, 16(1):117–125, 1 2019.

[114] Gordon J. Berman, Daniel M. Choi, William Bialek, and Joshua W. Shaevitz. Mapping the stereotyped behaviour of freely moving fruit flies. *Journal of the Royal Society Interface*, 11(99), 10 2014.

[115] Alexander Y. Katsov and Thomas R. Clandinin. Motion Processing Streams in Drosophila Are Behaviorally Specialized. *Neuron*, 59(2):322–335, 7 2008.

[116] Douglas Bates, Martin Mächler, Ben Bolker, and Steve Walker. Fitting Linear Mixed-Effects Models Using lme4. *Journal of Statistical Software*, 67(1), 2015.

[117] Eshin Jolly. Pymer4: Connecting R and Python for Linear Mixed Modeling. *Journal of Open Source Software*, 3(31):862, 11 2018.

[118] David Firth. Bias reduction of maximum likelihood estimates. *Biometrika*, 80(1):27–38, 9 1993.

APPENDIX

Technical Methods

1. Technical Methods for Chapter 2

1.1. Fly strains

All fruit flies used in this study were bred and reared in a 12:12 day-night cycle, on a diet of standard cornmeal agar medium, at room temperature and controlled humidity. The following strains were used: Canton-special, UAS-Kir2.1, UAS-DTI, HC-Gal4 [**11**], HC-LexA [**15**], AC-Gal4 [**7**], TRPA1^{1} (BDSC#26504, backcrossed 5 times), Df-TRPA1 (Df(3 L)ED4421; BDSC#8066), Df Gr28B (Df(2 L)Exel7031), VT46265-Gal4, UAS-GFP, UAS-GCaMP7f [**87**], hs-FLPG5.PEST and tubP-FRT>GAL80-FRT> [**88**].

The Gr28b.d-LexA line used in this study labels the 3 hot arista TRNs which project to the hot glomerulus in the PAL and (as far as could be ascertained) no other neurons in the animal (see Figure 2.1). The HC-Gal4 line used here strongly labels the 3 hot responding arista TRNs and no other neurons in the antenna, brain, or ventral nerve cord (VNC). Additional off-target expression includes ∼1–2 neurons in leg tarsi and additional 1–2 putative chemosensory neurons innervating the sub-esophageal zone (SEZ; note that these projections do not respond to temperature in Ca^{2+} imaging experiments).

1.2. Experimental and statistical protocol for single flies

Experimental conditions were essentially as described above, except flies were run individually instead of in groups. Unless otherwise stated, we used a set sequence of test temperatures

(BT/TT): 25° /25°C, 25° /35°C, 25° /30°C, 25° /40°C. Tracking of single flies and all data analysis was done in Python. Basic image processing (edge detection and ellipse approximation of body) was done using openCV. To calculate an avoidance index for single flies, we tracked the centroid position of the fly for the duration of the trial and used the following equation $AI = \frac{\text{time at BT} - \text{time at TT}}{\text{total time}}$. To calculate the translation and rotational velocities at each time point, we determined the centroid position and angle of orientation of the fly. Velocity was projected along the body axis of the fly to obtain the velocities in the forward and sideways moving directions. Direction of movement was calculated using the heuristic that the vast majority of movement is in the forward direction, as done in [**115**]. In Figure 2.3b and g, AI values and speeds were compared using 1 or 2-way ANOVA, as appropriate (threshold $P = 0.05$). We used a standard two-tailed t-test (threshold $P = 0.05$) to determine if AIs were different from zero.

Fly tracks were additionally segmented to identify maneuvers executed in the boundary region- between the hot and cool quadrants. The boundary region was defined as starting at the 25.5°C isotherm and extending 5 mm into the hot quadrant (a position characterized by stable temperature in all 3 experimental conditions according to our simulation- see below). Maneuvers were classified as "U-turns" if the fly started on the 25°C quadrant, invaded the border region, and eventually returned to the 25°C quadrant. "Border crossings" were defined as events that terminated with exit on the hot side. Crossover-to-turn ratio was defined as (# U-turns) / (# U-turns + # border crosses). In order to compare the ratios of U-turns vs border crosses in control and experimental animals (while taking into account the potential impact of fly-to-fly idiosyncrasies) we used a generalized linear mixed model (GLMM) with fly ID as a random effect and Wald testing to determine significance (threshold

P = 0.05; data shown in Figure 2.3)([**116, 117**]). This GLMM has the form

$$Y = g(X\beta + Z\gamma) + \epsilon, \tag{.1}$$

where Y is the dependent variable (e.g., U-turn or cross), X, β are the predictor variables and their corresponding coefficients (fixed effects), Z, γ are the design matrix for random effects (i.e., fly ID) and corresponding coefficients, g is an inverse link function (i.e., logistic or linear), and ϵ is the residual. The random effects coefficients are assumed to be normally distributed with mean zero.

1.3. Analysis of turn direction

To analyze the relationship between incoming angle and turning direction within the hot/cool border regions (Figure 2.7), we extracted the first turn performed within the boundary upon entry from the cool side. Here, "turns" were defined as segments containing a deviation from the fly's trajectory resulting in a rotational velocity of at least 45°/second. A positive rotational velocity corresponds to a left turn, while a negative rotational velocity corresponds to a right turn. To define the incoming angle, the starting point of the turn was defined by stepping back along the fly track until the rotational velocity component changed sign or until there was no longer a monotonic decrease in velocity. The angle of the body axis at this location relative to the isothermal lines of the hot/cool boundary was considered as the incoming angle. Testing for changes in turning bias following ablation or silencing of antennae was performed using a GLMM with both approach angle and fly ID as random effects and Wald testing for significance (see above, threshold P=0.05). For bilaterally ablated animals,

this test was modified to test if removal of the antennae abolished predicted turning bias (i.e., based on the behavior of the non-ablated control).

To estimate accuracy in predicting turn direction based upon differential temperature readings at the antennae at turn initiation (Figure 2.7c), we first estimated the temperature at each antenna at each turn's starting point (as defined above). We then calculated an inter-antennal temperature difference (left-right). Here, a negative number indicated a cooler temperature at the left and therefore would predict a left turn, while a positive number would predict a right turn. If this prediction was met we assigned a value of 1 to the event, a zero otherwise. We then binned the data according to inter-antennal temperature difference using a bin size of 0.1°C, and calculated a mean prediction accuracy by taking the mean of the string of 1s and 0s for each bin. Standard deviation was obtained by bootstrapping the data within each bin 1000 times. In order to check for potential turning bias resulting from asymmetric ablation or silencing, we calculated left/right turning frequencies at constant 25°C (note that "turns" are deviations in rotational velocity reaching at least 45°C per second in magnitude). Frequencies were then calculated by taking the ratio of counts between left and right turns (Figure 2.8).

1.4. Analysis of casting

To quantify casting we segmented maneuvers executed in the boundary region as described above. A "cast" was defined as an event containing at least one left and one right turn (as defined above) in close succession. We then quantified the fraction of border interactions that contained at least one cast for each test temperature (Figure 2.11e). To test the relationship between initial inter-antennal temperature difference (at start of first turn) and the probability of performing multiple turns in the boundary region (Figure 2.11f), we

used a GLMM with fly ID as a random effect and Wald testing to determine significance (threshold P = 0.05). For plotting in Figure 2.11f, cast probability was calculated within each bin as P(casting) = casts/ (simple turns + casts). To estimate the potential change in inter-antennal temperature difference between the first and last turn within a cast (Figure 2.11g), ΔT at the start of first and last turns was compared using a Linear Mixed Model (LMM) with fly ID as a random effect and ANOVA for significance(threshold P = 0.05).

1.5. Boundary region analysis and repeated trial experiment

For experiments testing the response of flies to uniform heat or heating (Figure 2.11a-c and Figure 2.12), the arena was heated uniformly from 25°C to 40°C and fly movement was recorded during a defined heating window (10 seconds, from ∼28°C to ∼38°C) or at stable temperature (40°C). To establish the direction of the first turn induced by heating, we limited our analysis to flies that happened to be stationary at the beginning of the heating period. Vehicle simulations in constant heat were designed to match the conditions of fly experiments.

Boundary region tracks were analyzed over the course of each 25 vs 40°C individual fly trial and the position of the head at maximum distance into the hot region was recorded (for schematic see Figure 2.11j). The plot in Figure 2.11k was constructed using the maximum temperatures reached during each interaction with the hot boundary (the first interaction with the border was considered time zero). To test for significance of the decreasing trend (while taking into account the potential impact of fly-to-fly idiosyncrasies) we used a linear mixed model (LMM) with fly ID as a random effect and ANOVA for testing (threshold P=0.05). In Figure 2.11h,i,l, we binned boundary foray depths using the positions of select isotherms. The differences in turning frequency in the 25.5-26.5°C temperature bin between

vehicles and flies, as well as between trials in the repeated trials experiment were tested using a generalized linear mixed model with fly ID as a random effect and Wald testing to determine significance (threshold P=0.05).

As shown in Figure 2.11l, we also performed a repeated trial experiment, in which naïve flies were tested in a series of subsequent 25 vs 40°C trials. Each trial lasted for 2 min. Subsequent trials were interleaved by a 30s pause at constant temperature (33°C). At each new trial, the spatial configuration of hot and cool tiles was flipped, as shown in the schematic in Figure 2.11l. After a set of 8 trials (day 1), flies were individually collected and placed in food vials at 25°C overnight. They were then tested again the next day (day 2).

1.6. Analysis of maximum temperature experienced

Boundary region tracks were analyzed over the course of each 25 vs 40 °C individual fly trial and the position of the head at maximum distance into the hot region was recorded (for schematic see Figure 2.11j). The plot in Figure 2.11k was constructed using the maximum temperatures reached during each interaction with the hot boundary (the first interaction with the border was considered time zero). To test for significance of the decreasing trend (while taking into account the potential impact of fly-to-fly idiosyncrasies) we used a linear mixed model (LMM) with fly ID as a random effect and ANOVA for testing (threshold P = 0.05). In Figure 2.11h, i, l, we binned boundary foray depths using the positions of select isotherms. The differences in turning frequency in the 25.5–26.5 °C temperature bin between vehicles and flies, as well as between trials in the repeated trials experiment were tested using a generalized linear mixed model with fly ID as a random effect and Wald testing to determine significance (threshold P = 0.05).

2. Technical Methods for Chapter 3

2.1. Tracking of fly navigation in the linear gradient

To estimate fly position and orientation, we first performed background subtraction by subtracting the 20th percentile value of each pixel from a random sample of 200 frames. Binarization and morphological opening and closing operations were then performed, and position was calculated as the average x and y position of the nonzero pixels.

2.2. Statistical testing of navigational phenotype

To compare different average distances walked to each isothermal line, significance was determined using a 1 or 2-way ANOVA, depending on the type of manipulation. Testing for different frequency of reaching each line was performed using a 1 or 2 way logistic regression model, and significance was determined using a likelihood ratio test (LRT). Firth's method was used in the case of complete or quasi-complete separation [**118**].

2.3. Analysis of fly walking speed and heading

For all analysis of fly walking directionality, we binned possible orientations into 6 groups, evenly spaced over $[0, 2\pi)$. We then calculated relative frequency of walking in each bin ("$\vec{v}$ direction" as well as the average walking speed while in that heading bin ("Av. speed"). We restricted our analysis to timepoints in which the fly walked at least 1 mm/s, as it was robust to error in our estimation of fly position, yet captured observable walking behavior well.

2.4. Fly brain connectome analysis

To analyze connectivity between the TRNs and the EPGs/PFNvs, we used the hemibrain connectome made available by the FlyEM Project at Janelia Research Campus [**17**]. All analysis was performed in python after querying the *neuprint-python* API. Identities of these neurons were already annotated in the dataset (hemibrain v1.2). Shortest path analysis was performed using Dijkstra's method [**106**].